U.PORTO

FACULDADE DE CIÊNCIAS
UNIVERSIDADE DO PORTO

PhD

PhD

3°
CICLO

FCUP
2019

U.PORTO

Correlated Disorder in One-dimensional Electronic Systems

Niaz Ali Khan

FC

U.PORTO

FACULDADE DE CIÊNCIAS
UNIVERSIDADE DO PORTO

dfis
universidade
de aveiro

Universidade do Minho
Escola de Ciências

PhD

Correlated Disorder in One-dimensional Electronic Systems

Niaz Ali Khan

Tese de Doutoramento apresentada à
Faculdade de Ciências da Universidade do Porto
Física

2019

PhD

Correlated Disorder in One-dimensional Electronic Systems

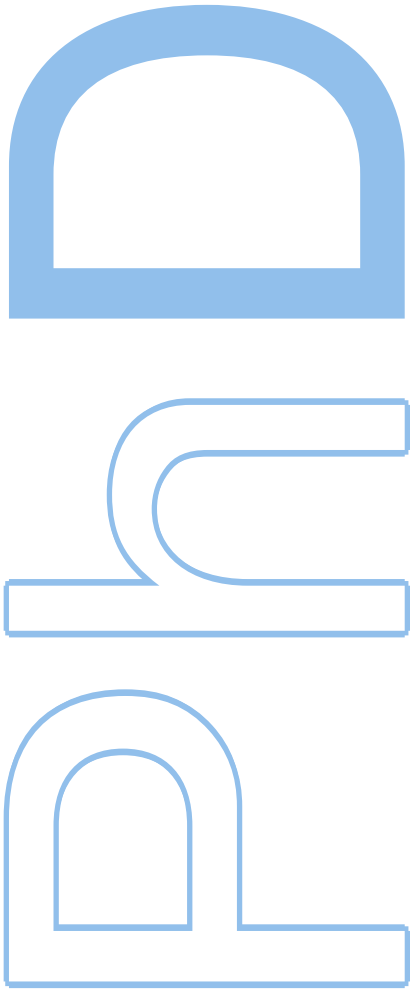

Niaz Ali Khan
Program Doutoral em Física
Departamento de Física e Astronomia
2019

Orientador
J. M. B. Lopes dos Santos, Faculdade de Ciências, Universidade do Porto

Co-orientador
J. M. Viana Parente Lopes, Faculdade de Ciências, Universidade do Porto

Niaz Ali Khan

Correlated Disorder in One-dimensional Electronic Systems

Departamento de Física e Astronomia
Faculdade de Ciências da Universidade do Porto
Maio 2019

Niaz Ali Khan

Correlated Disorder in One-dimensional Electronic Systems

Tese submetida Faculdade de Ciências da Universidade do Porto para obtenção do grau de Doutor em Física

Departamento de Física e Astronomia
Faculdade de Ciências da Universidade do Porto
Maio 2019

To Family, especially Parents with Love

Abstract

In this dissertation, we study free fermion lattice systems with different models of static disorder. In particular, we examine one-dimensional (1D) systems with power-law correlated random site energies (de Moura-Lyra class of models), at zero temperature.

We report numerical calculations of the spectral functions of Bloch states in the de Moura-Lyra model, based on the Kernel polynomial method (KPM), which has an $\mathcal{O}(N)$ computational complexity, where N is the system size. The spatial correlations in the limit $\alpha \to 1^+$ give rise to non-perturbative spectral functions shaped as the probability distribution of the random on-site energies, even at low disorder strengths, which reflects the appearance of a classical limit, and finds an excellent agreement with analytical calculations. In addition, we observe a self-averaging behavior of the spectral function for $\alpha \leq 1$, as the standard deviation decays $1/\sqrt{N}$, at the band center, but ceases to do so for $\alpha > 1$.

The main focus is to examine delocalization transition in de Moura-Lyra model, which has been the object of a long standing discussion in the literature. We report the first numerical evidences that such a transition happens at $\alpha = 1$, where the localization length (measured from the scaling of the conductance) is shown to diverge as $(1-\alpha)^{-1}$, in the thermodynamic limit. The persistent finite-size scaling of the data is shown to be caused by a very slow convergence of the nearest-neighbor correlator to its infinite-size limit, and controlled by the choice of a proper scaling parameter. This last conclusion leads to a re-interpretation of the localization in these models which appears to be dominated by the first neighbor variance rather than the long range power-law tail. Finally, the numerical results are confirmed by analytical perturbative calculations which are built on previous work. In addition, we report the kernel polynomial simulations of localization length for the de Moura-Lyra model. For the Anderson model, the KPM results show an excellent agreement with perturbative result in large system size limit, confirming the validity of the kernel polynomial procedure. For the de Moura-Lyra model, we verify our results by comparing with the localization length obtained by scaling the conductance as well as analytical result.

We review entanglement analysis of the disordered system and also compute the KPM estimates of entanglement entropy based on KPM for the Anderson model. In addition, we present evidence regarding the area law of entanglement entropy by employing a quantum information inspired technique, entanglement contour: a tool to quantify the spatial structure of entanglement. We also report on the entanglement contour as a diagnostic tool for delocalization transition in the disordered system. In particular, we numerically explore the scale invariant feature of the scaled entanglement contour in the vicinity of phase transition for the power-law correlated disorder model.

Contents

List of Figures

Acknowledgments

I was fortunate of being part of a group with an extremely enjoyable and stimulating working atmosphere. First and foremost I would like to express my sincere gratitude to my supervisor, Prof. J. M. B. Lopes dos Santos for giving me the opportunity to work in his group. Over the course of this thesis, he has offered invaluable guidance, helpful suggestions and comments.

Special regard to my co-adviser Prof. J. M. Viana Parente Lopes, who taught me a most fascinating numerical method, "Kernel Polynomial Method". Discussions with him were always fruitful and his ideas were a constant source of inspiration. Without his guidance and patience, this thesis would not exist in this form. He was very friendly, socially active and often had social gatherings at his place. I would like to thank to J. P. Santos Pires for being always open to share his knowledge and new findings with me. He was very friendly, always available for help and I learned a lot from him about doing research.

I would like to thank CFP group members and officemates: Catarina, Robert, Daniel, Goncalo and Simão with whom I have always had great discussions about physics. Special regards to my other friends: Mushtaq Raza, Aftab Rashid, Ali Awan, Kashif, and Syed Tahir Amin for being with whom I feel at home, away from home.

I will forever be thankful to my former advisers, Prof. Salman Khan and Khalid Khan. Dr. K.K was gratefully acknowledged for the financial support. Dr. S. Khan was the reason why I decided to go to pursue a career in research.

I would gratefully acknowledge the INTERWEAVE Project, Erasmus Mundus Action 2 Strand 1 Lot 11, EACEA/42/11 Grant Agreement 2013-2538/ 001-001 EM Action 2 Partnership Asia-Europe and the FCT research grant under the reference UID/FIS/04650/2013 for the financial support.

On a personal note, I would like to thank my family, specially my parents, sisters and brothers for their patience, prayers and moral support throughout my studies.

Publications

This thesis is based on the following publications:

- Chapter. 2 & 4: N. A. Khan, J. M. Viana Parente Lopes, J. P. Santos Pires, and J. M. B. Lopes dos Santos. "Spectral functions of one-dimensional systems with correlated disorder". J. Phys.: Condens. Matter, 31(17):175501, (2019).

- Chapter. 5: J. P. Santos Pires, N. A. Khan, J. M. Viana Parente Lopes, and J. M. B. Lopes dos Santos. "Global Delocalization Transition in the de Moura-Lyra Model". Phys. Rev. B. 99, 205148 (2019).

- Chapter. 3 & 5: N. A. Khan, J. P. Santos Pires, J. M. Viana Parente Lopes, and J. M. B. Lopes dos Santos. "The Kernel Polynomial Simulations of Localization Length: Probing Delocalization Transition", (To appear in EPJ Web Conference) .

Manuscript (unsubmitted)

- Chapter. 6.I: N. A. Khan, J. M. Viana Parente Lopes, J. P. Santos Pires, and J. M. B. Lopes dos Santos. "The Kernel Polynomial Simulations of Entanglement Entropy".

- Chapter. 6.II: N. A. Khan, J. M. B. Lopes dos Santos, J. M. Viana Parente Lopes and J. P. Santos Pires, "Probing Anderson Transition with Entanglement Contour".

Nomenclature

Γ	Correlation function of the local disorder
κ	Inverse localization length
λ	Eigenvalues of $\mathcal{C}_{ij}$
$\mathcal{C}_{ij}$	One-particle correlation function
$\mathcal{H}$	Hamiltonian
μ_m	Chebyshev moments of order m
σ_ε	Standard deviation of disorder
Υ	Lyapunov exponent
ε	Diagonal random potential
Υ	Disorder induced Spectral width
ξ	Localization length
ζ	Correlation length
C_n	Fluctuations contour
C_s	Entanglement contour
g_m	Jackson kernel
l	Mean free path
$T_n(x)$	Chebyshev polynomials of the 1st kind
$U_n(x)$	Chebyshev polynomials of the 2nd kind
W	Disorder strength
1D	One-dimensional
CMP	Condensed matter physics

DOS Density of states

KPM Kernel polynomial method

LDOS Local density of states

OBC Open boundary conditions

PBC Periodic boundary conditions

QIT Quantum information theory

TBM Tight binding model

Chapter 1

Introduction

1.1 Context

The study of electronic properties of quantum systems is one of the most fundamental problems in Condensed Matter Physics (CMP). The electronic states in a perfectly ordered crystal are translationally invariant with probability amplitudes extending to all lattice sites. Such extended states are described by plane waves (Bloch's theorem) and lead to the metallic nature of the system. However, the situation becomes much more complicated for real systems with electron-electron correlations or/and disorder. The aim of this thesis is to study the electronic properties of non-interacting disordered fermions at zero temperature. More specifically, we study the delocalization mechanism of the quantum systems in the presence of different models of static disorder.

The phenomena of metal-insulator transition (MIT) [8, 9] is one of the important pillars underpinning condensed matter systems. It was Anderson [10], who first proposed the idea of electronic phase transition in a lattice model under certain conditions, the so-called Anderson Transition. He argued that a non-interacting tight-binding system of electrons with uniformly distributed random energies (Anderson disorder) would be localized at the Fermi level if:

- The disorder is strong enough;
- The Fermi energy lies in the region of sufficiently small density of states (at band edges).

The localized wavefunctions typically have an envelope with an exponential tail,

$$\Psi(\vec{r}) = \exp(-\frac{r}{\xi}) \sum_i c_i e^{i\phi_i} \psi_i(\vec{r}_i - \vec{r}_0) \tag{1.1}$$

where ϕ_i are the random phases, ψ_i are the site wavefunctions and $\vec{r}_0$ gives the locations of the state. The parameter ξ quantifies the localization of wavefunctions and is referred as the localization length [11, 12]. It is one of the most fascinating tools used to characterize

the behavior of the disordered system. For an exponentially localized states the localization length is finite and typically smaller than the linear size of system. In contrast, the localization length tends to infinity for extended states.

It is a well established fact that all eigenstates of a one dimensional (1D) system are localized in the presence of infinitesimal Anderson disorder [10]. There is no room for diffusion of electrons [13, 14], since the localization length is of the order of mean free path (the mean distance between two impurities). However, Anderson transition may occur in a non-interacting cubic lattice for a sufficiently large Anderson disorder (critical disorder) at zero temperature ($T = 0$) [15]. Typically electron states in the tails of the disorder-broadened bands can easily be restricted to a finite region of space, where the localization length is much smaller than the system size. In addition, Mott [9], proposed the idea of mobility edge which separate localized and extended states.

Traditionally, much interest has been given to the standard Anderson model, both by rigorous analytical methods [12] and numerical simulations [13, 16]. On the contrary, the role played by space correlations in the disordered potential remains unclear. The early attempts to deal with correlated disorder models [17] did not show any qualitative differences in the physics of the system, other than by changing the specific values of the localization length. The main focus of this work is to fill this gap by studying the behavior of the 1D Anderson model with correlated disorder, in particular, power-law correlated disorder model (de Moura-Lyra model).

There exists a considerable amount of work dedicated to numerical study of the strongly disordered systems. We use a powerful numerical method —Kernel Polynomial Method (KPM)— for our investigations, which in general plays a very prominent role in this research area [18, 19, 20, 21]. It is based the on polynomial expansions of the target function, which yield results of high accuracy with modest computational effort. The Chebyshev polynomials — with good convergence properties of the corresponding series and close relation to Fourier transform [22]— turn out to be a judicious choice of KPM expansion for most applications. It is important to mention that the numerical convergence and accuracy of the KPM estimates can be controlled by the number of polynomial moments and by the choice of an optimal kernel (see section 3.2).

The spectral function plays a fundamental role in illustrating the single particles properties of a interacting and a disordered quantum systems [23, 24]. It describes the energy distribution for a particle in a given momentum state k. In a non-interacting translation invariant system, it is simply a Dirac delta function of energy, peaked at the single particle energy E_k. Typically, the disorder turns the ideal Dirac delta of the spectral function into a broadened profile with a finite width [1, 24]. This broadening of the spectral function can trigger a strong suppression of the peak, as the spectral weight shifts from the center to its tails. Most theoretical work [1, 23, 24] show that the spectral function follows Lorentzian distributions in the perturbative regime for the Anderson model. The width of the Lorentzian reflects the finite lifetime $\tau = \hbar\Gamma^{-1}$, and equivalently, the finite scattering

mean free path l, as given by

$$\boldsymbol{l} \coloneqq v_F \tau = \frac{2t}{\hbar\Gamma}, \qquad E_F = 0. \tag{1.2}$$

The calculation of lifetime relies on the Born approximation

$$\frac{\hbar\Gamma}{t} = \frac{\overline{\varepsilon^2}}{2t^2}. \tag{1.3}$$

where $\overline{\varepsilon^2} = W^2/12$ is the variance of the local disorder potential of strength W. It is worthwhile to mention that the mean free path shows a power-law divergence in the limit of vanishing disorder at the band center [5].

The knowledge of spectral function also plays a crucial role in the de Moura-Lyra model [1] (see also chapter 4 for detail). The spectral function reveals a perturbative Lorentzian like behavior in the limit of Anderson model ($\alpha \to 0$), (α an exponent that characterize the algebraic decay of correlations). For $\alpha = 0$ ones recover the fully localized uncorrelated model, while in the opposite limit ($\alpha \to \infty$) the system becomes ordered and there is a complete delocalization. By varying α we observe a change from a Lorentzian shape to a Gaussian line shape for $\alpha \to 1^+$, that reflects the classical limit. In this limit, the spectral function converge towards the probability distribution of the random potential. In addition, the spectral function turns out to be self-averaging for $\alpha \leq 1$, as its standard deviation decay $1/\sqrt{N}$ with size N of the system at the band center. In the extreme case $\alpha \to \infty$, the correlated disorder system corresponds to a tight-binding model with a cosine potential of wavelength N and the spectral function reveal similar behavior as the density of states in real space. Moreover, a quantum to classical transition has been also experimentally investigated in the framework of one-particle spectral function for a non-interacting ultra-cold atoms in continuous three dimensional laser speckle disordered potentials [25].

The possibility of having a delocalization transition in the 1D de Moura-Lyra class of models has been the object of a long standing discussion in the literature [1, 17, 26, 27] (see also chapter 5 for detail). The first evidence of the delocalization transition could appear in 1D stemmed from the study of self-affine potentials pioneered by [17]. They defined a random potential with a power-spectrum decaying as $k^{-\alpha}$, which is known to occur naturally in the assembly of biological macro molecules, such as DNA [28]. By numerically studying the Lyapunov exponent as a function of α, de Moura and Lyra concluded that an Anderson transition happens at $\alpha = 2$, followed by the emergence of a mobility edge in the spectrum. These results were contested [29] on the basis of the ill-defined thermodynamic limit in these potentials. Eventually, it was understood that the presumed transition is an artifact of the anomalous scaling of the Lyapunov exponent, due to the non-stationarity of the potential for any $\alpha \geq 1$ [29, 30]. However, most recently, we reported the numerical evidences that such a transition happens at $\alpha = 1$, where the localization length is shown

to diverge as $(1-\alpha)^{-1}$ in the thermodynamic limit [27].

The notion of quantum entanglement has been intensively studied for revealing the non-local features of quantum systems [31, 32, 33]. At the fundamental level, it is widely considered as a cornerstone of quantum information theory (QIT) and an essential resource for quantum teleportation, quantum cryptography, and quantum metrology [34]. Nevertheless, it has been also recognized as an inter-disciplinary tool, which combine elements of condensed matter theory, quantum mechanics and information theory. The most peculiar property of entanglement is the characterization of a quantum system relative to a given subsystem. Most theoretical research show that he entanglement entropy of the ground state of a translationally invariant quantum lattice gaped model with local interactions scales with the size of the boundary [35]. However, the entanglement entropy as a function of system size has a logarithmic scaling law in 1D quantum critical systems [36, 37, 38]. Moreover, the entanglement entropy in a 1D critical lattice system in the presence of uniformly distributed on-site disorder satisfies area law for $l \gg \xi$, while it shows logarithmic behavior for $l \ll \xi$, where l is the subsystem size and ξ is the localization length [37, 39].

Recent development in the characterization of entanglement has been introduced by Chen and Vidal [40]: the entanglement contour. These authors have introduced a way to express the entanglement entropy as a sum of contributions associated with each degree of freedom of the subsystem, which satisfies certain consistency conditions that legitimate an interpretation of each term as the contribution of the corresponding degrees of freedom to the total entropy. It thus possible to discuss the spatial distribution of entanglement among the untraced degrees of freedom. The consistency conditions do not entail a unique definition of the entanglement contour, but in case of fermions, there is a very natural and intuitive definition. They came up with a conclusion that the contribution of local states to the total entanglement in a free fermions with translational invariance decays as a power law with the distance to the boundary for the gapless, and as a exponential for gaped systems. It has been investigated that the contribution of local states to the total entanglement in the system decays exponentially with the distance to the boundary for critical Anderson model [41]. In addition, the contour function can be used as a theoretical tool for the characterization of delocalization transition in de Moura-Lyra model.

1.2 Organization of the Thesis

The structure of this thesis is as follows:

In Chapter 2, we briefly introduce the basic concepts of condensed matter physics and quantum information theory, which are relevant to the problems studied in remaining chapters of the thesis. In particular, we consider a one-dimensional non-interacting tight-binding chain of fermions with different models of disorder. We briefly review the quantum information inspired techniques, entanglement entropy and contour function.

In Chapter 3, we discuss an efficient algorithm for the computation of an eigenvector

of the corresponding known eigenvalue of a tridiagonal matrix. This algorithm is known as the Fernando technique [42]. In addition, we employ a polynomial expansion based technique, kernel polynomial method, to calculate the density of states, spectral function and localization length of the system as described in chapter 2. Indeed, we test and confirm the utility of numerical implementations for a full understanding of these problems in the limit of a perfectly clean system.

In Chapter 4, we will employ KPM for the computations of spectral function of Bloch states in an one-dimensional tight-binding non-interacting chain with power-law correlated disorder at zero temperature. We examine the appearance of a classical limit in a single-band lattice system. In addition, we prove the self-averaging behavior of the spectral function for $\alpha \leq 1$.

In Chapter 5, we study the delocalization mechanisms of the de Moura-Lyra model by means of conductance and localization length. We address that the delocalization transition in the model occur at a point where localization length diverge as $(1-\alpha)^{-1}$ in the thermodynamic limit. We numerically calculate the localization length by two different techniques and verify them by comparing with analytical result first obtained explicitly in this work as an application of the generalized Thouless formula [43].

In Chapter 6, we study the entanglement analysis of Anderson model at zero temperature. We review the scaling of entanglement for the model in detail. Moreover, we address the area law of entanglement from the perspective of entanglement contour. In addition, we also investigate the delocalization transition in the de Moura-Lyra model from the perspective of entanglement and entanglement contour.

In Chapter 7, we close this thesis with the conclusions, as well as, a brief discussion on the possible future directions of our work.

Chapter 2

Theoretical Background

In this chapter we briefly introduce the basic concepts that will be needed in the remainder of the thesis. The first part of this chapter is devoted to the theoretical background of the condensed matter systems, related to one-dimensional tight-binding non-interacting chains with different models of static disorder. The second part, we will review the concepts of the quantum information theory. In particular, we will be concerned with the measures of entanglement and entanglement contour in a quantum system.

2.1 Condensed Matter Physics

In this section we will recall certain aspects of condensed matter physics, relevant to the problems addressed in the following chapters.

2.1.1 The Disorder Model

This section is based on [1], introduces a one-dimensional non-interacting disordered electronic system. In particular, we study tight-binding model with nearest neighbor hopping and random site energies. The Hamiltonian of the corresponding system has the following general form [1],

$$\mathcal{H} = -t \sum_{m=0}^{N-1} |\varphi_{m+1}\rangle \langle\varphi_m| + |\varphi_m\rangle \langle\varphi_{m+1}| + \sum_{m=0}^{N-1} \varepsilon_m |\varphi_m\rangle \langle\varphi_m| \tag{2.1}$$

where $\{|\varphi_m\rangle\,;\, m = 0, \ldots, N-1\}$ are the local Wannier states. In what follows, we impose periodic boundary conditions by setting $|\varphi_m\rangle = |\varphi_{m+N}\rangle$ and the lattice parameter a is taken as 1. This model is based on certain simplifications. For instance, the second or third nearest neighbor hopping that might have some contributions in a real system, are considered to be zero. The term ε_m is the on-site random potential at site m.

2.1.1.1 Anderson Model

Anderson Model [10] is a standard model that describes the disorder induced MIT in a non-interacting lattice electronic system. In the model (see Eq. 2.1), the site energies of the lattice are chosen be uncorrelated random variables. The standard choice of their probability distributions is the uniform distribution in the interval $]-W/2, W/2[$. The parameter W is a positive constant describing the strength of disorder. The probability distribution $P(\varepsilon_m)$, of ε_m is

$$P(\varepsilon_m) = \begin{cases} \frac{1}{W}, & |\varepsilon_m| < \frac{W}{2}, \\ 0, & \text{elsewhere.} \end{cases} \tag{2.2}$$

The variance of the random potential is $\sigma_\varepsilon^2 \equiv \overline{\varepsilon^2} = W^2/12$.

2.1.1.2 Correlated Disorder Model

Most of the work on electronic system refers to uncorrelated disorder [5, 14, 15, 24, 44], where all the eigenstates of a non-interacting one-dimensional electronic chain in the presence of infinitesimal disorder are found to be localized. Here, we pay attention to the case in which the site energies are the set of correlated random variables for any arbitrary correlation [1]. We will be concerned with the long-range Gaussian and power-law correlated disorder models from the perspective of spectral function, as studied in [1].

The exact eigenstates of the Hamiltonian (given by Eq. 2.1) in the absence of disorder would be the Bloch states

$$|k\rangle = \frac{1}{\sqrt{N}} \sum_{m=0}^{N-1} e^{ikm} |\varphi_m\rangle , \tag{2.3}$$

The presence of static disorder causes scattering of $|k\rangle \rightarrow |k+q\rangle$, characterized by the matrix elements of the random potential $\mathcal{V} := \sum_m \varepsilon_m |\varphi_m\rangle \langle\varphi_m|$ that connect two Bloch states, *i.e.*,

$$\langle k+q| \mathcal{V} |k\rangle = \frac{1}{N} \sum_m \varepsilon_m e^{-iqm}, \tag{2.4}$$

seen here to depend only on the transferred momentum q[1]. We easily invert Eq. 2.4 to express the local energies as a Fourier sum,

$$\varepsilon_m = \sum_q \langle k+q| \mathcal{V} |k\rangle e^{iqm}, \tag{2.5}$$

We choose to model the randomness by taking these matrix elements as

$$\langle k+q| \mathcal{V} |k\rangle = V(q) e^{i\phi_q}, \tag{2.6}$$

[1] q is in the first Brillouin zone.

where $V(q) := |\langle k+q| \mathcal{V} |k\rangle|$ is a specified even function of q and ϕ_q is a random phase with a uniform probability distribution in the circle $[0, 2\pi[$. The different phases are independent variables except for the constraints $\phi_q = -\phi_{-q}$, which ensure the hermiticity of the Hamiltonian. Using the property $V(q) = V(-q)$, the local energies turns out to be

$$\varepsilon_m = \sum_{q\neq 0} V(q) e^{i\phi_q} e^{iqm}, \tag{2.7}$$

$$= 2\sum_{q>0} V(q)\cos(qm + \phi_q). \tag{2.8}$$

With these definitions, the mean of the site energies is $\overline{\varepsilon_m} = \sum_q V(q)\overline{e^{i\phi_q}} e^{iqm} = V(0)$, since the condition $\phi_q = -\phi_{-q}$ fixes $\phi_0 = 0$ and the individual phase averages are zero, $\overline{e^{i\phi_q}} = \delta_{q,0}$. Since $\overline{\varepsilon_m}$ merely shifts the spectrum, we will always choose $\overline{\varepsilon_m} = 0$, meaning that $V(0) = 0$.

In general, the values of the energies in different sites will be correlated in this model of disorder. The two-site covariance of the potential can be written as

$$\overline{\varepsilon_n \varepsilon_m} = \sum_{q,q'\neq 0} V(q)V(q')\overline{e^{i\phi_{q'}} e^{i\phi_q}} e^{i(qm+q'n)}, \tag{2.9}$$

where all the phase averages factorize unless $q = -q'$, and the average of a single phase is zero,

$$\overline{e^{i\phi_q}} := \delta_{q,0}. \tag{2.10a}$$

$$\overline{e^{i\phi_{q'}} e^{i\phi_q}} := \delta_{q+q',0}. \tag{2.10b}$$

Hence (using the property $V(q) = V(-q)$),

$$\overline{\varepsilon_n \varepsilon_m} = 2\sum_{q>0} V(q)V(-q)\delta_{q+(-q),0}\cos\left(q(n-m)\right),$$

$$= 2\sum_{q>0} V^2(q)\cos\left(q(n-m)\right). \tag{2.11}$$

From Eq. 2.11, we see that $V^2(q)$ can be related to the Fourier transform of the correlation of the disorder potential $\overline{\varepsilon_n \varepsilon_0}$, as follows

$$V^2(q) = \frac{1}{N}\sum_n \overline{\varepsilon_n \varepsilon_0} e^{iqn}. \tag{2.12}$$

In the case of an uncorrelated disorder, the usual Anderson's model, we have

$$\overline{\varepsilon_n \varepsilon_m} = \sigma_\varepsilon^2 \delta_{n,m}, \tag{2.13}$$

with $\sigma_\varepsilon^2 := \overline{\varepsilon^2}$, or, equivalently

$$V^2(q) = \frac{1}{N}\sigma_\varepsilon^2. \tag{2.14}$$

Thus, for uncorrelated site disorder, the magnitude of the scattering matrix element from $k \to k+q$ is independent of the transferred momentum, q .

2.1.1.3 Gaussian Correlated Disorder

Our first model of correlated disorder is the Gaussian case. For that, we choose

$$V(q) := \frac{A(q_c)}{\sqrt{N}} \exp\left(-\frac{q^2}{4q_c^2}\right), \tag{2.15}$$

where $A(q_c)$ is a measure of the strength of disorder. The $N^{-\frac{1}{2}}$ factor in Eq. 2.15 is introduced in order to have a well-defined thermodynamic limit for the local variance and correlation functions of the disorder potential. The parameter q_c is the correlation length that controls the correlation of the random potential. In the limit, $q_c \gg \pi$, one recovers the Anderson model with uncorrelated disorder. As shown in Fig. 2.1, the smaller the q_c the smoother are the random profiles.

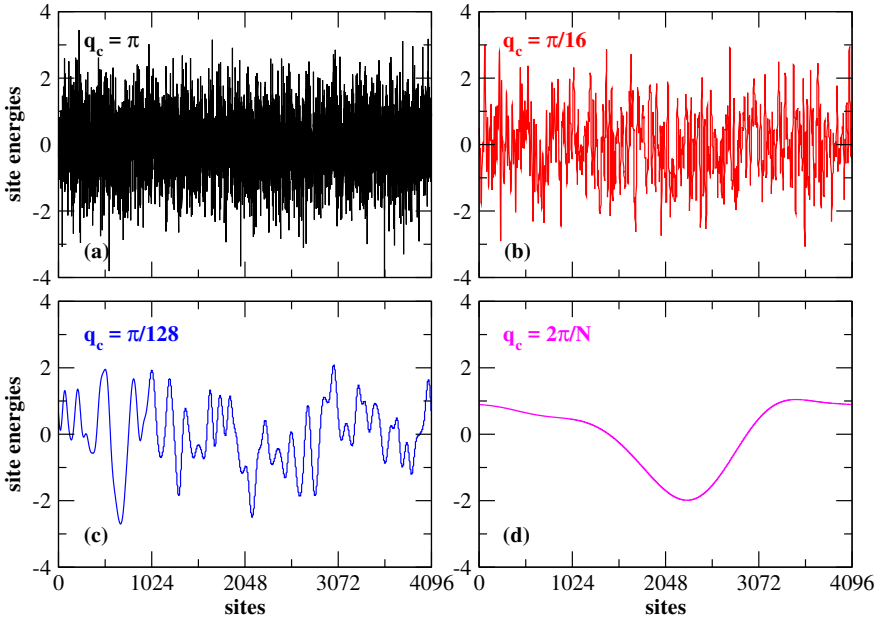

Figure 2.1: Typical normalized on-site energy landscapes for Gaussian correlated disorder with $N = 4096$ for (a) $q_c = \pi$, (b) $q_c = \pi/16$, (c) $q_c = \pi/128$, and (d) $q_c = 2\pi/N$.

In this model, the values of $V(q)$ are only significant in an interval of linear size q_c

around $q = 0$. This means that the disordered potential couples Bloch states with nearby momenta, more strongly[2]. The statistical properties of the corresponding potential can be calculated through Eq. 2.11, in the thermodynamic limit ($N \to \infty$), yielding

$$\overline{\varepsilon_n \varepsilon_m} = A^2(q_c) \int_{-\pi}^{\pi} \frac{dq}{2\pi} e^{-\frac{q^2}{2q_c^2}} e^{iqr_{nm}}, \tag{2.16}$$

where $r_{nm} = (n - m)$. This integral can be solved analytically in the limit of $q_c \ll \pi$. In this case, the integration intervals can be extended to $k \in]-\infty, +\infty[$, i.e.,

$$\overline{\varepsilon_n \varepsilon_m} = A^2(q_c) \int_{-\infty}^{\infty} \frac{dq}{2\pi} e^{-\frac{q^2}{2q_c^2} + iqr_{nm}}, \tag{2.17}$$

$$= A^2(q_c) e^{-\frac{q_c^2 r_{nm}^2}{2}} \int_{-\infty}^{\infty} \frac{dq}{2\pi} e^{-\frac{1}{2q_c^2}\left(q - iq_c^2 r_{nm}\right)^2}, \tag{2.18}$$

$$= A^2(q_c) e^{-\frac{q_c^2 r_{nm}^2}{2}} \frac{q_c}{\sqrt{2\pi}}, \tag{2.19}$$

The variance of the potential is

$$\sigma_\varepsilon^2 := \overline{\varepsilon^2} = A^2(q_c) \int_{-\infty}^{\infty} \frac{dq}{2\pi} e^{-\frac{q^2}{2q_c^2}}, \tag{2.20}$$

$$= A^2(q_c) \frac{q_c}{\sqrt{2\pi}}. \tag{2.21}$$

In this same limit, we can also relate the parameter $A(q_c)$ with the local disorder strength, using Eq. 2.21

$$A^2(q_c) = \sqrt{2\pi} \frac{\sigma_\varepsilon^2}{q_c}. \tag{2.22}$$

meaning that,

$$V(q) = (2\pi)^{\frac{1}{4}} \frac{\sigma_\varepsilon}{\sqrt{q_c N}} \exp\left(-\frac{q^2}{4q_c^2}\right). \tag{2.23}$$

2.1.1.4 Power-law Correlated Disorder

In order to study the influence of long-range correlations of disorder, power-law correlated random potential was proposed [17]. Specifically, the site energies have approximately power-law spectral density $S(k) \propto k^{-\alpha}$, where k is the inverse of the wavelength $k = 1/\lambda$. The function $S(k)$ is the Fourier transform of the two point correlation function of the local potential. The power-law correlated site potential for a periodic chain of N sites is [4, 17]

$$\varepsilon_m = 2A(\alpha) \sum_{p=1}^{N/2} \left(\frac{2\pi}{N}\right)^{\frac{1-\alpha}{2}} \frac{1}{p^{\frac{\alpha}{2}}} \cos\left(\frac{2\pi p}{N} m + \phi_p\right). \tag{2.24}$$

[2]However, this does not mean an absence of back-scattering, since the full effect of this potential must take all the multiple scattering processes into account. As a matter of fact, these disordered potentials with short-range correlations are believed to cause an exponential localization of the eigenstates, in a manner similar to the 1D Anderson model with uncorrelated disorder.

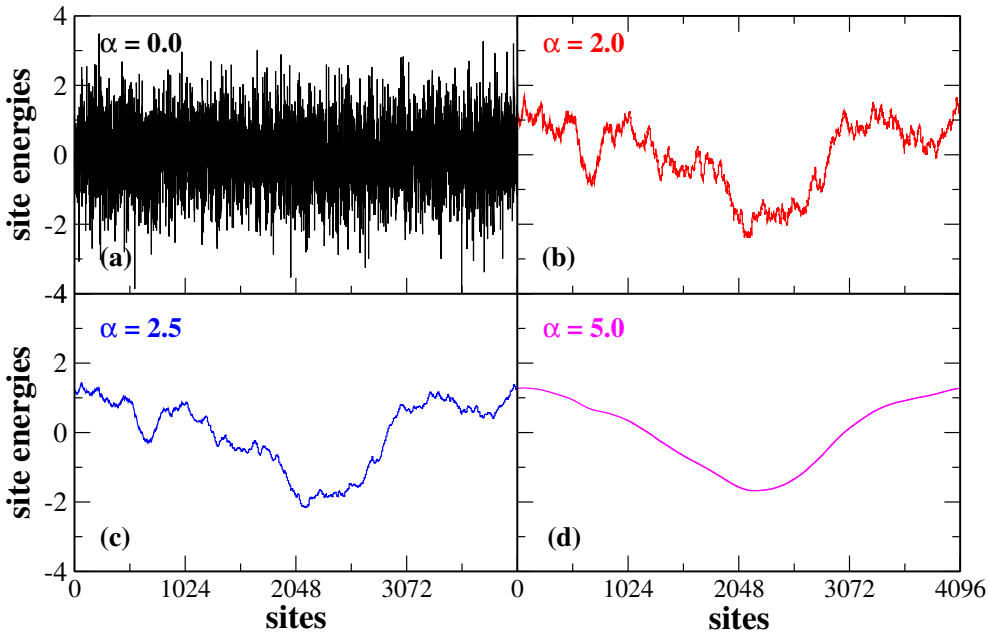

Figure 2.2: Typical normalized on-site energy landscapes with $N = 4096$ for the uncorrelated random sequency ($\alpha = 0$), the trace of a usual Brownian motion ($\alpha = 2$), the trace of a usual Brownian motion with persistent increments ($\alpha = 2.5$), and $\alpha = 5$.

The phases ϕ_p have the same properties as before, being uniformly distributed in $[0, 2\pi[$. The exponent α is called the correlation exponent, and quantifies the degree of correlation imposed in the system. In the limit $\alpha \to \infty$, Eq. 2.1 corresponds to a tight-binding model with a sinusoidal (cosine) potential and one expects extended electronic states due to the effective absence of disorder . For the case when $\alpha = 0$ (white-noise potentials), one recovers the Anderson model with uncorrelated disorder. Thus, the states of the quantum particles are exponentially localized. For $\alpha = 2$, the site energies will have the standard Brownian diffusion. As shown in Fig. 2.2, the larger α the smoother are the random profiles. We can reduce this definition to our formulation by defining the Bloch wave-vector as

$$q := \frac{2\pi}{N} p. \tag{2.25}$$

so that Eq. 2.24 becomes

$$\varepsilon_m = 2A(\alpha) \left(\frac{2\pi}{N}\right)^{\frac{1}{2}} \sum_{q>0} \frac{1}{q^{\alpha/2}} \cos\left(qm + \phi_q\right), \tag{2.26}$$

$$= A(\alpha) \left(\frac{2\pi}{N}\right)^{\frac{1}{2}} \sum_{q\neq 0} \frac{1}{q^{\alpha/2}} e^{i(qm+\phi_q)}. \tag{2.27}$$

Since this sum is only over the positive half of the first Brillouin zone (i.e., $q = 2\pi p/N$, $p = 1, \ldots N/2$), it can be rewritten as

$$\varepsilon_m = \sum_{q \neq 0} V(q) e^{i\phi_q} e^{iqm}, \tag{2.28}$$

with $V(q)$ defined as

$$V(q) = A(\alpha) \left(\frac{2\pi}{N}\right)^{\frac{1}{2}} \frac{1}{|q|^{\frac{\alpha}{2}}}, \tag{2.29}$$

and the independent random phases obeying the constraint $\phi_q = -\phi_{-q}$. The $q = 0$ term is excluded as before, and we have introduced a normalization factor $A(\alpha)$ that will define a finite variance for the local disorder.

2.1.2 Physical Quantities

This section is intended to provide the theoretical background of the physical quantities, that might be needed for the remaining chapters.

2.1.2.1 Density of States

The density of states (DOS) of a quantum system is one of the main observable quantities of interest in solid-state physics. It describes the number of states that are available in a quantum system and is essential for determining the particle concentrations and the energy distributions of particles. The DOS of an $N \times N$ Hamiltonian matrix $\hat{\mathcal{H}}$ with eigenvalues E_α is given by

$$\rho(E) = \frac{1}{N} \sum_{\alpha=0}^{N-1} \delta(E - E_\alpha), \tag{2.30}$$

where α is the set of quantum numbers labelling the eigenstates. In the thermodynamic limit, the DOS of one-dimensional tight-binding chain in first Brillion zone becomes

$$\rho(E) = \frac{1}{2\pi} \int dk \delta(E + 2t \cos k), \tag{2.31}$$

$$= \frac{1}{\pi} \frac{1}{\sqrt{4t^2 - E^2}}. \tag{2.32}$$

The DOS define a continuous distribution of the spectrum of the Hamiltonian in the thermodynamic limit. Moreover, the DOS (Eq. 2.32) is symmetric around the band center and displays Van Hove singularities at the band edges.

2.1.2.2 Local Density of States

Local density of state (LDOS) [44] is the density of states of a quantum system projected at a specific site. We start by defining the spectral matrix correlation, $\rho^{ij}(E)$, at energy

E, with different sites i and j, as given by

$$\rho^{ij}(E) = \frac{1}{N}\sum_{\alpha=0}^{N-1}\langle i|\alpha\rangle\langle\alpha|j\rangle\delta(E-E_\alpha), \tag{2.33}$$

where E_α and $|\alpha\rangle$ are the eigenvalues and eigenstates of the $N\times N$ Hamiltonian matrix $\hat{\mathcal{H}}$, respectively. The LDOS is defined as the spectral matrix correlation at $j=i$,

$$\rho^{ii}(E) \equiv \rho^{i}(E) = \frac{1}{N}\sum_{\alpha=0}^{N-1}|\langle i|\alpha\rangle|^2\,\delta(E-E_\alpha), \tag{2.34}$$

In a pure quantum system, due to the perfect translational symmetry of the lattice, the LDOS at an arbitrary site is the same as the DOS. Hence, the DOS of the tight-binding chain is expressed in terms of the LDOS $\rho^i(E)$, as,

$$\rho(E) = \frac{1}{N}\sum_{i=0}^{N-1}\rho^{i}(E), \tag{2.35}$$

The DOS of a clean 1D tight-binding chain has von Hove singularities at the band edges, which are smoothed out by introducing disorder in the system (see Fig. 3.5).

2.1.2.3 Spectral Function

A single-particle spectral function $\rho(k,E)$, is the key ingredient in the understanding of interacting and of disordered electronic systems. It can be thought of as the energy distribution of a state of momentum k, or the momentum distribution of a state of energy E. For free non-interacting particles, the zero temperature spectral function has the form [23, 24],

$$\rho(k,E) = \sum_{\alpha=0}^{N-1}|\langle k|\alpha\rangle|^2\,\delta(E_k-E_\alpha), \tag{2.36}$$

where $|k\rangle$ is a Bloch state of one electron system. In a non-interacting translationally invariant system it is simply a Dirac Delta function of energy, peaked at the single particle energy E_k. Thus, the probability density of the state k with energy E can only be happen by adding an electron to the state k given by $E=E_k$. In general, introducing interactions (electron-phonon, electron-electron) in the system will change the Dirac delta nature of the spectral function. However, the it may still be a peaked function around the single particle energy E_k. Moreover, the density of states can also be obtained by taking statistical average of the spectral function over energy or momentum distributions. In addition, the spectral function will always be positive and should satisfies the normalization condition

$$\frac{1}{2\pi}\int dk\rho(k,E) = \sum_{\alpha=0}^{N-1}|\langle k|\alpha\rangle|^2 = 1. \tag{2.37}$$

Also notice that, in the absence of disorder $\rho(k, E) = \delta(E - E_k)$, and by summing $\rho(k, E)$ over k, one gets the density of states.

2.1.2.4 Localization Length

The one-particle wave-functions for sufficiently strong disorder strength in macroscopic disordered quantum systems at absolute zero temperature are exponentially localized [12, 45]. In other words, the amplitudes of the one-particle wave-functions are exponentially decaying in space at infinity. For instance, the localized wavefunctions in one dimension can be written as

$$|\Psi(x)| \sim \exp\left(-\kappa\,|x - x_0|\right), \tag{2.38}$$

in the limit $|x - x_0| \to \infty$, where x_0 is the center of localization. The parameter κ is called the inverse localization length, and specifies the localization strength of the wave-functions. The wave-functions is weakly localized (widely spread wave) for a small and strongly localized (narrowly spread wave) for large value of κ.

Many theoretical works have been made for the calculations of localization length for the one-dimensional Anderson model (see Eq. 2.1). Herbert-Jones-Thouless formula [46], relates the localization length[3] $\xi = 1/\kappa$, of a one-dimensional disordered electronic system in terms of the density of states, as given by

$$\frac{1}{\xi(E)} = \int \rho(\epsilon) \ln|E - \epsilon|\,\mathrm{d}\epsilon - \ln|t|\,, \tag{2.39}$$

where $\rho(\epsilon)$ is the density of states at energy ϵ. It is well known that the density of states[4] of the Anderson model varies as $1/W$ [12], for large disorder in the energy limit, $|E| < \frac{1}{2}W$. The localization length in this limit can be obtained as,

$$\frac{1}{\xi(E)} = \frac{1}{W}\int_{-W/2}^{W/2} \ln|E - \epsilon|\,\mathrm{d}\epsilon - \ln|t|\,, \tag{2.40}$$

$$= \frac{1}{2}\ln\frac{W^2 - 4E^2}{4e^2t^2} + \frac{E}{W}\ln\frac{W + 2E}{W - 2E}. \tag{2.41}$$

Eq. 2.41, gives the localization length of the one-dimensional Anderson model in large disorder limit.

Now we focus on the localization length of the Anderson model in small disorder limit. The expression Eq. 2.39, in the thermodynamic limit can be written as (see Eq. 6.10 in Ref. [12]),

$$\frac{1}{\xi(E)} = \mathrm{Re}\int_{-\infty}^{E} \overline{G_{ii}(\epsilon)}\mathrm{d}\epsilon, \tag{2.42}$$

[3] in unit of lattice spacing, a

[4] Density of states is just the probability distributions of the random disorder, ($\rho(\epsilon) = P(\epsilon)$) in the large disorder limit.

This is a basic equation and will be used to calculate the $\xi(E)$ in units of lattice spacing, in the perturbative regime. Using perturbation, the averaged Green's function $\overline{G_{ii}(\epsilon)}$ has the following form:

$$\overline{G_{ii}(\epsilon)} = \sum_x \sum_y G^0_{0x}(\epsilon) G^0_{xy}(\epsilon) G^0_{y0}(\epsilon) \overline{\varepsilon_x \varepsilon_y}, \tag{2.43}$$

The variance of the uniformly distributed random potentials (Anderson model) is

$$\overline{\varepsilon_x \varepsilon_y} \equiv \varepsilon^2 \delta_{xy} = \frac{W^2}{12} \delta_{xy}. \tag{2.44}$$

Substitution of this into Eq. 2.42 gives the localization length as

$$\begin{aligned} \frac{1}{\xi(E)} &= \frac{W^2}{12} \int_{-\infty}^{E} \sum_{xy} G^0_{0x}(\epsilon) G^0_{xy}(\epsilon) G^0_{y0}(\epsilon) \delta_{xy} \mathrm{d}\epsilon, \\ &= \frac{W^2}{12} \int_{-\infty}^{E} \sum_{x} G^0_{0x}(\epsilon) G^0_{xx}(\epsilon) G^0_{x0}(\epsilon) \mathrm{d}\epsilon, \end{aligned} \tag{2.45}$$

The lattice Green's function $G^0_{pq}(\epsilon)$, at energy ϵ has the form

$$G^0_{pq}(\epsilon) = \frac{1}{2\pi} \int_{-\pi}^{\pi} \mathrm{d}k \frac{e^{ik(p-q)}}{\epsilon - 2t\cos k}. \tag{2.46}$$

Inserting in Eq. 2.45 gives the localization length as

$$\frac{1}{\xi(E)} = \frac{W^2}{12} \frac{1}{(2\pi)^3} \int_{-\infty}^{E} \int_{-\pi}^{\pi} \int_{-\pi}^{\pi} \int_{-\pi}^{\pi} \frac{\sum_x e^{ix(k_3-k_1)} \mathrm{d}k_1 \mathrm{d}k_2 \mathrm{d}k_3 \mathrm{d}\epsilon}{(\epsilon - 2t\cos k_1)(\epsilon - 2t\cos k_2)(\epsilon - 2t\cos k_3)}, \tag{2.47}$$

The sum term gives

$$\sum_x e^{ix(k_3-k_1)} = \sum_{x=-\infty}^{\infty} e^{ix(k_3-k_1)} = 2\pi\delta(k_3 - k_1). \tag{2.48}$$

Inserting in Eq. 2.47, we get,

$$\begin{aligned} \frac{1}{\xi(E)} &= \frac{W^2}{12} \frac{1}{(2\pi)^2} \int_{-\infty}^{E} \int_{-\pi}^{\pi} \int_{-\pi}^{\pi} \int_{-\pi}^{\pi} \frac{\delta(k_3 - k_1) \mathrm{d}k_1 \mathrm{d}k_2 \mathrm{d}k_3 \mathrm{d}\epsilon}{(\epsilon - 2t\cos k_1)(\epsilon - 2t\cos k_2)(\epsilon - 2t\cos k_3)}, \\ &= \frac{W^2}{24} \frac{1}{4t^2 - E^2}. \end{aligned} \tag{2.49}$$

This formula allows us to determine the localization distance for known energy spectrum. The localization length shows a power-law divergence in the limit of vanishing disorder.

2.2 Quantum Information Theory Concepts

In this section, we recall basic notions of quantum information theory [34, 47].

2.2.1 State Vector

The state of an isolated quantum system can be represented by a normalized state vector $|\psi\rangle$ in a Hilbert space $\mathscr{H}$. It contains all the possible information about the quantum system. The simplest examples of a two-level quantum system are spin half particle and a two-level atom. The basis states of a two level system are denoted by $|0\rangle$ and $|1\rangle$, and could represent the spin up and spin down for the spin half particle, or the ground and excited state for the two-level atom. The two level system is the basic unit of information in quantum computing, and is called the qubit, which is short for quantum bit.

What is the difference between qubit and ordinary bit.? An ordinary bit (classical bit), the fundamental concept of classical computation and information, may exist either in the state 0 or 1, while a qubit may exist in any linear combination of the states $|0\rangle$ and $|1\rangle$. The superposition state $|\psi\rangle$, can be written as

$$|\psi\rangle = \alpha\,|0\rangle + \beta\,|1\rangle\,, \tag{2.50}$$

where α and β are the complex numbers. According to the laws of quantum mechanics, the modulus squared value of α or β gives the probability of finding the qubit in state $|0\rangle$ or $|1\rangle$, respectively. Mathematically,

$$\begin{aligned} p_0 &= |\langle 0|\psi\rangle|^2 = |\alpha|^2\,. \\ p_1 &= |\langle 1|\psi\rangle|^2 = |\beta|^2\,. \end{aligned} \tag{2.51}$$

where p_0 and p_1 is the probability of the qubit in the state $|0\rangle$ and $|1\rangle$, respectively. The sum of the probabilities of all possible outcomes must be 1, so that the qubit's state (Eq. 2.50) must be normalized.

2.2.2 Density Operator

The concept of density operator [34] is a more general description of a quantum system than the state vector, as it allows the study of the individual subsystems of a composite quantum system, and the description the statistical mixture of the states. A state vector can only describe a pure state, while a density operator can describe both pure and mixed states of a quantum system.

2.2.2.1 Pure and Mixed States

The state of a quantum system can be represented as a linear superposition of basis vectors. Consider a system that is in some known state $|\phi\rangle$, given by

$$|\phi\rangle = \sum_i c_i |i\rangle \tag{2.52}$$

The density operator for the system of state $|\phi\rangle$ can be written as,

$$\begin{aligned}\rho &= |\phi\rangle \langle\phi| , \\ &= \sum_{i,j} c_i c_j^* |i\rangle \langle j| , \\ &= \sum_{i,j} \rho_{ij} |i\rangle \langle j| . \end{aligned} \tag{2.53}$$

where $\rho_{ij} = \langle i | \rho | j \rangle$ are the matrix elements of the density operator. If measurement is made on the system, the diagonal matrix element ρ_{ii} gives the probability of finding the system in state $|i\rangle$, and are called populations. The off-diagonal matrix element $\rho_{ij} = \rho_{ji}^*$ depends on the relative phase c_i and c_j, therefore often called coherence terms.

The density operator for a pure state has the properties [48]:

$$\mathrm{Tr}(\rho) \equiv \sum_i \rho_{ii} = 1, \text{ and } |\rho_{ij}|^2 = |c_i|^2 |c_j|^2 = \rho_{ii}^2 \rho_{jj}^2. \tag{2.54}$$

it follows that

$$\mathrm{Tr}(\rho^2) = 1, \text{ and } \rho^2 = \rho, \tag{2.55}$$

i.e., the density operator for a pure state is idempotent. The density operator for a statistical mixture of the states $|\Psi\rangle$ with respective probabilities p^Ψ can be written as

$$\rho^\Psi = \sum_\Psi p^\Psi |\Psi\rangle \langle\Psi| , \tag{2.56}$$

where the states, $|\Psi\rangle$'s

$$|\Psi\rangle = \sum_i c_i^\Psi |i\rangle \tag{2.57}$$

are required to be normalized to one ($\langle\Psi|\Psi\rangle = 1 \Rightarrow \sum_i \left|c_i^\Psi\right|^2 = 1$), but are not necessarily orthogonal. On inserting Eq. 2.57 into Eq. 2.56, results

$$\rho^\Psi = \sum_\Psi \sum_{ij} p^\Psi c_i^\Psi (c_j^\Psi)^* |i\rangle \langle j| , \tag{2.58}$$

$$= \sum_\Psi \sum_{ij} p^\Psi \rho_{ij}^\Psi |i\rangle \langle j| . \tag{2.59}$$

where $\rho_{ij}^\Psi = c_i^\Psi (c_j^\Psi)^*$ is the density matrix for the state $|\Psi\rangle$ (Eq. 2.57). The trace of the

density operator is

$$\mathrm{Tr}(\rho^{\Psi}) \equiv \sum_i p^{\Psi} \rho_{ii}^{\Psi} = \sum_{\Psi} p^{\Psi} \sum_i \left| c_i^{\Psi} \right|^2 = \sum_{\Psi} p^{\Psi}. \tag{2.60}$$

where $0 \leqslant p^{\Psi} \leqslant 1$ and $\sum_{\Psi} p^{\Psi} = 1$, which is consistent with the interpretation of p^{Ψ}, as the probability for the system to be in the state $|\Psi\rangle$. Under these conditions, we say that the system is in a mixed state. The density operator has the following properties:

- The density operator is Hermitian, $\rho = \rho^{\dagger}$.

- The density operator on a finite dimensional Hilbert space is a positive operator $\rho \geqslant 0$ with trace equal to one. The density operator is positive if and only if all of its eigenvalues are greater than or equal to zero.

- $\mathrm{Tr}(\rho^2) \leqslant 1$, where the equality is verified only for pure state. The density operator for pure states is idempotent, $\rho^2 = \rho$.

2.2.2.2 Expectation Value of an Operator

The mean or average value of an operator with respect to a quantum state is the expectation value of that operator. For an operator $\mathcal{O}$, the expectation value is simply the scalar product of a quantum state $|\phi\rangle$ with the vector $\mathcal{O}|\phi\rangle$ resulting from the action of operator $\mathcal{O}$ on $|\phi\rangle$. Mathematically,

$$\langle \mathcal{O} \rangle = \langle \phi | \mathcal{O} | \phi \rangle . \tag{2.61}$$

When a system is in pure state $|\phi\rangle$ (see Eq. 2.52), then the expectation value of the operator $\mathcal{O}$ is given by

$$\begin{aligned} \langle \mathcal{O} \rangle &= \sum_i \sum_j c_i c_j^* \langle j | \mathcal{O} | i \rangle , \\ &= \sum_i \sum_j \rho_{ij} \mathcal{O}_{ji} = \sum_i (\rho \mathcal{O})_{ii}, \\ &= \mathrm{Tr}(\rho \mathcal{O}) = \mathrm{Tr}(\mathcal{O} \rho). \end{aligned} \tag{2.62}$$

where $\rho_{ij} = c_i c_j^*$ and $\mathcal{O}_{ji} = \langle j | \mathcal{O} | i \rangle$. This shows that for known density matrix, the expectation value of any operator can be calculated by taking the trace of the product of that operator in matrix representation with the density matrix.

The expectation value of $\mathcal{O}$ for the ensemble or mixture of states $|\Psi\rangle$ (see Eq. 2.57),

with respective probabilities p^{Ψ} can be written as

$$\begin{aligned}\langle\mathcal{O}\rangle &= \mathrm{Tr}(\rho^{\Psi}\mathcal{O}),\\ &= \sum_{\Psi}\sum_{ij} p^{\Psi} c_i^{\Psi}(c_j^{\Psi})^{*}\mathcal{O}_{ji},\\ &= \sum_{\Psi}\sum_{ij} p^{\Psi}\rho_{ij}^{\Psi}\mathcal{O}_{ji},\\ &= \sum_{\Psi} p^{\Psi} Tr(\rho_{ij}^{\Psi}\mathcal{O}),\\ &= \sum_{\Psi} p^{\Psi}\left\langle\Psi|\mathcal{O}|\Psi\right\rangle. \end{aligned} \tag{2.63}$$

From Eq. 2.63, it is clear that the expectation value of operator $\mathcal{O}$ is the statistical average of its expectation values $\langle\Psi|\mathcal{O}|\Psi\rangle$ in the pure states $|\Psi\rangle$.

2.2.2.3 Reduced Density Matrix

The density operator is a very useful tool for the characterization of the properties of subsystems in a composite system. A composite system is made up of two or more individual subsystems. The reduced density operator, all that is required to define the properties of the subsystem regardless the size and state (pure or mixed) of the complete system, can be constructed by an operation on density matrix of the total system, called the partial trace.

Let us consider a composite system of $\mathcal{A}$ and $\mathcal{B}$. $\mathscr{H}_{\mathcal{A}}$ is the Hilbert space of system $\mathcal{A}$, with an orthonormal basis $|i_{\mathcal{A}}\rangle$. Similarly $\mathscr{H}_{\mathcal{B}}$ is the Hilbert space of system $\mathcal{B}$, with an orthonormal basis $|j_{\mathcal{B}}\rangle$. Here $i(j) = 0, 1, 2, ...d_{\mathcal{A}} - 1(d_{\mathcal{B}} - 1)$, with $d_{\mathcal{A}}$ and $d_{\mathcal{B}}$ are the dimensions of the Hilbert space of system $\mathcal{A}$ and $\mathcal{B}$ respectively. The Hilbert space of the composite system of dimension $d_{\mathcal{A}}d_{\mathcal{B}}$ is the the tensor product of the two spaces, $\mathscr{H} = \mathscr{H}_{\mathcal{A}}\otimes\mathscr{H}_{\mathcal{B}}$. The state of the composite system is [49],

$$|\Psi_{\mathcal{AB}}\rangle \equiv \sum_{ij} c_{ij}\,|i_{\mathcal{A}}\rangle\,|j_{\mathcal{B}}\rangle = \sum_{ij} c_{ij}\,|i_{\mathcal{A}}j_{\mathcal{B}}\rangle\,, \tag{2.64}$$

with a density matrix

$$\rho_{\mathcal{AB}} = |\Psi_{\mathcal{AB}}\rangle\,\langle\Psi_{\mathcal{AB}}| = \sum_{ijkl} c_{ij}c_{ik}^{*}\,|i_{\mathcal{A}}j_{\mathcal{B}}\rangle\,\langle k_{\mathcal{B}}l_{\mathcal{A}}|\,, \tag{2.65}$$

A reduced density of a subsystem $\mathcal{B}$ can be obtained by taking the partial trace of $\rho_{\mathcal{AB}}$

with respect to system $\mathcal{A}$:

$$\begin{aligned}
\rho_{\mathcal{B}} &= \mathrm{Tr}_{\mathcal{A}}(\rho_{\mathcal{AB}}), \\
&= \sum_{i_{\mathcal{A}}} \langle i_{\mathcal{A}}|\Psi_{\mathcal{AB}}\rangle\langle\Psi_{\mathcal{AB}}|i_{\mathcal{A}}\rangle, \\
&= \sum_{i} c_{ij}c^{*}_{lk}\langle i_{\mathcal{A}}|i_{\mathcal{A}}\rangle \left|j_{\mathcal{B}}\right\rangle \left\langle k_{\mathcal{B}}\right| \langle l_{\mathcal{A}}|i_{\mathcal{A}}\rangle, \\
&= \sum_{i} c_{ij}c^{*}_{ik}\langle i_{\mathcal{A}}|i_{\mathcal{A}}\rangle \left|j_{\mathcal{B}}\right\rangle \left\langle k_{\mathcal{B}}\right| \langle i_{\mathcal{A}}|i_{\mathcal{A}}\rangle, \qquad (2.66) \\
&= \sum_{i} c_{ij}c^{*}_{ik} \left|j_{\mathcal{B}}\right\rangle \left\langle k_{\mathcal{B}}\right|. \qquad (2.67)
\end{aligned}$$

where c^{*}_{ik} is the complex conjugate of c_{ik}. Similarly, we can trace out the degree of freedom of the subsystem $\mathcal{B}$ in order to find reduced density of subsystem $\mathcal{A}$, i.e., $\rho_{\mathcal{A}} = \mathrm{Tr}_{\mathcal{B}}(\rho_{\mathcal{AB}})$.

2.2.3 Schmidt Decomposition

The Schmidt decomposition [34], is a tool characterizing pure states of a composite system in quantum information theory. This decomposition shows that, any pure bipartite state can be decomposed as a superposition of corresponding states. By the singular value decomposition, c_{ij} of the composite quantum system $|\Psi_{\mathcal{AB}}\rangle$ given by Eq. 2.64 can be written by using singular value decomposition, as

$$c_{ij} = (UDV^{\dagger})_{ij}. \qquad (2.68)$$

where $D = \mathrm{diag}(\lambda_1, \lambda_2, \lambda_3, ...\lambda_\chi)$ is a positive diagonal matrix of dimension $\chi \times \chi$, U and V are unitary matrices. χ is the Schmidt rank of the bipartite state and is equal to the number of λ_α in its Schmidt decomposition and satisfies

$$\chi \leq \min(d_{\mathcal{A}}, d_{\mathcal{B}}). \qquad (2.69)$$

The linear combinations of $|i_{\mathcal{A}}\rangle$ with the columns of U and $|j_{\mathcal{A}}\rangle$ with the rows of $V^{\dagger}$ leads to the Schmidt decomposition form of $|\Psi_{\mathcal{AB}}\rangle$, as [34]

$$|\Psi_{\mathcal{AB}}\rangle = \sum_{ij\alpha} U_{i\alpha}D_{\alpha\alpha}V_{\alpha j} \left|i_{\mathcal{A}}\right\rangle \left|j_{\mathcal{B}}\right\rangle, \qquad (2.70)$$

Defining $|\alpha_{\mathcal{A}}\rangle \equiv \sum_i U_{i\alpha} |i_{\mathcal{A}}\rangle$, $|\alpha_{\mathcal{B}}\rangle \equiv \sum_j V_{\alpha j} |j_{\mathcal{B}}\rangle$, and $\lambda_\alpha = D_{\alpha\alpha}$, we get

$$|\Psi_{\mathcal{AB}}\rangle = \sum_{\alpha=0}^{\chi-1} \lambda_\alpha \left|\alpha_{\mathcal{A}}\right\rangle \left|\alpha_{\mathcal{B}}\right\rangle. \qquad (2.71)$$

where $|\alpha_{\mathcal{A}}\rangle$ and $|\alpha_{\mathcal{B}}\rangle$ form an orthonormal basis (Schmidt bases) for the system $\mathcal{A}$ and $\mathcal{B}$, respectively. The expansion coefficients λ_α, also known as Schmidt coefficients, are

non-negative real numbers, $\lambda_\alpha \geq 0$, satisfying $\sum_\alpha \lambda_\alpha^2 = 1$[5]. The density matrix $\rho_\mathcal{A}$ of the system $\mathcal{A}$ can be obtained by employing Eq. 2.67,

$$\rho_\mathcal{A} \equiv \mathrm{Tr}_\mathcal{B}(|\Psi_{\mathcal{AB}}\rangle \langle\Psi_{\mathcal{AB}}|) = \sum_\alpha \lambda_\alpha^2 |\alpha_\mathcal{A}\rangle \langle\alpha_\mathcal{A}| . \tag{2.72}$$

Similarly, the reduced density matrix of the system $\mathcal{B}$, can be found as $\rho_\mathcal{B} = \sum_\alpha \lambda_\alpha^2 |\alpha_\mathcal{B}\rangle \langle\alpha_\mathcal{B}|$. The eigenvalues of $\rho_\mathcal{A}$ and $\rho_\mathcal{B}$ for a pure state of a composite system are identical, so many important properties of the quantum systems of a composite system will be the same for both systems.

The number of non-zero eigenvalues of a matrix is called Schmidt number. This is an important property of a composite quantum system and quantifies entanglement in a system. For instance, the Schmidt number for separable state of a composite quantum system is one, while for entangled state it turns out to be greater than one.

Example 1. A possible state of a composite system $\mathcal{AB}$ is [47],

$$|\Psi_{\mathcal{AB}}\rangle = \frac{1}{\sqrt{2}} (|0\rangle_\mathcal{A} |0\rangle_\mathcal{B} + |0\rangle_\mathcal{A} |1\rangle_\mathcal{B}) . \tag{2.73}$$

The density matrix of the subsystem $\mathcal{A}$ is

$$\rho_\mathcal{A} = \frac{1}{2} |0\rangle \langle 0| . \tag{2.74}$$

The eigenvalues of $\rho_\mathcal{A}$ are $\lambda_1 = 1/2$ and $\lambda_2 = 0$. Since, the Schmidt number is 1, therefore the state of the composite system is separable. Eq. 2.73, can be rewritten as

$$|\Psi_{\mathcal{AB}}\rangle = \frac{1}{\sqrt{2}} |0\rangle_\mathcal{A} (|0\rangle_\mathcal{B} + |1\rangle_\mathcal{B}) . \tag{2.75}$$

which is clearly a separable state.

Example 2. Consider the single state of a composite system $\mathcal{AB}$ is [47],

$$|\Psi_{\mathcal{AB}}\rangle = \frac{1}{\sqrt{2}} (|0\rangle_\mathcal{A} |1\rangle_\mathcal{B} - |1\rangle_\mathcal{A} |0\rangle_\mathcal{B}) . \tag{2.76}$$

The density matrix of the subsystem $\mathcal{A}$, can be found as

$$\rho_\mathcal{A} = \frac{1}{2} |0\rangle \langle 0| + |1\rangle \langle 1| . \tag{2.77}$$

The eigenvalues of $\rho_\mathcal{A}$ are $\lambda_1 = \lambda_2 = 1/2$. Since, the Schmidt number is 2, therefore the state of the composite system is entangled.

[5]By normalizing, $\sum_\alpha \lambda_\alpha^2 = 1$, λ_α are real positions, because one can absorb phases in $|\alpha_\mathcal{A}\rangle |\alpha_\mathcal{B}\rangle$.

2.2.4 The von Neumann Entropy

The von Neumann entropy is the most common way of quantifying the uncertainty in the state of a quantum system. It is the quantum analog of the Shannon entropy, which measures the uncertainty associated with a classical probability distribution. The von Neumann entropy, $S(\rho)$, for a quantum system characterized by the density operator ρ, is defined as

$$S(\rho) = -\mathrm{Tr}\left(\rho \log \rho\right). \tag{2.78}$$

It can be expressed in terms of the eigenvalues, λ_i, of the density matrix, as

$$S(\rho) = -\sum_i \lambda_i \log \lambda_i. \tag{2.79}$$

Here, we use $0 \log 0 \equiv 0$, as defined for the Shannon entropy[6]. The von Neumann entropy has the following basic properties [34], which play a fundamental role in quantum information theory.

- From the Schmidt decomposition, if the eigenvalues of the reduced density operator of system $\mathcal{A}$ and system $\mathcal{B}$ are the same, then $S_{\mathcal{A}} = S_{\mathcal{B}}$.

- The von Neumann entropy is non-negative, and vanishes $S(\rho) = 0$, if and only if the system is in a pure state.

- For a completely mixed state $\rho = I/N$, (I is an $N \times N$ identity matrix), the von Neumann entropy attains its maximum value, as given by

  $$S(\rho) = \log N \tag{2.80}$$

  where N is the dimension of the corresponding Hilbert space.

- The von Neumann entropy of the tensor product of $\mathcal{A} \otimes \mathcal{B}$ is the sum of the entropies of system $\mathcal{A}$ and system $\mathcal{B}$,

  $$S(\mathcal{A} \otimes \mathcal{B}) = S(\mathcal{A}) + S(\mathcal{B}). \tag{2.81}$$

- The von Neumann entropy of the density matrix ρ_i with probability p_i has the property,

  $$S(\sum_i p_i \rho_i) = H(p_i) + \sum_i p_i S(\rho_i). \tag{2.82}$$

  where $H(p_i) \equiv -\sum_i p_i \log(p_i)$ is the Shannon entropy of the set of probability p_i.

[6] Intuitively, an event with zero probability should not contribute to the entropy, so by convention we agree that the Shannon entropy $0 \log 0 \equiv 0$. More formally, note that $\lim_{x \to 0} x \log x \equiv 0$, which provides further support for our convention.

2.2.5 Quantum Entanglement

A pure composite quantum system has zero uncertainty, but the state of one of the subsystems (determined by a reduced density operator) may have finite von Neumann entropy, associated with the uncertainty of the subsystem. This von Neumann entropy is the entanglement entropy of the two subsystem.

The von Neumann entropy [34] is favored unique measure of entanglement of subsystems, and has been commonly used to characterize the entanglement properties of a quantum lattice models in condensed matter physics [32].

2.2.5.1 Entanglement Entropy

The entanglement entropy for a pure state $|\Psi\rangle \in \mathscr{H}_{\mathcal{A}} \otimes \mathscr{H}_{\mathcal{B}}$ is the von Neumann entropy of the reduced density matrix of each part of the system. The entanglement entropy, $S_{\mathcal{A}}$, of the subsystem $\mathcal{A}$ can be written as

$$S_{\mathcal{A}} = -\mathrm{Tr}_{\mathcal{A}} \left(\rho_{\mathcal{A}} \log \rho_{\mathcal{A}} \right). \tag{2.83}$$

where $\rho_{\mathcal{A}}$ is the reduced density operator of the system $\mathcal{A}$, obtained by taking the partial trace of the total density operator ρ with respect to system $\mathcal{B}$ (see Eq. 2.67). If λ_α are the eigenvalues of the reduced density matrix $\rho_{\mathcal{A}}$, then entanglement entropy can be computed as

$$S_{\mathcal{A}} = -\sum_{\alpha} \lambda_\alpha \log \lambda_\alpha. \tag{2.84}$$

The entanglement entropy of the system $\mathcal{A}$, can easily be obtained, zero for the separable state as given by Eq. 2.73, and $\log 2$ for the entangled state, (see Eq. 2.76).

2.2.6 Entanglement in free Fermions

We turn our attention to the study of the ground state bipartite entanglement entropy for a non-interacting Fermionic system. For non-interacting case, the ground state of the lattice sites can be describe by a Slater determinant. Let $|\Psi\rangle$ be the ground state of the system, then the higher order correlation function can be expressed in terms of one-particle correlation function [50],

$$\left\langle \hat{c}_k^\dagger c_l^\dagger \hat{c}_m \hat{c}_n \right\rangle = \left\langle \hat{c}_k^\dagger \hat{c}_n \right\rangle \left\langle \hat{c}_l^\dagger \hat{c}_m \right\rangle - \left\langle \hat{c}_k^\dagger \hat{c}_m \right\rangle \left\langle \hat{c}_l^\dagger \hat{c}_n \right\rangle. \tag{2.85}$$

where the two-point one-particle correlation function $\mathcal{C}_{ij}$ can be describe as

$$\mathcal{C}_{ij} = \left\langle \Psi | \hat{c}_j^\dagger \hat{c}_i | \Psi \right\rangle.$$

with $\hat{c}_i^\dagger (\hat{c}_i)$ are the creation (annihilation) Fermionic operator of site i, obeying anti-commutation relations. The two-point correlation function can also be computed by using

the density matrix ρ as [50]

$$\mathcal{C}_{ij} = \mathrm{Tr}[\rho \hat{c}_j^\dagger \hat{c}_i]. \tag{2.86}$$

The ground state correlation function of the free Fermionic chain at half filling in the asymptotic limit is given by [51]

$$\mathcal{C}_{ij} = \frac{1}{2\pi} \int_{-\frac{\pi}{2}}^{\frac{\pi}{2}} dq e^{-iq(i-j)}, \tag{2.87}$$

$$= \frac{1}{\pi(i-j)} \sin(\frac{\pi\,(i-j)}{2}). \tag{2.88}$$

If Eq. 2.85 (Wick's theorem), holds for a subsystem $\mathcal{A}$ of size $L_\mathcal{A}$, then the reduced density matrix $\rho_\mathcal{A}$ of the corresponding subsystem can be expressed as the exponential of a free fermions operator [50]

$$\rho_\mathcal{A} = \mathscr{F}^{-1} \exp[-\mathfrak{H}], \tag{2.89}$$

where $\mathscr{F}$ is the normalization constant satisfying

$$\mathrm{Tr}(\rho_\mathcal{A}) = 1 \rightarrow \mathscr{F} = \mathrm{Tr}[\exp[-\mathfrak{H}]], \tag{2.90}$$

and $\mathfrak{H}$ is the entanglement Hamiltonian of the subsystem $\mathcal{A}$, and expressed as

$$\mathfrak{H} = \sum_{ij}^{L_\mathcal{A}} H_{ij} \hat{c}_i^\dagger \hat{c}_j, \tag{2.91}$$

Let $\psi_k(i)$ be the eigenvectors of H with eigenvalues E_k. Then the transformation of $\hat{c}_i = \sum_k \psi_k(i) a_k$, will diagonalize the Hamiltonian $\mathfrak{H}$, and the reduced density matrix becomes

$$\rho_\mathcal{A} = \mathscr{F}^{-1} \exp[-\sum_k E_k\ \hat{a}_k^\dagger \hat{a}_k], \tag{2.92}$$

The normalization constant can be calculated as

$$\begin{aligned} \mathscr{F} &= \mathrm{Tr}[\exp[-\sum_k E_k\ \hat{a}_k^\dagger \hat{a}_k]], \\ &= \prod_k (1 + e^{-E_k}). \end{aligned} \tag{2.93}$$

The entanglement entropy (see Eq. 2.78) of the subsystem $\mathcal{A}$ becomes

$$S(\rho_\mathcal{A}) = -\mathrm{Tr}\left(\rho_\mathcal{A} \log \rho_\mathcal{A}\right), \tag{2.94}$$

$$= -\sum_k (\frac{e^{-E_k}}{1+e^{-E_k}}) \log(\frac{e^{-E_k}}{1+e^{-E_k}}) + (\frac{1}{1+e^{-E_k}}) \log(\frac{1}{1+e^{-E_k}}), \tag{2.95}$$

$$= -\sum_k (\frac{1}{1+e^{E_k}}) \log(\frac{1}{1+e^{E_k}}) + (1 - \frac{1}{1+e^{E_k}}) \log(1 - \frac{1}{1+e^{E_k}}). \tag{2.96}$$

The correlation function of the subsystem is

$$\mathcal{C}_{ij} = \sum_k \psi_k^\star(i)\psi_k(j)\frac{1}{e^{E_k}+1}, \tag{2.97}$$

On other hand, H has the representations

$$H_{ij} = \sum_k \psi_k^\star(j)\psi_k(i)E_k, \tag{2.98}$$

In matrix form, the correlation function and the Hamiltonian H can be written as

$$\mathcal{C} = \hat{\psi}^\dagger.\frac{1}{\exp[E_k]+1}.\hat{\psi}. \tag{2.99}$$

$$H = \hat{\psi}^\dagger.[E_k].\hat{\psi}. \tag{2.100}$$

where $[E_k]$ denotes the diagonal matrix with diagonal elements E_k and $\hat{\psi}$ is the matrix formed by $\psi_k(i)$. The eigenvalues of correlation matrix $\mathcal{C}(\lambda_k)$ and Hamiltonian H (E_k) are related by [50]

$$\lambda_k = \frac{1}{e^{E_k}+1}. \tag{2.101}$$

The entanglement entropy (see Eq. 2.96) in terms of the eigenvalues of the correlation matrix can be computed as

$$S_\mathcal{A} = -\sum_{k=1}^{L_\mathcal{A}} \lambda_k \log(\lambda_k) + (1-\lambda_k)\log(1-\lambda_k). \tag{2.102}$$

The expression Eq. 2.102, gives the entanglement entropy of the Fermionic chain, and has been vigorously studied for the disordered system [5, 26, 36].

2.2.7 Entanglement Contour

In order to examine the spatial distribution of entanglement entropy, Chen and Vidal [40] introduced the concept of entanglement contour (EC) in the context of Fermionic quadratic systems. It is found that the entanglement contour $C_s(l,\, L)$, for a lattice site of state $|\phi_l\rangle$, of sub-region $\mathcal{A}$ can be obtained as

$$C_s(l,\, L) = \sum_k |\langle\phi_l|\psi_k\rangle|^2 \, S_\mathcal{A}(\lambda_k). \tag{2.103}$$

where $\lambda_k \in [0,\, 1]$, and $|\psi_k\rangle$ are the eigenvalues and the eigenstates of the correlation matrix. The function, $S_\mathcal{A}(\lambda_k)$,

$$S_\mathcal{A}(\lambda_k) = -\lambda_k \log\lambda_k - (1-\lambda_k)\log(1-\lambda_k). \tag{2.104}$$

is the local entanglement entropy of the sub-region $\mathcal{A}$.

Chapter 3

Computational Techniques

In this chapter we introduce a variety of numerical methods for studying non-interactive electronic systems with disorder and illustrate them with some examples. We will briefly describe the exact diagonalization scheme for the eigenvalue problem. In addition, we will discuss a most efficient algorithm [42] for the computations of an eigenvector of the corresponding known eigenvalue of a tridiagonal matrix.

We will discuss the computational details and applications of the Kernel Polynomial Method (KPM). In particular, we will study the KPM simulations of various physical observables in the context of tight-binding model in the presence of diagonal disorder. As guidance examples, we will compute the density of states, spectral function, and localization length for a one-dimensional non-interacting Anderson model at zero temperature. For the localization length, we employ the kernel polynomial approximation of Thouless formula [12, 46], which expresses the localization length in terms of density of states. We find an excellent agreement with the perturbative result in the large system limit, confirming the validity of the kernel polynomial procedure.

At the end of this chapter, we review Landauer formalism for the calculation of conductance in one-dimensional systems. It is a very useful tool to obtain localization length of the disordered system in chapter 5.

3.1 Exact Diagonalization Method

The eigenvalue problem (exact diagonalization method) [52] is one of the most basic and fascinating problem of the numerical analysis and has a central importance in understanding various physical quantities —density of states, inverse participation ratio, and entanglement entropy, etc— in condensed matter physics. The essentials of the method are based on the solution of the set of homogeneous equations

$$(\mathcal{T} - \lambda I)z = 0, \tag{3.1}$$

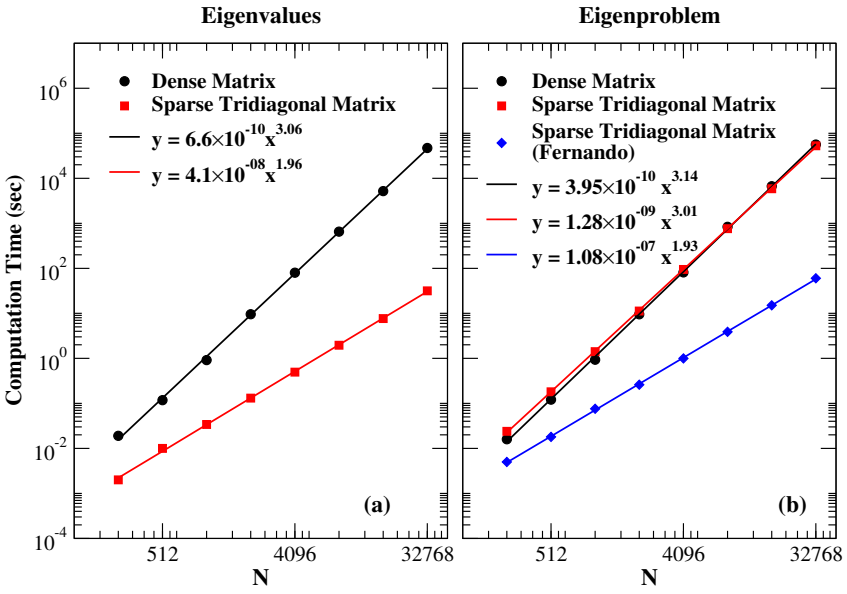

Figure 3.1: Execution time (sec) as a function of size for a one-dimensional lattice system with open boundary condition. The lines are the corresponding fit of the data.

where z are the eigenvectors and λ are the eigenvalues of a square $N \times N$ matrix $\mathcal{T}$, I is the order N identity matrix. The general theory of simultaneous algebraic linear equations suggests a non-trivial solution of Eq. 3.1 for the singular matrix $\mathcal{T} - \lambda I$, if

$$\det(\mathcal{T} - \lambda I)z = 0. \tag{3.2}$$

This determinant can be expanded in characteristic equation of the $\mathcal{T}$, as

$$a_0 + a_1\lambda + ... + a_{N-1}\lambda^{N-1} + a_N\lambda^N = 0 \tag{3.3}$$

In general, Eq. 3.3 has N roots, which may or may not be complex, even if the matrix is real. The roots are called eigenvalues or characteristic values of the matrix $\mathcal{T}$. The set of Eq. 3.1 has at least one non-trivial solution for any eigenvalue, called the eigenvector or the characteristic vector of that eigenvalue.

We will briefly discuss the cost of computations of solving a dense symmetric eigenproblem. The cost of solving a dense symmetric matrix require $\mathcal{O}(N^3)$ operations [52], where N is the order of the matrix. Thus, a straightforward diagonalization scheme for the eigenproblem is limited to small systems.

Throughout the work presented in this thesis we are concerned with non-interacting tight-binding models with nearest neighbor interactions. Fortunately, the Hamiltonian of

the system turns out to be a symmetric tridiagonal sparse matrix. Thus, we can take advantage of the sparse structure of the Hamiltonian matrix by using less memory (without storing the zeros of the matrix), and can perform standard matrix computations economically.

A detailed comparison of numerical complexity of the diagonalization scheme for computing eigenvalues and eigenproblem is depicted in Fig. 3.1. One can see that, the numerical complexity of the dense Hamiltonian matrix for the computation of eigenvalues and eigenproblem (eigenvalues and the associated eigenvectors) is $\mathcal{O}(N^3)$. However, the computational cost for the eigenvalues of a symmetric tridiagonal sparse Hamiltonian matrix is $\mathcal{O}(N^2)$. It is worthwhile to mention that a built-in function with *Eigen library*[1] in C++ has been used for computing the eigenvalues of the symmetric tridiagonal sparse Hamiltonian matrix, i.e.,

```
Eigen::SelfAdjointEigenSolver<Eigen::MatrixXd> Matrix;
Matrix.computeFromTridiagonal(diag , subdiag, Eigen::EigenvaluesOnly);
```

Here, diag and subdiag are the diagonal and subdiagonal entries in a one-dimensional array of N and $N-1$ values, respectively. This is a very fast operation as it uses less storage space. This technique is more appropriate for the computations of eigenvalues only, which has $\mathcal{O}(N^2)$ numerical cost as shown in Fig. 3.1.a. However, the computational cost for the full eigenproblem turns out to be $\mathcal{O}(N^3)$ for a symmetric sparse tridiagonal matrix [2].

To solve the eigenproblem of the symmetric tridiagonal sparse Hamiltonian matrix with controlled computational cost, we discuss an algorithm [42] for the solution of the eigenproblem of a symmetric tridiagonal sparse matrices. The main concern of this algorithm is to compute an accurate eigenvector of the corresponding approximated eigenvalue of the matrix.

Since, the systems of linear equations (Eq. 3.1), are under-determined (see Eq. 3.2), therefore at least one equation is redundant. By putting $z_k = 1$, for the kth redundant equation, one can compute all other components of z. However, the accuracy of the eigenvector depends on the choice of the redundant equations of a tridiagonal matrix [52]. More precisely, an accurate eigenvector can be computed by eliminating high redundant equations. Dropping less redundant equations can lead to a disastrous results. This fact can be explained by considering an order 2 matrix F [42, 52],

$$F = \begin{bmatrix} 0.713263 & 0.000984 \\ 0.000984 & 0.121665 \end{bmatrix}, \quad \lambda_1 = 0.71326463, \quad \lambda_2 = 0.12166336. \tag{3.4}$$

where λ_1 and λ_2 are the eigenvalues of F. Let $\lambda \approx 0.713265$ with an approximate error

[1] https://eigen.tuxfamily.org/dox/index.html

[2] The *Eigen library* uses a symmetric QR algorithm [53] for the solution of eigenproblem of a symmetric matrix. Hence, the computational cost for the eigenproblem turned $\mathcal{O}(N^3)$ for a symmetric sparse tridiagonal matrix.

0.36×10^{-6}; eliminating the second equation of the homogeneous system $(F - \lambda I)z = 0$, Wilkinson obtained the following eigenvector

$$z^t = \begin{bmatrix} 1 & 0.002033 \end{bmatrix}. \tag{3.5}$$

Similarly dropping the first equation, he obtained the following eigenvector

$$z^t = \begin{bmatrix} 1 & 0.00166329 \end{bmatrix}. \tag{3.6}$$

The eigenvector given by Eq. 3.5 is accurate only to 3 decimal places while the eigenvector Eq. 3.6 is accurate to 8 decimal places (Mathematica[3] gives $z^t = [\ 1 \quad 0.00166328\ ]$).

In order to get some intuition of the algorithm developed by Fernando [42], based on choosing an optimal number k such that $z_k = 1$, and to compute all other components of z, we consider a tridiagonal matrix $\mathcal{T}$,

$$\mathcal{T} = \begin{bmatrix} a_1 & b_1 & & & \\ c_1 & a_2 & b_2 & & \\ & . & . & . & \\ & & c_{N-2} & a_{N-1} & b_{N-1} \\ & & & c_{N-1} & a_N \end{bmatrix}, \tag{3.7}$$

The tridiagonal matrix $\mathcal{T}$[4] is unreduced, in the sense that all off-diagonal elements are non-zero. The LDU factorization of the $\mathcal{T} - \lambda I$ is computed as

$$\mathcal{T} - \lambda I = LDU, \tag{3.8}$$

$$= \begin{bmatrix} 1 & & & \\ l_1^+ & 1 & & \\ & . & . & . \\ & & & 1 \\ & & l_{N-1}^+ & 1 \end{bmatrix} \begin{bmatrix} d_1 & & & & \\ & d_2 & & & \\ & & . & . & \\ & & & d_{N-1} & \\ & & & & d_N \end{bmatrix} \begin{bmatrix} 1 & u_1^+ & & & \\ & 1 & & & \\ & & . & . & \\ & & & 1 & u_{N-1}^+ \\ & & & & 1 \end{bmatrix}, \tag{3.9}$$

where the pivots d_n are given by

$$d_1(\lambda) = a_1 - \lambda. \tag{3.10a}$$

$$d_i(\lambda) = a_i - \lambda - c_{i-1}u_{i-1}^+, \qquad i = 2, 3, ..., N. \tag{3.10b}$$

$$u_i^+ = b_i/d_i, \qquad \text{and} \qquad l_i^+ = c_i/d_i. \tag{3.10c}$$

[3] Exact diagonalization of F using mathematica.
[4] The empty entries of the matrix has zeroes.

In similar way, the UDL factorization is formulated as

$$\mathcal{T} - \lambda I = UDL, \tag{3.11}$$

$$= \begin{bmatrix} 1 & u_1^- & & & \\ & 1 & u_2^- & & \\ & . & . & . & \\ & & & 1 & u_{N-1}^- \\ & & & & 1 \end{bmatrix} \begin{bmatrix} \delta_1 & & & & \\ & \delta_2 & & & \\ & & . & . & . \\ & & & \delta_{N-1} & \\ & & & & \delta_N \end{bmatrix} \begin{bmatrix} 1 & & & & \\ l_1^- & 1 & & & \\ & . & . & . & \\ & & & 1 & \\ & & & l_{N-1}^- & 1 \end{bmatrix}, \tag{3.12}$$

where the pivots $\delta_i(\lambda)$ are computed recursively as

$$\delta_N(\lambda) = a_N - \lambda, \tag{3.13a}$$

$$\delta_i(\lambda) = a_i - \lambda - b_i l_i^+; \qquad i = N-1, ..., 2, 1, \tag{3.13b}$$

$$u_i^- = b_i/\delta_{i+1}; \qquad \text{and} \qquad l_i^- = c_i/\delta_{i+1}. \tag{3.13c}$$

For LDU and UDL factorization of $(\mathcal{T} - \lambda I)$, the pivots should not be zero,

$$d_i(\lambda) \neq 0, \qquad \text{for} \qquad i = 1, 2, ...N-1.$$
$$\delta_i(\lambda) \neq 0, \qquad \text{for} \qquad i = N, N-1..., 2.$$

In practice, Eq. 3.1 will only be satisfied for an exact eigenvalue of $\mathcal{T}$, however, λ is the approximate eigenvalue of $\mathcal{T}$ with rounding errors. Thus, for an approximate eigenvalue Eq. 3.1 will have the form

$$(\mathcal{T} - \lambda I)\, z_k = \mu_k e_k. \tag{3.14}$$

with residual μ_k, and e_k unit vector. There are two ways to compute μ_k [42],

$$\mu_{k+1} = \frac{\mu_k \delta_{k+1}}{d_k}; \qquad k = 1, 2, ...N-1; \qquad \text{with} \qquad \mu_1 = \delta_1. \tag{3.15}$$

and

$$\mu_k = \frac{\mu_{k+1} d_k}{\delta_{k+1}}; \qquad k = N-1, ..., 2, 1; \qquad \text{with} \qquad \mu_N = d_N. \tag{3.16}$$

It was Fernando [42] who proposed a more effective way of computing a highly accurate components of eigenvector z by choosing a number $k^{'}$ that gives minimum residual value.

$$k^{'} = \min\left(\mu_k\right), \qquad k = 1, ...N. \tag{3.17}$$

A remarkable fact is that a very small $\min|\mu_k|$ reflects a good approximate eigenvalue of $\mathcal{T}$. Thus, on eliminating $k^{'}th$ equation and putting $z_{k'} = 1$, one compute all other components

of z by using the following equations

$$z_j = -\frac{b_i}{d_i} z_{j+1}, \qquad j = k^{'} - 1, ..., 1. \tag{3.18}$$

and

$$z_j = -\frac{c_{i-1}}{\delta_i} z_{j-1}, \qquad j = k^{'} + 1, ..., N. \tag{3.19}$$

This algorithm substantially improves the arithmetic complexity of the eigen decomposition of the sparse tridiagonal matrix from $\mathcal{O}(N^{3.06})$ to $\mathcal{O}(N^2)$, as illustrated in Fig. 3.1(b). Thus, we can compute the eigenproblem based quantities, such as local density of states, and inverse participation ratio etc., with a controllable computational cost.

3.2 The Kernel Polynomial Method

The Kernel Polynomial Method (KPM) [18, 19, 20] has played a significant role in the fields of condensed matter systems for simulating quantum systems. This is a very efficient algorithm that can evaluate various physical quantities, such as DOS without diagonalizing the Hamiltonian of the system. It is a polynomial expansion-based technique with a controlled accuracy and convergence. A scalar product between two integrable functions $f, g : [a, b] \to \mathbb{R}$ can be defined as

$$\langle f|g\rangle = \int_a^b w(x) f(x) g(x) \mathrm{d}x, \tag{3.20}$$

where $w(x)$ is a positive weight function defined on the interval $[a, b]$. In addition, there exist a complete set of polynomials $p_m(x)$, which satisfy the orthogonality conditions

$$\langle p_m|p_n\rangle = \frac{1}{h_m}\delta_{m,n}. \tag{3.21}$$

where $h_m = 1/\langle p_m|p_m\rangle$ is the inverse of the squared norm of p_m. These orthogonality relations allow us to expand a piece-wise smooth function $f(x)$ in terms of a complete set of orthogonal polynomials $p_m(x)$,

$$f_{KPM}(x) = \sum_{m=0}^{\infty} \alpha_m p_m(x); \qquad x \in [-1,\, 1], \tag{3.22}$$

where $f_{KPM}(x)$ is the KPM estimate of the function $f(x)$. The expansion coefficients α_m are obtained by taking the inner products of $f(x)$ with polynomial p_n

$$\alpha_m = \langle p_m|f\rangle h_m. \tag{3.23}$$

Any type of orthogonal polynomials can be used for the kernel polynomial approach. However, the Chebyshev polynomials take a significant position for most applications in com-

putational condensed matter physics, because they have optimal convergence properties and a close relation to the Fourier transform.

There are several kinds of Chebyshev polynomials. We shall use the first, $T_m(x)$, and second kind, $U_m(x)$, polynomials. These polynomials are defined on the interval $[-1, 1]$. The Chebyshev polynomial of the first kind is a polynomial in x of degree m, defined by the relation [22],

$$T_m(x) = \cos\left(m \arccos(x)\right); \qquad m \in \mathbb{N}. \tag{3.24}$$

More generally we may define Chebyshev polynomials appropriate to any given finite range $[a, b]$ of x by suitable re-scaling. The Chebyshev polynomials $T_m(x)$ satisfy the following three-term recurrence relation [22],

$$T_m(x) = 2xT_{m-1}(x) - T_{m-2}(x); \qquad m > 1. \tag{3.25}$$

starting with $T_0(x) = 1$ and $T_1(x) = x$. Thus using Eq 3.25, we can recursively generate all the polynomials very efficiently. Depending on the degree m, the Chebyshev polynomials $T_m(x)$ is an even or odd function. Furthermore, the Chebyshev polynomial of first kind has the following special property [22],

$$T_m(T_n(x)) = T_{mn}(x). \tag{3.26}$$

In addition, the weight function of the first kind of Chebyshev polynomial $w_T(x)$, is

$$w_T(x) = \frac{1}{\pi\sqrt{1-x^2}}. \tag{3.27}$$

The second kind of Chebyshev polynomial $U_n(x)$, is a polynomial in x of degree n, defined by

$$U_m(x) = \frac{\sin\left((m+1)\arccos(x)\right)}{\sin\left(\arccos(x)\right)}, \qquad m \in \mathbb{N}. \tag{3.28}$$

with a weight function $(w_U(x))$, as given by

$$w_U(x) = \pi\sqrt{1-x^2}. \tag{3.29}$$

and satisfies the recurrence relation

$$U_m(x) = 2xU_{m-1}(x) - U_{m-2}(x), \qquad m > 1. \tag{3.30}$$

which together with the initial conditions

$$U_0(x) = 1, \text{ and } U_1(x) = 2x,$$

provides an efficient procedure for generating the polynomials. The relation between the

Chebyshev polynomials of the first and second kinds is

$$U_m(x) - U_{m-2}(x) = 2T_m(x). \tag{3.31}$$

The Chebyshev polynomials are a complete set of mutually orthogonal functions and satisfy the following orthogonality relations [22],

$$\int_{-1}^{1} w_T(x)T_m(x)T_n(x)\mathrm{d}x = \frac{1}{2}\delta_{mn}(\delta_{m0}+1). \tag{3.32}$$

Thus, the expression Eq. 3.22, in terms of Chebyshev polynomial of the first kind can be written as

$$f_{KPM}(x) = \mu_0 + 2\sum_{m=1}^{\infty}\mu_m T_m(x), \tag{3.33}$$

with coefficients, μ_m,

$$\mu_m = \langle f|T_m\rangle = \int_{-1}^{1} w_T(x)f(x)T_m(x)\mathrm{d}x. \tag{3.34}$$

Eqs. 3.33 and 3.34 are the general basis for the polynomial expansion. In the next section we will explain the truncated polynomial expansions of Eqs. 3.33, and the convergence of the approximation.

3.2.1 Truncated Expansions of a Function

In practical numerical calculation, the KPM simulations of a function can only be evaluated for a finite Chebyshev series. For this purpose, one needs to truncate the infinite Chebyshev polynomial series. In the truncated form, Eq. 3.33 can be written as

$$f_{KPM}(x) = \mu_0 + 2\sum_{m=1}^{M-1}\mu_m T_m(x), \tag{3.35}$$

where M is the number of polynomial series. However, this truncation results in some unwanted oscillations (Gibbs oscillations) near points where the function is not continuously differentiable. The situation is even worse for discontinuities or singularities of a function, for instance, rectangular function, or Dirac delta function, as depicted in Fig. 3.2 and 3.3, respectively.

It turns out that the Gibbs oscillations can be filtered out by modifying the moments, i.e., $\mu_m \to \mu_m g_m$, where g_m is the Gibbs damping factor. Thus, the accuracy and the quality of Chebyshev series expansions of a function can be improved by using an appropriate damping factor.

The accuracy and numerical convergence of the KPM estimates can be controlled by increasing the number of Chebyshev polynomial moments and using an appropriate Gibbs

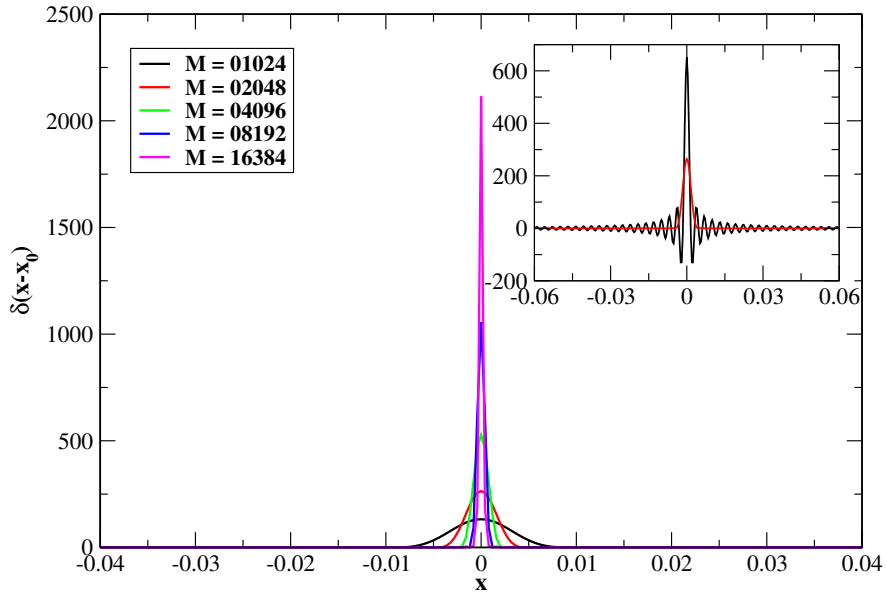

Figure 3.2: The KPM estimates of Dirac delta function for various Chebyshev moments M with Jackson kernel. In the inset, we show the Dirac delta approximations for $M = 2048$ with (red curve) and without (black curve) kernel.

damping kernel. More precisely, the absolute difference between the function $f(x)$ and its KPM estimates $f_{KPM}(x)$ defined on the interval $[-1+\epsilon, 1-\epsilon]$ goes to zero,

$$\|f(x) - f_{KPM}(x)\|_{\infty}^{\epsilon} = \max_{-1+\epsilon<x<1-\epsilon} |f(x) - f_{KPM}(x)| \overset{M\to\infty}{\to} 0. \tag{3.36}$$

There are various kernels satisfying Eq. 3.36 at different rates. The simplest kernel, is Dirichlet kernel, whose all coefficients are one,

$$g_m^D = 1. \tag{3.37}$$

and equivalent to truncation of the series without filtering. It works perfectly for a continuous function (see Fig. 3.4), however, leads to the disadvantages for functions shown in Fig. 3.2 and 3.3.

The most judicious choice of kernel is the Jackson kernel which improves the quality of Chebyshev series expansions of a function. The explicit mathematical form of the Jackson kernel g_m, is

$$g_m = \frac{1}{M+1}\left((M-m+1)\cos\left(\frac{m\pi}{M+1}\right) + \sin\left(\frac{m\pi}{M+1}\right)\cot\left(\frac{\pi}{M+1}\right)\right). \tag{3.38}$$

The Gibbs damping factor implicitly depends on the number of Chebyshev moments M. The g_m corresponds to a specific kernel polynomial which determines the quality of kernel polynomial approximations. Examples of the KPM expansions with Jackson kernel are shown in Fig. 3.2 and 3.3.

In general, the kernels have the following properties [19].

- The kernel should be of M degree Chebyshev moments polynomial.
- The kernel estimates of a function $f(x)$ should be strictly positive for a positive $f(x)$, for example, the density of states, spectral function etc.,.
- The kernel is normalized, $g_0 = 1$.
- The second coefficient g_1 approaches 1 as $M \to \infty$.

In the following, we will briefly discuss the KPM approximations of the Dirac delta, rectangular and Lorentzian functions.

3.2.2 Dirac Delta Function

The Dirac delta function $\delta(x - x_0)$ plays a very important role in physics. It may be thought as an infinitely high and thin spike at x_0. It may be represented by a rectangular function or Lorentz function in the limit of vanishing broadening with constant area. The KPM approximation of Dirac delta function is given by

$$\delta(x - x_0) = \frac{2}{\pi} \sum_{m=0}^{M-1} \frac{\mu_m g_m}{1 + \delta_{m,0}} T_m(x), \tag{3.39}$$

where, x and x_0 are in the range $]-1, 1[$, and μ_m are the Chebyshev coefficients, computed as

$$\mu_m = \int_{-1}^{1} \frac{1}{\sqrt{1 - x^2}} T_m(x) \delta(x - x_0) dx = \frac{T_m(x_0)}{\sqrt{1 - x_0^2}}. \tag{3.40}$$

Eq. 3.39, can be rewritten as

$$\delta(x - x_0) = \frac{2}{\pi \sqrt{1 - x_0^2}} \sum_{m=0}^{M-1} \frac{g_m}{1 + \delta_{m,0}} T_m(x_0) T_m(x). \tag{3.41}$$

The Dirac delta, Eq. 3.39, can be characterized by evaluating the variance σ_x^2,

$$\sigma_x^2 = \left\langle x^2 \right\rangle - \left\langle x \right\rangle^2, \tag{3.42}$$

where using the first three Chebyshev polynomials, one can find

$$x = T_1(x), \tag{3.43}$$

$$x^2 = \frac{T_2(x) + T_0(x)}{2}, \tag{3.44}$$

Thus, the average of x and x^2 is,

$$\langle x \rangle = \int_{-1}^{1} x\delta(x - x_0) = g_1 T_1(x_0), \tag{3.45}$$

$$\langle x^2 \rangle = \int_{-1}^{1} x^2\delta(x - x_0) = \frac{g_0 T_0(x_0) + g_2 T_2(x_0)}{2}, \tag{3.46}$$

Putting these equations in Eq. 3.42,

$$\begin{aligned}
\sigma_x^2 &= x_0^2(g_2 - g_1^2) + \frac{g_0 - g_2}{2}, \\
&= \frac{M - x_0^2(M-1)}{2(M+1)} \left(1 - \cos\frac{2\pi}{M+1}\right), \\
&\simeq \left(\frac{\pi}{M}\right)^2 \left(1 - x_0^2 + \frac{3x_0^2 - 2}{M}\right).
\end{aligned} \tag{3.47}$$

At $x_0 = 0$, the expansion of delta function function has a broadened peak of width $\sigma_x = \pi/M$, whereas close to the boundary $x_0 = \pm 1$, one find $\sigma_x = \pi/M^{3/2}$. The KPM estimates of Dirac delta function are presented in Fig. 3.2.

3.2.2.1 Rectangular Function

A rectangular function $f(x)$, with broadening parameter γ, has the following form

$$f(x) = \begin{cases} \frac{1}{\gamma} & -\frac{\gamma}{2} \leq x \leq \frac{\gamma}{2}, \\ 0 & \text{otherwise.} \end{cases} \tag{3.48}$$

Following Eq. 3.35, the approximated rectangular function $F(x)$, will have the form

$$F(x) = \frac{2}{\pi} \sum_{m=0}^{M-1} \frac{\mu_m g_m}{1 + \delta_{m,0}} T_m(x), \tag{3.49}$$

where μ_m are the Chebyshev coefficients, and can be computed as

$$\mu_m = \int_{-\gamma/2}^{\gamma/2} \frac{f(x) T_m(x)}{\sqrt{1 - x^2}} dx, \tag{3.50}$$

The zeroth moment is

$$\mu_0 = \frac{2}{\gamma} \arcsin(\frac{\gamma}{2}), \quad \gamma \leq 2. \tag{3.51}$$

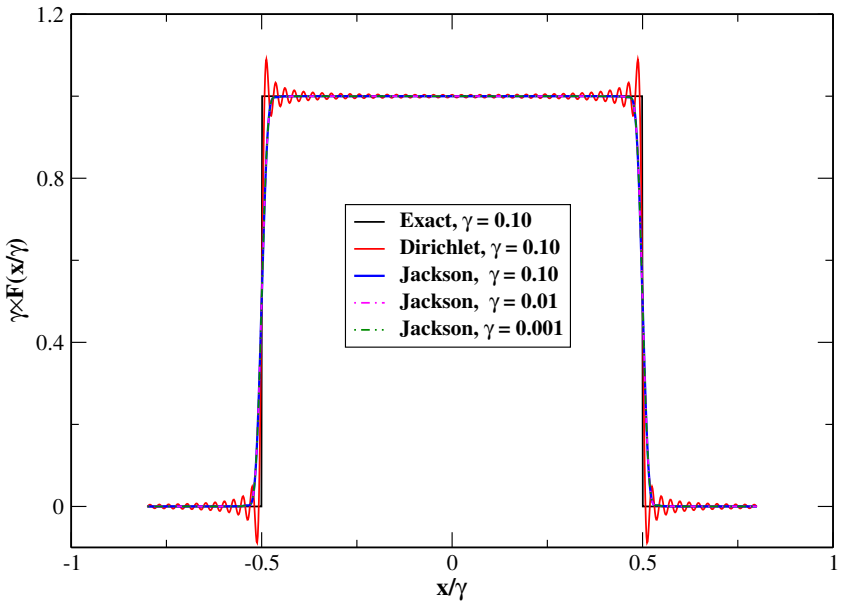

Figure 3.3: The KPM estimates of the rectangular function for various broadening γ. The KPM converge fully for $M = 256/\gamma$, moments with different γ. The KPM approximations with Jackson kernel show a very good agreement with the exact function. Red curve shows the estimates with Dirichlet kernel ($g_m = 1$).

and for $m > 0$,we have

$$\mu_m = \frac{2}{m\gamma} \cos\left(\frac{m\pi}{2}\right) \sin\left(m \arcsin\left(\frac{\gamma}{2}\right)\right), \qquad \gamma \leq 2. \tag{3.52}$$

For a better resolutions, the KPM estimates of rectangular function require large amount of moments for a finite broadening parameter γ. Indeed, the moments and broadening are inversely related. Suppose M_0 Chebyshev moments are required for the broadening γ_0, then

$$M_0\gamma_0 = \text{const.} \tag{3.53}$$

Fig. 3.3, illustrates the KPM estimates of rectangular function for various broadenings. We found a good resolutions of the estimated rectangular function of $\gamma_0 = 1$ with $M_0 = 256$ Chebyshev moments. However, in the limit of vanishing broadening $\gamma \to 0$, one needs to have large number of polynomials for better convergence. For $\gamma_0 < 0.1$, we follow

$$M = \frac{M_0\gamma_0}{\gamma}. \tag{3.54}$$

The KPM estimate of rectangular function with Dirichlet kernel (red curve) has large fluctuations that are successfully filtered out by using the Jackson kernel.

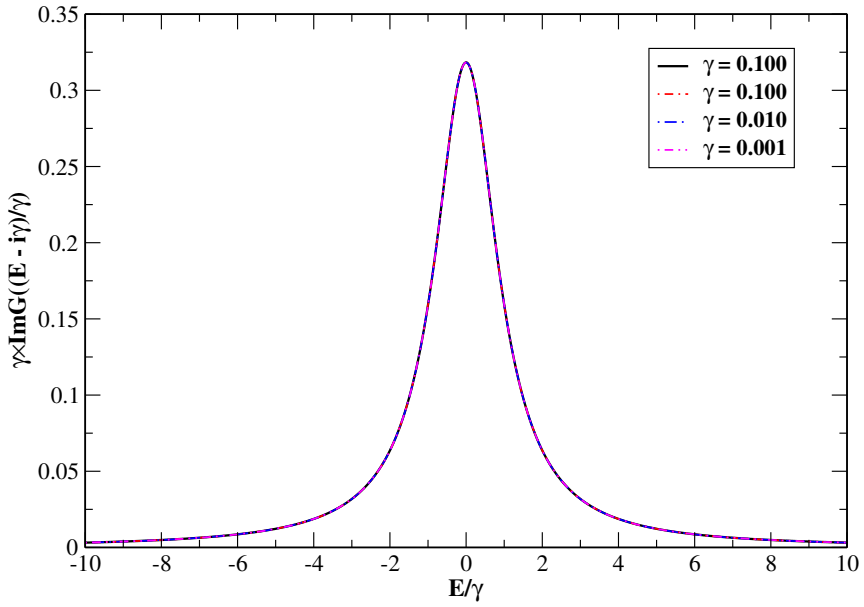

Figure 3.4: The KPM estimates of the imaginary part of the Green's function for various broadenings γ. The KPM converges fully for $M = 8/\gamma$, moments with different γ. The KPM approximations (dashed curves) have a very good agreement with the exact result (bold curve).

3.2.3 Chebyshev Polynomial Green's function method

The Green's function method has versatile applications in several fields in Physics. In general, it can be used to express the physical properties of the system, such as density of states, conductivities and spectral functions. Here, we derive an exact spectral decomposition of the lattice Green's function in terms of Chebyshev polynomials of first kind following ref. [54]. The Green function for a finite broadening γ at energy E is

$$\hat{G}(E + i\gamma) = \frac{1}{E - \hat{\mathcal{H}} + i\gamma}, \tag{3.55}$$

$$= \frac{1}{i}\int_0^\infty dt e^{i(E-\hat{\mathcal{H}}+i\gamma)t}, \tag{3.56}$$

$$= \frac{1}{i}\int_0^\infty dt e^{i(E+i\gamma)t}\boldsymbol{e^{-i\hat{\mathcal{H}}t}}, \tag{3.57}$$

where $\hat{\mathcal{H}}$ is the Hamiltonian of the system. In terms of Chebyshev expansions, we make use of the identity (for $\boldsymbol{e^{-i\hat{\mathcal{H}}t}}$)[55]

$$e^{-ixt} = \sum_{m=0}^{\infty} \frac{2i^{-m}}{1+\delta_{m,0}} J_m(t)T_m(x), \quad |x| \leq 1. \tag{3.58}$$

Inserting into Eq. 3.57, we get

$$\hat{G}(E+i\gamma) = \frac{1}{i}\int_0^\infty dt e^{i(E+i\gamma)t} \sum_{m=0}^{\infty} \frac{2i^{-m}}{1+\delta_{m,0}} J_m(t) T_m(\hat{\mathcal{H}}), \tag{3.59}$$

where $J_m(t)$ is the Bessel function of order m. Let $z := E + i\gamma$ be a rescaled complex energy variable, then

$$\hat{G}(z) = \frac{1}{i}\sum_{m=0}^{\infty} \frac{2i^{-m}}{1+\delta_{m,0}} T_m(\hat{\mathcal{H}}) \int_0^\infty dt e^{-(-iz)t} J_m(t), \tag{3.60}$$

The integral, in fact, is the Laplace transform of the Bessel function, which has the following solution,

$$\int_0^\infty dt e^{-st} J_m(t) = \frac{1}{\sqrt{1+s^2}} \left(\sqrt{1+s^2} - s\right)^m, \tag{3.61}$$

Using this expression, one can express Eq. 3.60 as follows,

$$\hat{G}(z) = \sum_{m=0}^{\infty} g_m(z) T_m(\hat{\mathcal{H}}), \tag{3.62}$$

where

$$g_m(z) = \frac{2i^{-1}}{1+\delta_{m,0}} \frac{(z - i\sqrt{1-z^2})^m}{\sqrt{1-z^2}}. \tag{3.63}$$

Specifically, the exact lattice Green's function expansion was discovered independently by Ferreira & Mucciolo [54] and Braun & Schmitteckert [56]. Different from the KPM approximation to the lattice Green's function, the spectral expansion in Eq. 3.62 always converges. This approach also provides a control over the energy resolution (via the inelastic broadening γ) and thus it is very convenient for studies of quantum criticality.

A comparison of KPM estimates of the imaginary part of the Green's function with exact Lorentzian function for various γ are shown Fig. 3.4.

3.3 Applications

The spectral approach [19] enables us to efficiently calculate several physical quantities without exactly diagonalizing the Hamiltonian of the system. In what follows, the KPM [19] is demonstrated for the computations of DOS, LDOS in the context of tight binding Anderson model.

3.3.1 Spectral Matrix Correlation

Let us briefly explain the spectral expansion technique for the real space spectral matrix correlation (SMC) of a lattice quantum system. To fit the energy spectrum of the Hamilto-

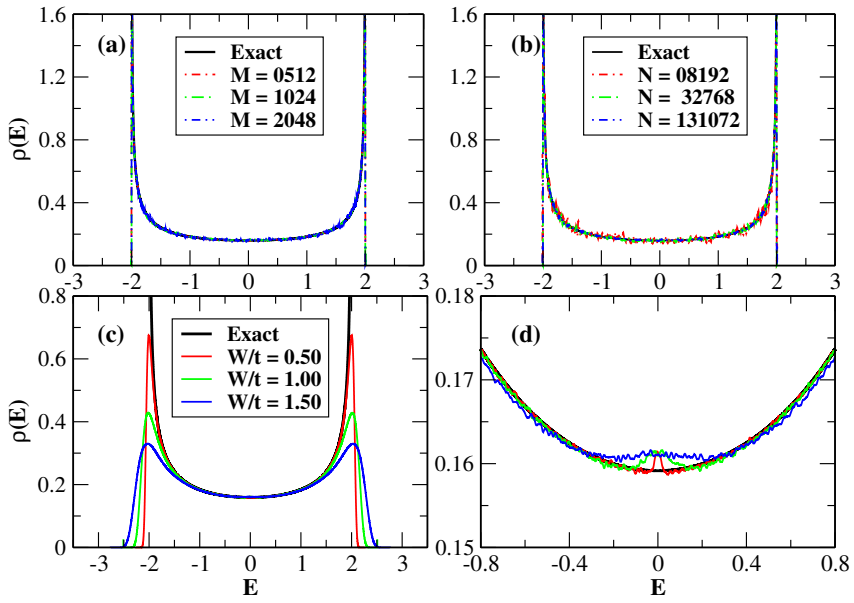

Figure 3.5: The DOS of the one-dimensional Anderson lattice model with periodic boundary condition at $T = 0$. (a) The numerical convergence of KPM estimates of DOS for (a) various Chebyshev moments with fixed system size $N = 131072$, and (b) increasing system size with $M = 1024$ for $W/t = 0$. (c) The approximated DOS of the system with size $N = 131072$ for various disorder strength and 1024 moments with 2048 realizations of disorder. In (d): Zoom of the DOS in (c) around the band center ($E = 0$).

nian matrix $\hat{\mathcal{H}}$ in the standard domain of orthogonality of the Chebyshev polynomials, we employ a linear transformation to Hamiltonian and all energy scales [5]. It is worthwhile to mention that the calculation of moments Eq. 3.34 requires integration over weight function, however, in practical applications to matrix problems prohibits a simple iterative scheme. Thus, following ref. [19], the truncated Chebyshev polynomials expansion of the SMC (see Eq. 2.33) can be expressed as

$$\rho^{ij}_{KPM}(E) = \frac{1}{\pi\sqrt{1-E^2}}\left[1 + 2\sum_{m=1}^{M-1} g_m \mu^{ij}_m T_m(E)\right], \tag{3.64}$$

where μ^{ij}_m are the coefficients of expansion series with no weight function in the integrand, and E is the rescaled energy, and i, or j are the tight-binding basis. The expression Eq. 3.64, can be used to compute the LDOS, DOS, and spectral function under certain conditions.

The main challenge in the KPM approach is to calculate the Chebyshev moments for the corresponding physical quantity. For instance, the Chebyshev moments of the SMC of

[5]The Hamiltonian matrix $\hat{\mathcal{H}}$ and all energy scales can be renormalized by dividing $(2D + W/2)$, where D is the dimension of the quantum system.

the $N \times N$ rescaled Hamiltonian matrix $\hat{\mathcal{H}}$ can have the following expression

$$\begin{aligned}
\mu_m^{ij} &= \int_{-1}^{1} T_m(E)\rho^{ij}(E)\, dE, \\
&= \frac{1}{N}\sum_{\alpha=0}^{M-1} \langle i|\alpha\rangle\langle\alpha|j\rangle T(E_\alpha), \\
&= \frac{1}{N}\sum_{\alpha=0}^{M-1} \langle i|T_m(\hat{\mathcal{H}})|\alpha\rangle\langle\alpha|j\rangle, \\
&= \langle i|T_m(\hat{\mathcal{H}})|j\rangle. \qquad (3.65)
\end{aligned}$$

where $\rho^{ij}(E)$ is the SMC as given by Eq. 2.33. It is important to notice that these moments can be computed recursively by using Eq. 3.25. Starting from the state $|j\rangle$, one can iteratively construct the states

$$|j_m\rangle = T_m(\hat{\mathcal{H}})|j\rangle \qquad (3.66)$$

with

$$|j_0\rangle = T_0(\hat{\mathcal{H}})|j\rangle = |j\rangle, \qquad (3.67)$$

$$|j_1\rangle = T_1(\hat{\mathcal{H}})|j\rangle = \hat{\mathcal{H}}|j\rangle, \qquad (3.68)$$

$$|j_{m+1}\rangle = 2\hat{\mathcal{H}}|j_m\rangle - |j_{m-1}\rangle, \qquad (3.69)$$

and Eq. 3.65

$$\mu_m^{ij} = \langle i|j_m\rangle. \qquad (3.70)$$

This iterative calculation of the moments is the most expensive part of KPM simulations. For a sparse Hamiltonian matrix $\hat{\mathcal{H}}$, of dimension N, the matrix vector multiplication process is an order $\mathcal{O}(N)$, and the computational complexity for the calculation of M Chebyshev moments require $\mathcal{O}(NM)$.

Eq. 3.70, is very general expression and can be modified for the local density of states. For instance, the KPM approximations of the LDOS, $\rho^i_{KPM}(E)$, at site i is

$$\rho^i_{KPM}(E) = \frac{1}{\pi\sqrt{1-E^2}}\left[1 + 2\sum_{m=1}^{M-1} g_m \mu_m^i T_m(E)\right], \qquad (3.71)$$

where the explicit expression of the polynomial coefficients is [19, 57],

$$\mu_m^{ii} \quad := \mu_m^i = \quad \langle i|T_m(\hat{\mathcal{H}})|i\rangle = \langle i|i_m\rangle. \qquad (3.72)$$

The DOS of the $N \times N$ rescaled Hamiltonian matrix $\hat{\mathcal{H}}$ can have the following expression [19, 57],

$$\rho_{KPM}(E) = \frac{1}{\pi\sqrt{1-E^2}}\left[1 + 2\sum_{m=1}^{M-1} g_m \mu_m T_m(E)\right], \qquad (3.73)$$

The Chebyshev moments are

$$\begin{aligned}\mu_m &= \int_{-1}^{1} T_m(E)\rho(E)\,dE, \\ &= \frac{1}{N}\sum_{\alpha=0}^{M-1} T(E_\alpha), \\ &= \frac{1}{N}\sum_{\alpha=0}^{M-1} \langle\alpha|T_m(\hat{\mathcal{H}})|\alpha\rangle, \\ &= \frac{1}{N}\mathrm{Tr}[T_m(\hat{\mathcal{H}})]. \end{aligned} \tag{3.74}$$

where $|\alpha\rangle$ is the αth eigenstate of the Hamiltonian. The trace in Eq. 3.74, can also be evaluated by the stochastic evaluation method of traces [19]. In this method the trace can be replaced by a stochastic average and the Chebyshev moments have the following form

$$\mu_m = \frac{1}{R}\sum_{r=0}^{R-1}\langle r|T_m(\hat{\mathcal{H}})|r\rangle, \tag{3.75}$$

where

$$|r\rangle = \sum_{n=0}^{N-1}\zeta_{rn}\,|n\rangle\,, \tag{3.76}$$

are complex random vectors of an arbitrary basis, $|n\rangle$, and $\zeta_{rn} \in \mathbb{C}$, is a set of independent random variables distributed identically. The number of random vectors R can be a small fixed number, while for the disordered systems, an additional ensemble averaging can be carried out to arbitrary accuracy. The coefficients of the complex random vectors satisfying

$$\langle\zeta_{rn}\rangle = 0; \quad \left\langle\zeta_{rn}\zeta_{r'n'}\right\rangle = 0; \quad \left\langle\zeta^*_{rn}\zeta_{r'n'}\right\rangle = \delta_{rr'}\delta_{nn'} \tag{3.77}$$

Let $\Theta = \frac{1}{R}\sum_{r=0}^{R-1}\langle r|B|r\rangle$ be the statistical expectation value of the trace estimate for any arbitrary Hermitian operator B, with matrix elements $B_{nn'} = \langle n|B|n'\rangle$, then

$$\langle\Theta\rangle = \left\langle\frac{1}{R}\sum_{r=0}^{R-1}\langle r|B|r\rangle\right\rangle, \tag{3.78}$$

$$= \frac{1}{R}\sum_{r=0}^{R-1}\sum_{n,n'=0}^{N-1}\left\langle\zeta^*_{rn}\zeta_{r'n'}\right\rangle B_{n,n'}, \tag{3.79}$$

$$= \sum_{n=0}^{N-1} B_{n,n} = \mathrm{Tr}(B). \tag{3.80}$$

Similarly, the expectation value of $\left\langle\Theta^2\right\rangle$ is [19]

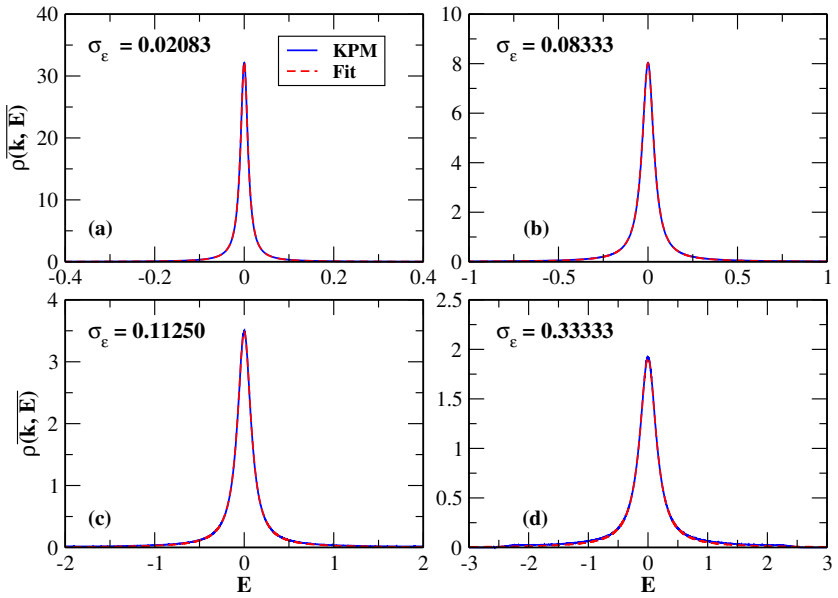

Figure 3.6: The disorder averaged spectral function $\rho(k, E)$ of the Anderson model at the band center ($k = \pi/2$, $E_k = 0$) for different variance σ_ε of the uncorrelated disorder potential. The spectral function is well represented by a Lorentzian [1].

$$\left\langle \Theta^2 \right\rangle = (\mathrm{Tr}(B))^2 + \frac{1}{R}\left(\mathrm{Tr}(B^2) + \left(\left\langle |\zeta_{rn}|^4 \right\rangle - 2 \right) \sum_{n=0}^{N-1} B_{n,n}^2 \right), \tag{3.81}$$

and the fluctuation $(\delta\Theta)^2 = \left\langle \Theta^2 \right\rangle - \left\langle \Theta \right\rangle^2$, become [19]

$$(\delta\Theta)^2 = \frac{1}{R}\left(\mathrm{Tr}(B^2) + \left(\left\langle |\zeta_{rn}|^4 \right\rangle - 2 \right) \sum_{n=0}^{N-1} B_{n,n}^2 \right), \tag{3.82}$$

where $\left\langle |\zeta_{rn}|^4 \right\rangle = \left\langle (\zeta_{rn}^*)^2 \, \zeta_{rn}^2 \right\rangle$. The trace of the matrix B^2 is of $\mathcal{O}(N)$, and the relative error of the trace estimate $\delta\Theta/\Theta$, turns out to be $\mathcal{O}(1/\sqrt{RN})$ for extremely sparse matrices. In general, the relative error of the trace estimates is $\mathcal{O}(1/\sqrt{RN^c})$, with $c \in [0, 1]$[6]

To give an impression of the physical content of the tight-binding model, we show in Fig. 3.5, the kernel polynomial expansions of DOS in one-dimensional Anderson model. We consider finite-size systems of linear size N with nearest-neighbor hopping parameter $t = 1$ and periodic boundary conditions at absolute zero temperature. In the absence of disorder, the DOS of the 1D tight-binding model has been verified for various moments as

[6] $c = 0$: fully dense matrices and $c = 1$: extremely sparse matrices (Identity matrix)

illustrated in Fig. 3.5. It is shown the DOS can be very well approximated by KPM for the system of size $N = 131072$ with 512 Chebyshev moments. In (b), we show the size dependence of DOS for fixed $M = 1024$. The DOS show fluctuations for small system size, which may be because of the large number of moments.

Introducing disorder in the system, results the breaking of translational periodicity due to scattering effects in the lattice system. As a consequence, the singularities at the band edges are progressively broadened with disorder strength, and its weight is redistributed to energies throughout and beyond the crystal band as presented in Fig. 3.5(c). By zooming the DOS around the band center (see Fig. 3.5(d)), we have pointed that, the DOS has a sharp peak at the band center in the presence of small disorder. Increasing disorder will progressively broaden the central part of the DOS, and consequently, the peak will disappear in the limit of strong disorder. This phenomena has also been studied for a disordered chains [58].

3.3.2 Spectral Function

The KPM approximation of the the spectral function (see Eq. 2.36), may have the form

$$\rho_{KPM}(k,E) = \frac{1}{\pi\sqrt{1-E^2}}\left[1 + 2\sum_{m=1}^{M-1} g_m \mu_m T_m(E)\right], \tag{3.83}$$

where the expansion coefficients μ_m are determined as

$$\mu_m \quad := \mu_m^{kk} = \int_{-1}^{1} T_m(E)\rho(k,E)\,dE = \langle k|\, T_m(\hat{\mathcal{H}})\,|k\rangle\,. \tag{3.84}$$

A plane-wave basis, $|k\rangle$, is used in the calculation of Chebyshev moments. The recursion relations obeyed by the Chebyshev polynomials carry over to these moments, and greatly simplify their calculation. The expression Eq. 3.83, represents the truncated sum of the Chebyshev series with Jackson kernel, g_m. The use of this kernel does not alter the series convergence to the intended function, as M goes to infinity. This makes the KPM approximations of $\rho(k,E)$ always positive, a rather describe feature, since by construction, $\rho(k,E) \geq 0$.

In Fig. 3.6 we show the approximated spectral function for various values of variance of random potential $\sigma_\varepsilon^2 = \overline{\varepsilon^2}$, at the band center $E_k = 0$ ($k = \pi/2$). It is well fitted by a Lorentzian, as expected from perturbation theory. The procedure of fitting the data provides us with more accurate estimates of the width of the spectral function. In Fig. 3.7(a), we show a comparison of the width parameter of the Lorentzian, obtained from the fits, with the value calculated from Born approximation

$$\frac{\hbar\Upsilon}{t} = \frac{\overline{\varepsilon^2}}{2t^2}. \tag{3.85}$$

Fig. 3.7(b) depicts data for the mean free path l obtained from the spectral width of the fitted Lorentzian spectral function for the 1D disordered lattice. The magenta curve represents the mean free path l, calculated from the Born approximation. It turns out that the perturbative results give a good account of the data until values $\sigma_\varepsilon \lesssim 1$.

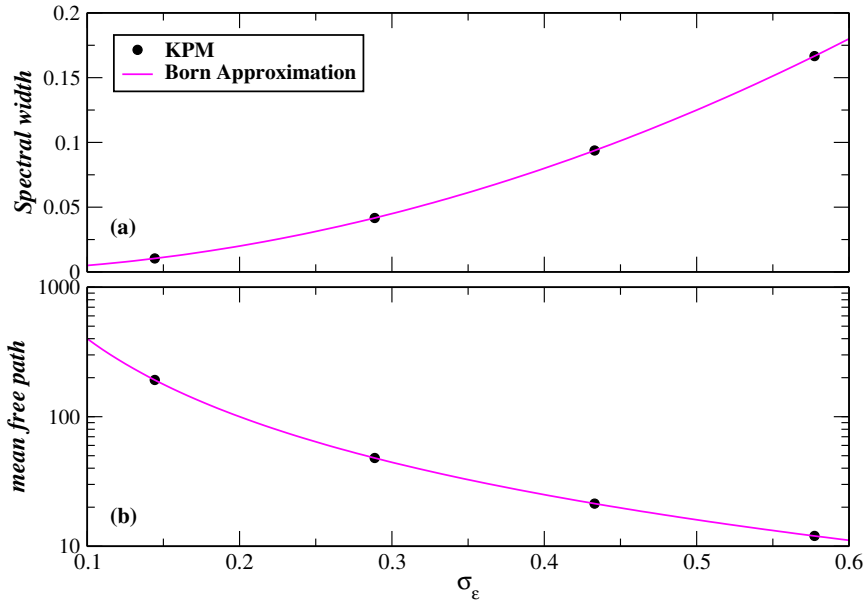

Figure 3.7: (a) The disorder induced spectral width Υ as a function of disorder variance of the fitted curves as presented in Fig. 3.6; the magenta line is the Born approximation (b) Log-linear plot of the mean free path obtained from the spectral width [1].

3.3.3 Localization Length

The localization length of one-dimensional quantum systems with statistically uncorrelated random potentials has been studied numerically [58]. They employ the Thouless formula [46] for the localization length $\xi(E)$ (see Eq. 2.39) of the Anderson model and imposing OBC. Here, we set, $t = 1$, so that $\ln|t| = 0$, and hence, the Thouless expression (see Eq. 2.39) of localization length is rewritten as

$$\frac{1}{\xi(E)} = \int_{-1}^{1} \rho_{KPM}(\epsilon) \ln|E - \epsilon| \, \mathrm{d}\epsilon, \tag{3.86}$$

where $\rho_{KPM}(\epsilon)$ is the KPM expansion of density of states at energy ϵ. After inserting the Chebyshev polynomial expansion of the density of states (see Eq. 3.73) into Eq. 3.86, we get

$$\frac{1}{\xi(E)} = \frac{2}{\pi} \sum_{m=0}^{M-1} \frac{\mu_m g_m}{1 + \delta_{m,0}} \mathcal{F}_m(E), \tag{3.87}$$

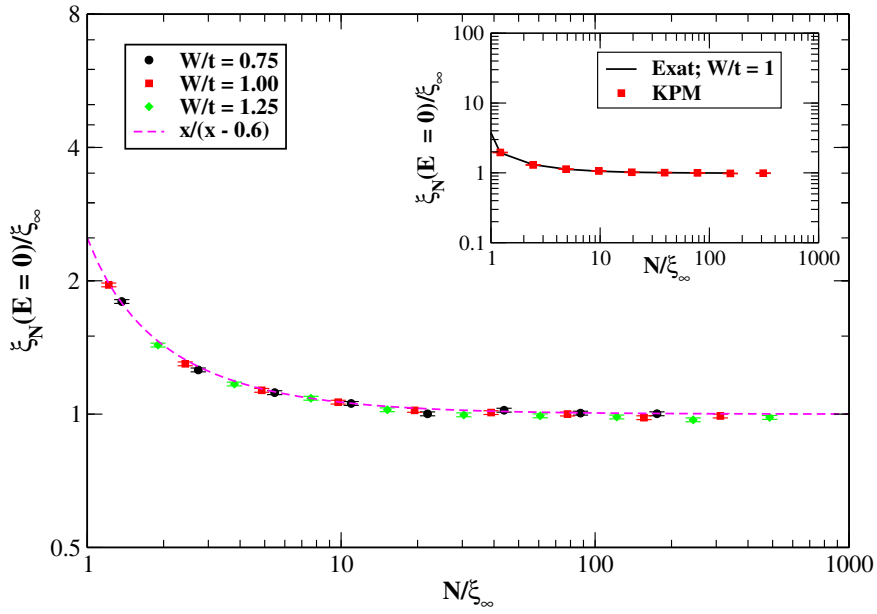

Figure 3.8: The numerical convergence of $\xi_N(E=0)/\xi_\infty$, as a function of $x = N/\xi_\infty$ for the 1D Anderson model with OBC at zero temperature. The data are computed for $M = 2048$ Chebyshev moments with 1% estimated error. The parameter ξ_∞ is the analytically calculated localization length in the perturbative regime for $N \to \infty$ [2, 3]. In the inset: we also validate the KPM estimates of the localization length by comparing with the results calculated by exact diagonalization (Eq. 2.39) for $W/t = 1$.

where μ_m are the Chebyshev moments as given by Eq. 3.74, M is the amount of Chebyshev moments, g_m is the Jackson kernel (see Eq. 3.38), and the function $\mathcal{F}_m(E)$, is given by

$$\mathcal{F}_m(E) = \int_{-1}^{1} T_m(\epsilon) \ln|E-\epsilon| \frac{\mathrm{d}\epsilon}{\sqrt{1-\epsilon^2}}, \tag{3.88}$$

In order to solve the integral, we first differentiate it with respect to E, i.e.,

$$\mathcal{F}_m^{'}(E) = \fint_{-1}^{1} \frac{T_m(\epsilon)}{(E-\epsilon)\sqrt{1-\epsilon^2}}\, d\epsilon, \tag{3.89}$$

It is found (see 7.344.1 in [59]) that,

$$\mathcal{F}_m^{'}(E) = -\pi U_{m-1}(E), \qquad m \geq 0, \tag{3.90}$$

where $U_{m-1}(E)$ is the Chebyshev polynomial of the second kind. For $m = 0$, we have $U_{-1}(E) = 0$, and hence $\mathcal{F}_0^{'}(E) = 0$, or $\mathcal{F}_0(E) =$ constant. For $m > 0$, we have

$$\mathcal{F}_m(E) = -\pi \int^E U_{m-1}(E)\, dE, \tag{3.91}$$

$$= -\frac{\pi}{m} T_m(E) + \text{const.} \tag{3.92}$$

It is also found that $\mathcal{F}_0(E) = -\pi \ln 2$, (see Eq.19 in [58]). The final expression of the localization length is

$$\frac{1}{\xi_N(E)} := \frac{1}{\xi(E)} = -\ln 2 - 2 \sum_{m=1}^{M-1} \frac{\mu_m g_m}{m} T_m(E). \tag{3.93}$$

The numerical convergence of the kernel polynomial simulations of localization length for a non-interacting 1D Anderson model with OBC at the band center ($E = 0$) is illustrated in Fig. 3.8. All computations are carried out for a fixed 1% estimated error with $M = 2048$ Chebyshev moments at the band center, $E = 0$. The estimated error is determined by the fluctuations in the localization length. One can clearly see that the KPM estimates show good convergence for a sufficiently large system with various disorder strength. In addition, we have found that the numerical data reported in Fig. 3.8 were very well fitted to the scaling function,

$$\frac{\xi_N(E=0)}{\xi_\infty} = \frac{x}{x - x_0}, \qquad x_0 \sim 0.6. \tag{3.94}$$

To explore the KPM procedure in more clarity, we compute the localization length as a function of disorder for various system sizes with a fixed numerical error 1%, as shown in Fig. 3.9. A small deviation of the estimated localization length from the perturbative results, $105.2/W^2$[3] is observed for a small disorder strength, which disappear in the large system limit as shown in Fig. 3.9 (left panel). The moments dependence on the KPM resolutions for a fixed system size $N = 2^{18}$ are shown in Fig. 3.9 (right panel). Interestingly, the KPM converges fully even for $M = 256$ moments. Most importantly, our numerical findings show excellent agreement with the perturbative results in the large N limit.

3.3.4 Numerical Complexity

The calculation of various physical quantities such as DOS, spectral function, and localization length by exact diagonalization method requires $\mathcal{O}(N^3 S)$ computational complexity [57], where N is the order of the dense matrix or the number of sites in lattice system and S is the realizations of disorder of Hamiltonian. The exact calculation are carried out by executing the diagonalization of the Hamiltonian matrix of the corresponding system as shown in Fig. 3.1.

However, the KPM simulations take the advantage of the matrix-vector multiplications over the diagonalization, and can compute for instance the DOS with an $\mathcal{O}(NMRS)$ numerical complexity for a sparse and $\mathcal{O}(N^2 MRS)$ for a dense Hamiltonian matrix by

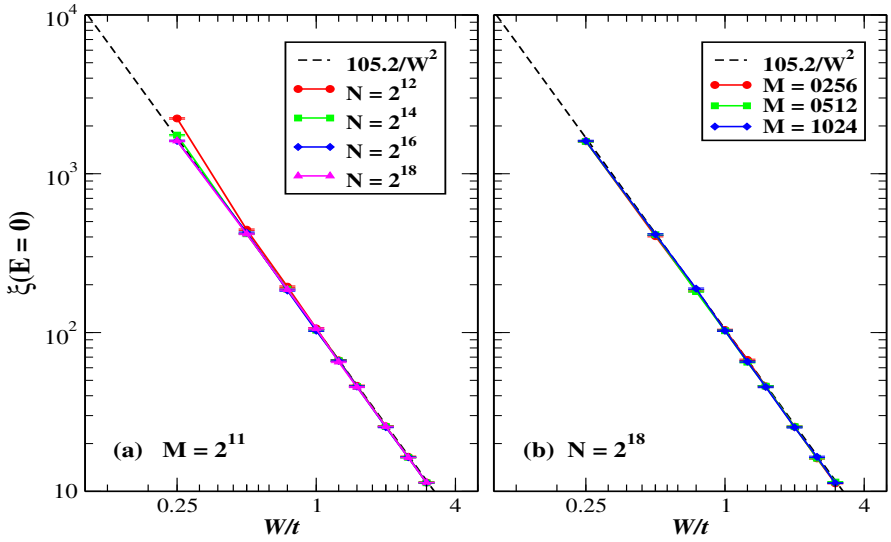

Figure 3.9: The KPM localization length $\xi_N(E=0)$, as a function of W/t for the 1D Anderson model with OBC at zero temperature. The deviations of the $\xi_N(E=0)$ from ξ_∞ (black dashed line) in the small disorder limit, start to disappear with increasing system size (left panel). We also show the numerical convergence of KPM for various expansion coefficients with fixed system size, $N = 2^{18}$ (right panel).

stochastic evaluation method, where M is the number of Chebyshev moments, and R is the number of random vectors. Thus, the KPM will be effective only when $MR \ll N^2$ for sparse and $MR \ll N$ for dense matrix. One can compute a self-averaging physical quantities (DOS) for a single random vectors with $S = 1$ in the large system limit. Hence, the cost of computations reduced to $\mathcal{O}(NM)$ for sparse Hamiltonian matrix.

The Chebyshev moments can also be computed by simple expectation values of Chebyshev polynomials in Hamiltonian matrix (see Eq. 3.65 and 3.72). As a consequence, the computational cost of M moments are $\mathcal{O}(NM)$ for a sparse Hamiltonian matrix.

3.4 Landauer Formalism

Now, we focus on the study of the transport properties of a non-interacting conductor in the presence of a diagonal random disordered potential, ε_n. An intuitive approach to quantum transport is based on the Landauer formalism [60, 61]. The standard theoretical view of the setup needed for the Landauer formalism with two linear leads is depicted in Fig. 3.10. In this approach, two semi-infinite clean leads are attached to a finite tight-binding disordered chain with a system Hamiltonian $\mathcal{H}_S$, and t hopping integral. Each lead is modeled by a clean tight-binding Hamiltonian, represented by $\mathcal{H}_L$ for left with a hopping matrix element t, and $\mathcal{H}_R$ for the right with the same hopping. Moreover, the

coupling between the left and right leads with the adjacent sites in the disordered system is described by t_{SL} and t_{RS}, respectively. We assume identical leads with a continuum of quantum energy levels and different constant chemical potentials. The chemical potential of the left and right leads are represented by μ_L and μ_R, respectively. Furthermore, we will always take the chemical potential of the sample to be its charge neutrality point, $\mu_S = 0$.

The tight-binding Hamiltonian of the system with two semi-infinite leads, $\mathcal{H}$, has the form,

$$\mathcal{H} = \mathcal{H}_L + \mathcal{H}_S + \mathcal{H}_R + \mathcal{H}_C, \tag{3.95}$$

where,

$$\mathcal{H}_S = -t\sum_{n=1}^{N}(c_{n+1}^{\dagger}c_n + c_n^{\dagger}c_{n+1}) + \sum_{n=1}^{N}\varepsilon_n c_n^{\dagger}c_n. \tag{3.96}$$

$$\mathcal{H}_L = -t\sum_{n=-\infty}^{-1}(c_{n+1}^{\dagger}c_n + c_n^{\dagger}c_{n+1}). \tag{3.97}$$

$$\mathcal{H}_R = -t\sum_{n=N+1}^{\infty}(c_{n+1}^{\dagger}c_n + c_n^{\dagger}c_{n+1}). \tag{3.98}$$

where N is the number of sites in the disordered sample. The Hamiltonian $\mathcal{H}_C = \mathcal{H}_{LS} + \mathcal{H}_{SR}$, connect two semi-infinite leads with the disordered system by boundary hoppings. Explicitly, it can be expressed as,

Figure 3.10: Theoretical view of the setup for the two-probe measurement of the conductance. Two semi-infinite clean leads (black filled circles) are connected to a disordered sample (red filled circles). The term t is the hopping matrix element of the disordered system, left, and right lead. The hopping integral t_{LS} and t_{SR}, connect leads with the disordered sample. The chemical potential of the system is assumed to be zero, while the left lead has μ_L and the right lead has μ_R chemical potential.

$$\mathcal{H}_{LS} = -t_{LS}(c_1^{\dagger}c_0 + c_0^{\dagger}c_1). \tag{3.99}$$

$$\mathcal{H}_{SR} = -t_{SR}(c_{N+1}^{\dagger}c_N + c_N^{\dagger}c_{N+1}). \tag{3.100}$$

Here, c_i and $c_i^{\dagger}$ are the local fermionic annihilation and creation operators, obeying the

anticommutations relations. For the sake of simplicity, we will take $t_{LS} = t_{SR} = t$.

Preliminary — The Periodic Chain: If we were dealing with independent electrons moving on an infinite periodic chain (no on-site disorder), with a single orbital per site. The Green's functions of the system in real space is given by

$$G_{ij}^{r/a}(E) = \sum_{\alpha} \frac{\psi_\alpha(i)\psi_\alpha^*(j)}{E - E_\alpha \pm i\gamma}, \tag{3.101}$$

where $\{\psi_\alpha\}$ and $\{E_\alpha\}$ are the eigenvectors and eigenvalues of the system[7]. The eigenvectors are the Bloch-waves and have the following form:

$$\psi_k = \frac{1}{\sqrt{N}} e^{-ikn}, \tag{3.102}$$

where k is a wavenumber, $k = \frac{2\pi}{N} n$, with $n \in \left\{-\frac{N}{2}+1, \cdots, -1, 0, 1, \cdots, \frac{N}{2}-1, \frac{N}{2}\right\}$, whereas $E_k = -2t\cos k$. Then, Eq. 3.101, can be rewritten as

$$G_{ij}^{r/a}(E) = \frac{1}{N} \sum_{k} \frac{e^{ik(i-j)}}{E + 2t\cos k \pm i\gamma}, \tag{3.103}$$

In the thermodynamic limit, Eq. 3.103 becomes

$$G_{ij}^{r/a}(E) = \int_{-\pi}^{\pi} \frac{dk}{2\pi} \frac{e^{ik(i-j)}}{E + 2t\cos(k) \pm i\gamma}, \tag{3.104}$$

This integral can be solved by converting it into a complex integral over the unit circle and finding the residues of the poles lying inside the circle. After some algebra, one obtains

$$G_{ij}^{r/a}(E) = \frac{(2t)^{-|i-j|}}{\sqrt{E^2 - 4t^2}} \left(-E \pm \sqrt{E^2 - 4t^2}\right)^{|j-i|}; \qquad E < -2t, \tag{3.105}$$

$$G_{ij}^{r/a}(E) = -\frac{(2t)^{-|i-j|}}{\sqrt{E^2 - 4t^2}} \left(-E \pm \sqrt{E^2 - 4t^2}\right)^{|j-i|}; \qquad E > 2t. \tag{3.106}$$

The General Case: Our aim, of course, is to calculate the non-equilibrium Green's function of the connected system, a task which can only be done numerically for a disordered sample. However, there are some general results which may be obtained by appealing to the local character of the Hamiltonian (Eq. 3.99 and 3.100). We may write the Dyson equations [61] for the Green's function, in the energy domain, as

$$\mathcal{G}_{i,j}^{r/a}(E) = G_{i,j}^{r/a}(E) + \sum_{k,l} G_{i,k}^{r/a}(E) V_{k,l} \mathcal{G}_{l,j}^{r/a}(E), \tag{3.107}$$

$$= G_{i,j}^{r/a}(E) + \sum_{k,l} \mathcal{G}_{i,k}^{r/a}(E) V_{k,l} G_{l,j}^{r/a}(E), \tag{3.108}$$

[7] $r/a = +/-$ stand for the retarded and advanced Green function

where $G^{r/a}_{i,j}(E)$'s are the Green functions of the unconnected system, $\mathcal{G}^{r/a}_{i,j}(E)$'s are the corresponding ones for the fully connected system, and $V_{i,j}$ are the matrix elements of the perturbation in position space.

3.4.1 Green's Function of a Semi-Infinite Chain

Our aim is to obtain expressions for the propagators in systems which are semi-infinite. This fact prevents us from using periodic boundary conditions and makes the infinite size limit much harder to achieve. Hence, to obtain the intended propagators, we resort to a different method which is based on the idea that an infinite periodic chain may be thought of as two semi-infinite ones, which are coupled by the hopping between their open-end sites. This situation is depicted in Fig. 3.11, where we baptize the two semi-infinite chains as the "left lead" and the "right lead" , respectively.

The interaction between the two semi-infinite leads is written, in the position basis, as

$$V_{n,m} = -t(\delta_{n,1}\delta_{m,0} + \delta_{n,0}\delta_{m,1}) \tag{3.109}$$

One can relate the Green's functions of the uncoupled system $G^{\overline{\infty}}_{i,j}(E)$ with the ones of the coupled system $G^{\infty}_{i,j}(E) = \mathcal{G}_{i,j}(E)$, via the Dyson equation, as given by

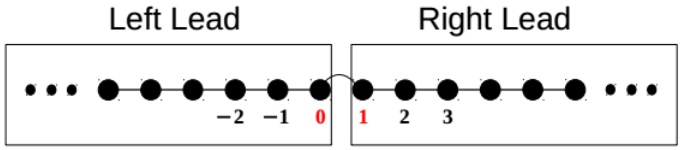

Figure 3.11: Scheme of the setup used to calculate the Green's functions of semi-infinite leads.

$$\begin{aligned} G^{\infty}_{i,j}(E) &= G^{\overline{\infty}}_{i,j}(E) + \sum_{n,m} G^{\infty}_{i,n}(E) V_{n,m} G^{\overline{\infty}}_{m,j}(E), \\ &= G^{\overline{\infty}}_{i,j}(E) - t\left(G^{\infty}_{i,1}(E) G^{\overline{\infty}}_{0,j}(E) + G^{\infty}_{i,0}(E) G^{\overline{\infty}}_{1,j}(E)\right), \end{aligned} \tag{3.110}$$

We are only interested in calculating the surface Green's functions, which are

$$\begin{aligned} g_L(E) &= G^{\overline{\infty}}_{0,0}(E), \\ g_R(E) &= G^{\overline{\infty}}_{1,1}(E), \end{aligned} \tag{3.111}$$

The Dyson equation Eq. 3.110, becomes

$$\begin{aligned} G^{\infty}_{1,0}(E) &= -tG^{\infty}_{1,1}(E) g_L(E), \\ G^{\infty}_{0,1}(E) &= -tG^{\infty}_{0,0}(E) g_R(E), \end{aligned} \tag{3.112}$$

Here, we use the fact that the Green's functions $G^{\frac{\infty}{2}}_{i,j}(E)$, for any i and j belonging to different leads are zero. The surface Green's functions can be reformulated as

$$\begin{aligned} g_L(E) &= -\tfrac{1}{t}\tfrac{G^{\infty}_{1,0}(E)}{G^{\infty}_{1,1}(E)}, \\ g_R(E) &= -\tfrac{1}{t}\tfrac{G^{\infty}_{0,1}(E)}{G^{\infty}_{0,0}(E)}, \end{aligned} \tag{3.113}$$

Supposing that a constant potential V is imposed on a semi-infinite lead, then the corresponding surface Green's function will have the following form

$$g_{L/R}(E, eV) = \frac{E + eV}{2t^2} \mp \frac{i}{2t^2}\sqrt{4t^2 - (E + eV)^2}. \tag{3.114}$$

In general, such a global energy shift has no physical meaning, however in the problem of non-equilibrium transport the situation is different because the global shift in the left lead is opposite to the one on the right lead. Such bias will yield physical consequences and must be taken into account.

3.4.2 Calculation of the Green's functions for a Sample with Leads

In this section, we will explore how to calculate the Green's functions —$\mathcal{G}^{r/a}_{i,j}(E)$ — between two positions inside the sample, when this is coupled (on both sides) to semi-infinite leads. The Dyson equations can be reformulated by using the fact that only few element of $V_{m,n}$ are non-zero (see Fig. 3.10), as given by

$$\mathcal{G}^{r/a}_{i,j} = G^{r/a}_{i,j} - t\left[G^{r/a}_{i,0}\mathcal{G}^{r/a}_{1,j} + G^{r/a}_{i,1}\mathcal{G}^{r/a}_{0,j} + G^{r/a}_{i,N}\mathcal{G}^{r/a}_{N+1,j} + G^{r/a}_{i,N+1}\mathcal{G}^{r/a}_{N,j}\right], \tag{3.115}$$

$$\mathcal{G}^{r/a}_{i,j} = G^{r/a}_{i,j} - t\left[\mathcal{G}^{r/a}_{i,0}G^{r/a}_{1,j} + \mathcal{G}^{r/a}_{i,1}G^{r/a}_{0,j} + \mathcal{G}^{r/a}_{i,N}G^{r/a}_{N+1,j} + \mathcal{G}^{r/a}_{i,N+1}G^{r/a}_{N,j}\right], \tag{3.116}$$

Since there are no correlations between leads and the scattering region i.e., $G^{r/a}_{i,0} = G^{r/a}_{i,N+1} = 0$, and $G^{r/a}_{0,j} = G^{r/a}_{N+1,j} = 0$, therefore, Eqs. 3.115 and 3.116 can be further simplified as,

$$\mathcal{G}^{r/a}_{i,j} = G^{r/a}_{i,j} - t\left[G^{r/a}_{i,1}\mathcal{G}^{r/a}_{0,j} + G^{r/a}_{i,N}\mathcal{G}^{r/a}_{N+1,j}\right], \tag{3.117}$$

$$\mathcal{G}^{r/a}_{i,j} = G^{r/a}_{i,j} - t\left[\mathcal{G}^{r/a}_{i,0}G^{r/a}_{1,j} + \mathcal{G}^{r/a}_{i,N+1}G^{r/a}_{N,j}\right], \tag{3.118}$$

At the same time, we can also find very simple expressions for $\mathcal{G}^{r/a}_{0,j}$, $\mathcal{G}^{r/a}_{N+1,j}$, $\mathcal{G}^{r/a}_{i,0}$ and $\mathcal{G}^{r/a}_{i,N+1}$ from Dyson's equations, which go as follows:

$$\mathcal{G}^{r/a}_{i,0} = -t\mathcal{G}^{r/a}_{i,1}G^{r/a}_{0,0} \tag{3.119}$$

$$\mathcal{G}^{r/a}_{0,j} = -tG^{r/a}_{0,0}\mathcal{G}^{r/a}_{1,j}, \tag{3.120}$$

$$\mathcal{G}^{r/a}_{i,N+1} = -t\mathcal{G}^{r/a}_{i,N}G^{r/a}_{N+1,N+1} \tag{3.121}$$

$$\mathcal{G}^{r/a}_{N+1,j} = -tG^{r/a}_{N+1,N+1}\mathcal{G}^{r/a}_{N,j}, \tag{3.122}$$

We will use the components of the retarded/advanced Green's functions of the sample coupled to metallic leads, to calculate the current I, using the Landauer formula for the current transversing the system [61]

$$I = \frac{et^4}{h} \int_{E_F - e\frac{\Delta V}{2}}^{E_F + e\frac{\Delta V}{2}} dE \gamma_L(E, \Delta V) \left| \mathcal{G}^r_{0,N+1}(E) \right|^2 \gamma_R(E, \Delta V) \tag{3.123}$$

where we use the fact that for non-interacting systems $\mathcal{G}^a_{nm}(E) = (\mathcal{G}^r_{mn}(E))^*$. The functions $\gamma_L(E, \Delta V)$ and $\gamma_R(E, \Delta V)$ are the given by,

$$\gamma_R(E, \Delta V) = -\frac{1}{t^2} \sqrt{4t^2 - (E - \frac{e\Delta V}{2})^2} \tag{3.124}$$

$$\gamma_L(E, \Delta V) = -\frac{1}{t^2} \sqrt{4t^2 - (E + \frac{e\Delta V}{2})^2}, \tag{3.125}$$

where $\gamma_R(E, \Delta V)$ and $\gamma_L(E, \Delta V)$ are the local density of states at the surface of the semi-infinite leads. That being said, the physical interpretation of Eq. 3.123 becomes clear, as $\left| \mathcal{G}^r_{0,N+1}(E) \right|^2$ is simply a probability of a state at the surface with energy E to tunnel through the sample.

The general Landauer Formula of Eq. 3.123 describes the steady-state non-equilibrium transport for any strength of the bias potential ΔV. However, the fields usually applied to real samples are ridiculously small when compared with the bandwidth t of the ordered chain. That being said, one is generally interested in the linear approximation to the full non-linear electric current, which is obtained by expanding the Eq. 3.123 in linear order with respect to the applied voltage, i.e.

$$I = \frac{e^2}{h} \int_{E_F - e\frac{\Delta V}{2}}^{E_F + e\frac{\Delta V}{2}} dE \sqrt{(4t^2 - (E + \frac{e\Delta V}{2})^2)(4t^2 - (E - \frac{e\Delta V}{2})^2)} \left| \mathcal{G}^r_{0,N+1}(E) \right|^2, \tag{3.126}$$

$$= \frac{e^2}{h} \left(4t^2 - E_F^2\right) \left| \mathcal{G}^r_{0,N+1}(E_F) \right|^2 \Delta V + \mathcal{O}\left(\Delta V^2\right), \tag{3.127}$$

which implies the following formula for the linear conductance $\mathrm{g}(E_F)$, of the sample with the infinite leads:

$$\mathrm{g}(E_F) = \frac{e^2}{h} (4t^2 - E_F^2) \left| \mathcal{G}^r_{0,N+1}(E_F) \right|^2. \tag{3.128}$$

The central quantity in the Landauer conductance Eq. 3.128, is $\mathcal{G}^r_{N+1,0}(E_F)$, which is computed very efficiently by employing recursive Green function method (RGFM), see appendix C for detail. In chapter 5, we will discuss this formalism for the computations of the conductance distributions of two different models of disorder in detail.

Chapter 4

Spectral Function

This chapter, based on [1], examines the spectral function of Bloch states in an one-dimensional non-interacting tight-binding chain with different models of static disorder at zero temperature. In particular, we will report numerical calculations of the single-particle spectral function based on the kernel polynomial method (KPM), which has an $\mathcal{O}(N)$ computational complexity.

We will focus on two models of correlated disorder: a Gaussian model and a power-law model. For power-law model, we will show a Lorentzian like behavior of the spectral function in the limit of Anderson model $\alpha \to 0$. This Lorentzian shape changes to a Gaussian line shape for $\alpha \to 1^+$, that reflects the classical limit in the single-band lattice system. In this limit ($\alpha \leq 1$), the spectral function shows a self-averaging behavior, as its standard deviation decays as $1/\sqrt{N}$ with size N of the system, at the band center. In the extreme limit $\alpha \to \infty$, the correlated disorder system corresponds to a tight-binding model with cosine potential of wavelength N and the spectral function reveals similar behavior to the density of state in real space.

We also investigate the phenomenon of Anderson transition in this system, by studying the distribution of the spectral function at the band center. In fact, we show a universal and a highly asymmetric distributions of the spectral function in the vicinity of phase transition. Moreover, we find that the spectral function distributions reflects Gaussian nature in the localized, while log-normal shape in the delocalized regime.

4.1 Correlation Function of the Local Disorder

In order to study the characteristics of the correlated random potential, we analytically calculate the auto correlation function of the local disorder potential. The auto-correlation function has the following definition,

$$\Gamma(r) = \frac{\overline{\varepsilon_n \varepsilon_{n+r}}}{\sigma_\varepsilon^2}, \tag{4.1}$$

where ε_n are the onsite random potentials as given by Eq. 2.5. Using Eq. 2.11, and Eq. 2.29, the auto correlation function for the power-law correlated model is expressed as

$$\Gamma(\alpha, r) = \frac{2A^2(\alpha)}{\sigma_\varepsilon^2} \left(\frac{2\pi}{N}\right) \sum_{q>0} |q|^{-\alpha} \cos(qr), \tag{4.2}$$

where the variance local disorder σ_ε^2 is,

$$\sigma_\varepsilon^2 = 2\sum_{q>0} V^2(q) = 2A^2(\alpha) \left(\frac{2\pi}{N}\right) \sum_{q>0} |q|^{-\alpha}, \tag{4.3}$$

Inserting into Eq. 4.2, the correlation function becomes

$$\Gamma(\alpha, r) = \frac{1}{\sum_{q>0} |q|^{-\alpha}} \sum_{q>0} |q|^{-\alpha} \cos(qr), \tag{4.4}$$

replacing $q = 2\pi p/N; \quad p = 1, \ldots N/2$, we get

$$\Gamma(\alpha, r) = \frac{\sum_{p=1}^{N/2} |p|^{-\alpha} \cos(\frac{2\pi p}{N} r)}{\sum_{p=1}^{N/2} |p|^{-\alpha}}, \tag{4.5}$$

In the large system limit $N \gg 1$, the correlation function for $\alpha = 1$ turns out

$$\Gamma(1, r) = -\frac{1}{H_{\frac{N}{2}}} \log\left(2\left|\sin(\frac{\pi r}{N})\right|\right) \approx -\frac{1}{\log(\frac{N}{2})} \log\left(2\left|\sin(\frac{\pi r}{N})\right|\right), \tag{4.6}$$

where $H_{\frac{N}{2}} = \sum_{p=1}^{N/2} |p|^{-1}$ is the $\frac{N}{2}$th harmonic number, and $\lim_{N\gg 1} H_{\frac{N}{2}} = \log(\frac{N}{2})$. The correlation functions, Eq. 4.6 is size-dependent, which goes to zero at $r = N/6$. Moreover, the correlation becomes negative for $r > N/6$, as shown in Fig. 4.1. For $r \ll N$, $\sin(\pi r/N) \approx \pi r/N$, and the correlator is

$$\Gamma(1, r) = -\frac{\log\left(\frac{2\pi r}{N}\right)}{\log(\frac{N}{2})} = 1 - \frac{\log(\pi r)}{\log(\frac{N}{2})}. \tag{4.7}$$

Thus, the first neighbor correlator is

$$\Gamma(1, 1) = 1 - \frac{\log(\pi)}{\log(\frac{N}{2})}. \tag{4.8}$$

For $\alpha \leq 1$, the denominator of Eq. 4.5 is divergent in the thermodynamic limit for $\gamma > 0$. At $\gamma = 0$, the denominator and numerator are equal[1], yields unit correlation. Thus, the correlation function is

$$\Gamma(\alpha, \gamma) = \delta_{\gamma,0}. \tag{4.9}$$

[1]The series for $\alpha = 0$, is not convergent but bounded.

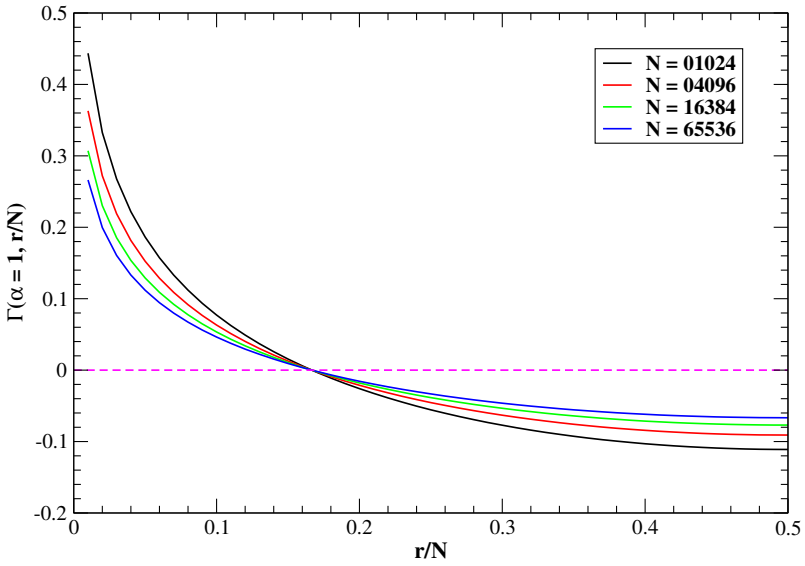

Figure 4.1: Correlation function of the power-law decay type correlated disorder potential as a function of lattice sites at $\alpha = 1$, (Eq. 4.6).

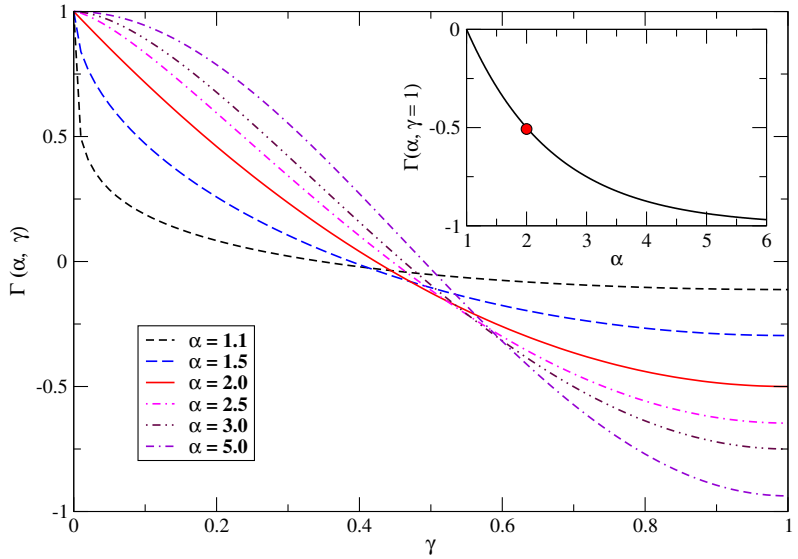

Figure 4.2: Correlation function of the power-law decay type correlated disorder potential as a function of lattice sites, for several values of the exponent α in the thermodynamic limit. The $\alpha \to \infty$ limit yields a perfect cosine correlation function. In the inset we show the characteristic of the correlation function for $\gamma = 1$ as function α [4].

for $\alpha \leq 1$ in the thermodynamic limit, where $\delta_{\gamma,0}$ is a Kronecker-delta function.

A more interesting case happens for $\alpha > 1$, where the integrals will have low-q singularities with a natural cut-off of $2\pi/N$. Also, in this case, the corresponding sum over p in

$$\sigma_\varepsilon^2 = 2A^2(\alpha)\left(\frac{2\pi}{N}\right)^{1-\alpha}\sum_{p=1}^{N/2}\frac{1}{p^\alpha}, \tag{4.10}$$

is found to converge as $N \to \infty$. These two facts mean that, no matter how large N is, the number of terms contributing to the sum is of $\mathcal{O}(1)$. Hence, we can never approximate it by an integral. In fact, the infinite sum in Eq. 4.10 is known to define the Riemann Zeta function [62],

$$\sum_{p=1}^{\infty}\frac{1}{p^\alpha} := \zeta(\alpha). \tag{4.11}$$

and the local variance of the disorder becomes

$$\sigma_\varepsilon^2 = 2A^2(\alpha)\left(\frac{2\pi}{N}\right)^{1-\alpha}\zeta(\alpha), \tag{4.12}$$

This allow us to express $A^2(\alpha)$ in terms of σ_ε, as follows,

$$A^2(\alpha) = \frac{\sigma_\varepsilon^2}{2\zeta(\alpha)}\left(\frac{2\pi}{N}\right)^{\alpha-1}. \tag{4.13}$$

and the two-site covariance of the potential (see Eq. 2.11) in this limit can also be calculated by using $q = 2\pi p/N$, as

$$\overline{\varepsilon_n\varepsilon_m} = 2A^2(\alpha)\left(\frac{2\pi}{N}\right)^{1-\alpha}\sum_{p=1}^{\infty}\frac{1}{|p|^\alpha}\cos\left(\frac{2\pi p}{N}(n-m)\right),$$

Hence, we can express the correlation function ($r_{nm} = n - m$) in terms of a polylogarithm function [62], $Li_\alpha(z) := \sum_{p=1}^{\infty} z^p/p^\alpha$, as follows,

$$\Gamma(\alpha, r_{nm}) = \frac{1}{\zeta(\alpha)}\mathrm{Re}\left[Li_\alpha\left(e^{\frac{2\pi i}{N}r_{nm}}\right)\right], \tag{4.14}$$

Defining a variable $\gamma = 2r_{nm}/N$ in the interval [0, 1] for $r_{nm} \in [0, N/2]$, allow us the size-independent correlation function, as follow:

$$\Gamma(\alpha, \gamma) = \frac{1}{\zeta(\alpha)}Re\left[Li_\alpha\left(e^{i\pi\gamma}\right)\right]. \tag{4.15}$$

Eq. 4.15, can be further simplified for $\alpha = 2$, as

$$\Gamma(2, \gamma) = \frac{\pi^2}{\zeta(2)}B_2(\gamma/2) = \frac{3}{2}\gamma^2 - 3\gamma + 1, \tag{4.16}$$

where $\zeta(2) = \pi^2/6$, and $B_2(x)$ is a second-order Bernoulli polynomial given by

$$B_2(\gamma/2) := \mathrm{Re}\left[Li_\alpha\left(e^{i\pi\gamma}\right)\right] = (\frac{\gamma}{2})^2 - \frac{\gamma}{2} + \frac{1}{6}. \tag{4.17}$$

The correlation function for $\alpha > 1$ in the thermodynamic limit is depicted in Fig. 4.2. It is shown that the correlations converge to a nonzero value and goes to negative for $\alpha = 1$. The correlations decrease with increasing α and at $\gamma = 1$, yields a value of $-1/2$ for critical exponent $\alpha = 2$ and converge to -1 for $\alpha \to \infty$. Also, the behavior of the correlation function is concave for $\alpha < 2$, linear for $\alpha = 2$ and convex for $\alpha > 2$ in the limit $\gamma \sim 0$. The negative correlation is "remarkable" in the sense that it drives the emergence of a periodic (sinusoidal) structure of the potential and the appearance of the extended low-energy states for $\alpha \geq 2$ [17].

As a last remark, we note that to ensure a finite $\overline{\varepsilon^2}$, we must choose $A^2(\alpha) \propto 1/N^{\alpha-1}$ as shown in Eq. 4.13. This implies that $A^2(\alpha) \to 0$, as $N \to \infty$ (for $\alpha > 1$).

The auto correlation function of the Gaussian correlated model $\Gamma(q_c, r)$, in the limit of $q_c \ll \pi$, (using Eq. 2.19 and Eq. 2.21 into Eq. 4.1) can be defined as

$$\Gamma(q_c, r) = e^{-\frac{q_c^2 r^2}{2}}. \tag{4.18}$$

The correlation function of site energies is Gaussian in real space with a decay length $\xi = q_c^{-1}$.

4.2 Spectral Function

As discussed in chapter 2, the single-particle spectral function is the energy distribution of a state of momentum k, or the momentum distribution of a state of energy E. In the absence of interactions or disorder, the spectral function is simply a Dirac delta peaked at a single-particle energy E_k.

Introducing disorder in a non-interacting disordered electronic system, can induce a finite width of the spectral function averaged over disorder. For Anderson model, the spectral function has a standard Lorentzian structure [24] with spectral width proportional to the disorder variance in the limit of weak disorder. Equivalently, the so-determined spectral width can give the decay rate of a momentum state due to scattering by the disorder as discussed in chapter 3. Here, we mainly focus on the disorder induced broadening of the spectral function of the correlated disorder models [1].

4.3 Spectral Function of a Disordered Free Fermions

In order to probe the single-particle properties of a disordered quantum system, we demonstrate the spectral function of a one-dimensional non-interacting free fermions in the pres-

ence of different models of disorder (see chapter 2 for detail). In practice, we tackle the single particle spectral function at a definite momentum.

4.3.1 Numerical Analysis of the Spectral Function

In this section, we pay attention to the study the spectral functions for one-dimensional non-interacting lattice in the presence of on-site Gaussian and power-law correlated disorder with periodic boundary conditions at zero temperature.

Numerical computations of the spectral function are carried out by a very efficient numerical method the so-called kernel polynomial method (KPM) for any strength of disorder. The resolution and numerical convergence of the KPM estimates are controlled by the number of M of Chebyshev moments used in the series of Eq. 3.83.

4.3.1.1 Gaussian Correlated Disorder

For other types of disorder, for instance, Gaussian correlated disorder (see Fig. 2.1), the spectral function of the tight-binding chain follows Lorentzian like function at cutoff wave vector $q_c = \pi$. In this case, the system with Gaussian correlated disorder is more like an Anderson model with uncorrelated disorder. In the thermodynamic limit, the cutoff wave vector $q_c \in (0, \infty)$.

The spectral function, at the band center ($E_k = 0, \quad k = \pi/2$), for Gaussian correlated disorder with different values of the cutoff wave vector q_c, is shown in Fig. 4.3 for unit variance of local disorder ($\sigma_\varepsilon = 1$). The red dashed curves are their corresponding fit of the spectral function. The best fit of the numerical data is found with a Lorentzian of width $\Upsilon \backsimeq 0.4456$ for $q_c = \pi$ (see Fig. 4.3(a)).

For $q_c = \pi/128$, the scattering becomes local in momentum space, and the spectral function is seen to be a Gaussian as shown in Fig. 4.3(b). It is worth mentioning that the spectral function for various strength of disorder is symmetric around the band center. Moreover, we have also shown the characteristic of the spectral function for various k as depicted in Fig. 4.3(c) and (d). For the given values, the spectral function shows similar distribution over energy. One can see, the peak of spectral function decreases for k values other than $\pm\pi/2$, as more clearly shown by the shifted curves in (c). For $q_c = \pi/128$, the spectral function shows no difference for other values of k. In this case, the spectral function just shift by an energy $E_k = -2\cos(\pm k)$. In addition, the spectral width turns out to be the variance of the site energies.

Furthermore, we have studied the spectral function of the system for various variance of local disorder σ_ε^2. We found that the spectral function for various σ_ε^2 display single universal curve in the limit of $\sigma_\varepsilon \gg \hbar v_k q_c$, where v_k is the Fermi velocity and $\hbar$ is the Plank constant. In particular, the spectral function for different values of σ_ε^2 are scaled to show that

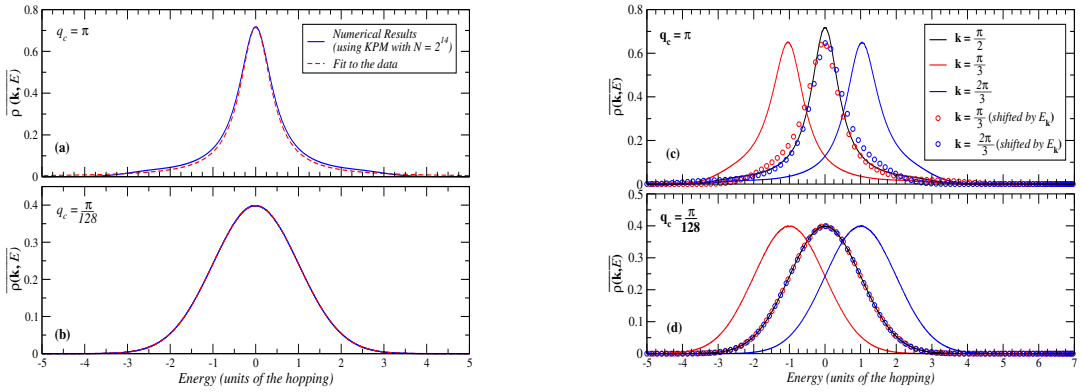

Figure 4.3: The disorder-averaged spectral function for Gaussian correlated disorder with unit variance $\sigma_\epsilon^2 = 1$, for (a) $q_c = \pi$, and (b) $q_c = \pi/128$. The spectral functions are reasonably fitted by a Lorentzian (upper panel) of half-width $\Upsilon \backsimeq 0.4456$, and very well fitted a Gaussian (lower panel) of variance $\sigma_\varepsilon^2 = 1$. The plots (c) and (d), show the spectral function for different values of k and how it relates to its shape at the band's center.

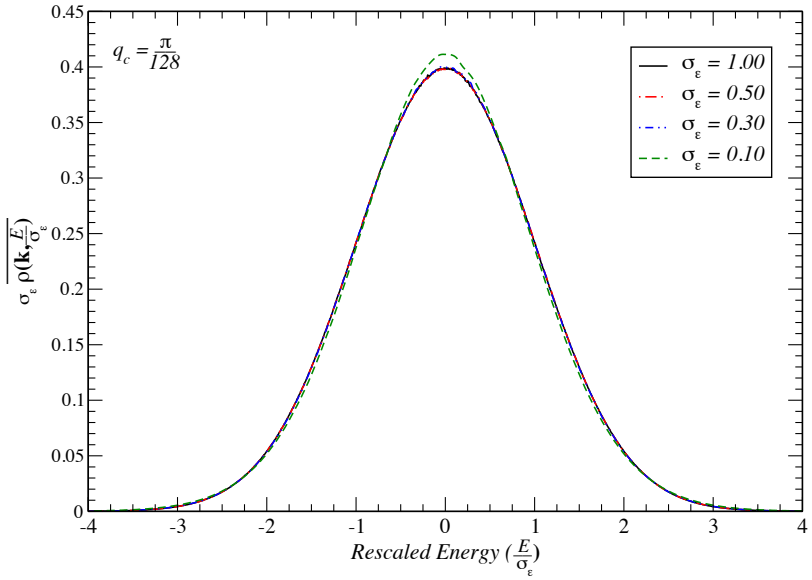

Figure 4.4: The normalized spectral function for the Gaussian correlated disorder of the system of size $N = 2^{14}$ with $M = 8192$ Chebyshev coefficients for different values of disorder variance σ_ε .

$$\overline{\rho(k = \pm\frac{\pi}{2}, E)} = \sigma_\varepsilon^{-1} \mathcal{N}(0, 1, E/\sigma_\varepsilon)\,, \quad \textbf{for } \sigma_\varepsilon \gg \hbar v_k q_c. \tag{4.19}$$

In Eq. 4.19, $\mathcal{N}(\mu, \sigma, \varepsilon)$ is the normal distribution of mean μ and variance σ. Fig. 4.4 illustrates a clear picture of the universal scaling of spectral function for various σ_ε. Obviously, the dashed green line does not obey the condition $\sigma_\varepsilon \gg \hbar v_k q_c$, and could not collapse with

other curves.

This result calls to mind the classical limit of the spectral function discussed by Trappe *et. al.* [63]. In that limit, the disordered potential dominates, and the spectral function merely reflects the probability distribution of local potential values. This in fact what is observed here. Since

$$\varepsilon_m = 2\sum_{q>0} V(q)\cos\left(qm + \phi_q\right), \tag{4.20}$$

in the thermodynamic limit, when $q_c \gg \pi/N$, the energy at each site is a sum of a large number of random independent variables, and by the central limit theorem, it is normally distributed. But what is significant here is that this limit is obtained even when the disorder strength is small enough to be considered a weak perturbation when compared to the bandwidth. As we will see later this will turn out to be a consequence of the local character of the scattering in momentum space.

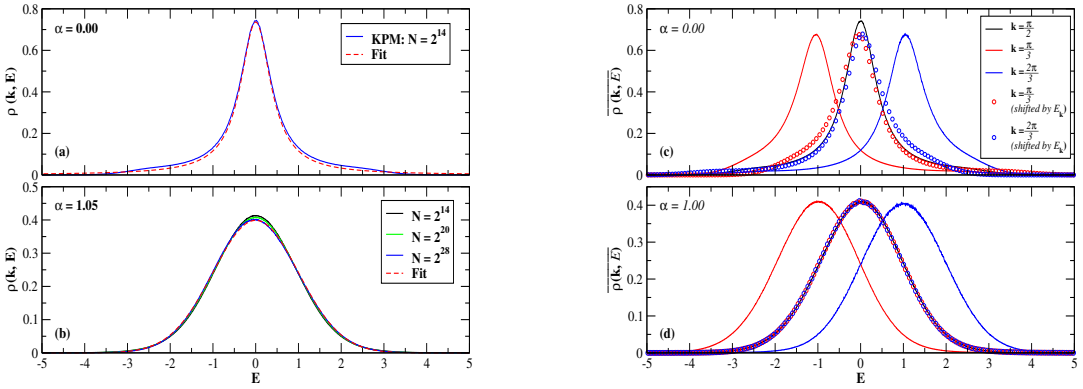

Figure 4.5: Mean spectral function for two values of the correlation exponent, α, and $\sigma_\varepsilon = 1$. The numerical plots show a good agreement with the following conclusions: (a) and (c) a Lorentzian fit of width $\Gamma \sim 0.433$ and a strong dependence of the shape with the value of k, for $\alpha < 1$; (b) and (d) a Gaussian fit of unit variance in the large L limit and a very weak dependence of the shape with the value of k for $\alpha \geq 1$.

4.3.1.2 Power-Law Correlated Disorder

We will now concentrate on the statistical properties of the spectral function for a system under the influence of power-law correlated disorder. As discussed in chapter 2, the power-law correlated disorder is characterized by the exponent α that determines how fast the Fourier transform of ε_n decays with wave vector, q,

$$V^2(q) \sim \frac{1}{|q|^\alpha}. \tag{4.21}$$

As α increases, scattering becomes increasingly dominated by small values of q ($q \ll \pi$).

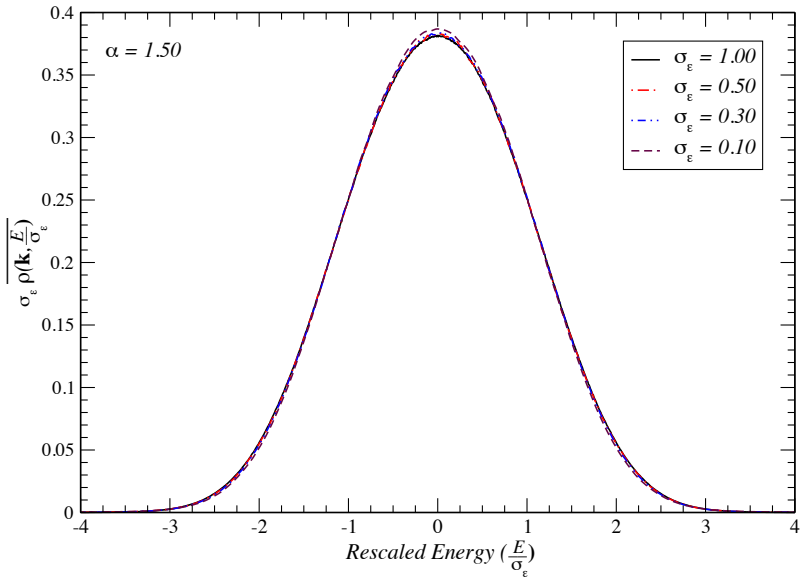

Figure 4.6: The normalized mean spectral function for the power-law correlated disorder, in a system of size $N = 2^{14}$ for different values of the on-site variance σ_ε. There were used 8192 Chebyshev coefficients for the calculation.

In Figure 4.5, we see that a transition for a Lorentzian to a Gaussian shape (with unit variance) of the spectral function at the band center for $\sigma_\varepsilon = 1$, occurs at $\alpha \approx 1.0$. This transition seems to hold for other values of k as well, except for a shift of the central energy value[2]. On closer scrutiny, however, a perfect Gaussian fit is only possible for $\alpha \to 1^+$, in the large N limit, and deviations become increasingly obvious as α increases; the spectral function develops a two peaked structure as a function of energy.

Even though the form of the spectral function is not a Gaussian, one still observes (Fig. 4.6) a universal behavior, for different disorder strengths, similar to the one found for Gaussian disorder, namely

$$\overline{\rho(k,E)} = \sigma_\varepsilon^{-1} \chi_\alpha \left(\frac{E}{\sigma_\varepsilon} \right). \tag{4.22}$$

with the $\chi_\alpha(E/\sigma_\varepsilon)$ depending on α, but not on the disorder variance σ_ε.

As for the Gaussian disorder case, we will show that the results of Figs. 4.5b and 4.6 reveal the emergence of the classical limit, as a consequence of the local character of scattering in momentum space.

[2]The shape of the Lorentzian $\overline{\rho(k,E)}$ depends much more strongly on the value of of k. This can be understood as the combined effect of a change in the central velocity (which affects the mean free path, i.e. the width) and the fact that the algebraic tails start to feel the effect of the finite bandwidth.

4.3.2 Statistical Properties of the Spectral Function in the Thermodynamic Limit

Thus far we have discussed the disorder-averaged spectral function. It is not however clear if this quantity represents a typical value for measurable quantity of macroscopic systems. This becomes specially concerning in the case of the power-law disorder model, which is known to have pathological properties in the thermodynamic limit [4]. To investigate this issue, we calculated the standard deviation of $\rho(k, E)$ for increasing number of sites and different values of the exponent α. These results are shown for two examples in Fig. 4.7.

From the numerical data, we conclude that for $\alpha < 1$ the standard deviation scales as $N^{-1/2}$, which clearly indicates a self-averaging behavior. On the other hand, for $\alpha > 1$ there seems to be a finite standard deviation for $\rho(k, E)$, even in the thermodynamic limit, i.e. $\rho(k, E)$ still fluctuates from sample to sample in the macroscopic limit. This property clearly indicates that $\alpha = 1$ is a special value for these models, not only because the shape of $\overline{\rho(k, E)}$ changes, but also because it becomes a non-self-averaging quantity.

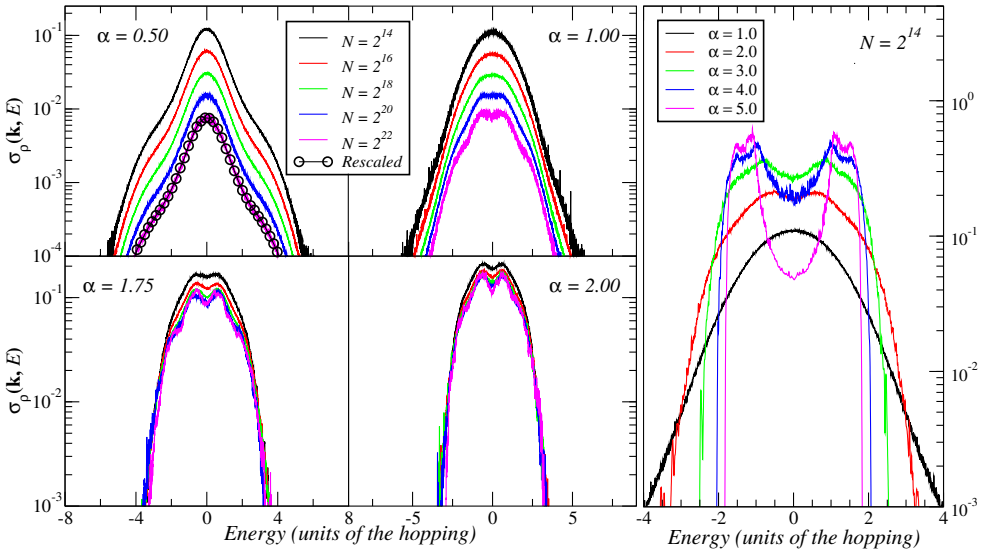

Figure 4.7: The standard deviation of the spectral function at $k = \pm\frac{\pi}{2}$, for $\alpha = 0.5$ (upper left panel), $\alpha = 1.0$ (upper right panel), $\alpha = 1.75$ (lower left panel) and $\alpha = 2.0$ (lower right panel). For $\alpha = 0.5$ the consecutive curves are shown to collapse when rescaled by a factor of $N^{-1/2}$ (black dots). For $\alpha > 1$, the curves coalesce to a non-zero limiting profile and no qualitative change of behavior is seen across $\alpha = 2$. In the extreme right panel, we show the decrease of the standard deviation for larger values of α (at a fixed size). All the calculations where done with $\sigma_\varepsilon = 1$.

In Fig. 4.7, we can also see an example of the same calculation done for $\alpha = 2$, where no qualitative changes in the scaling behavior of standard deviation of the spectral function

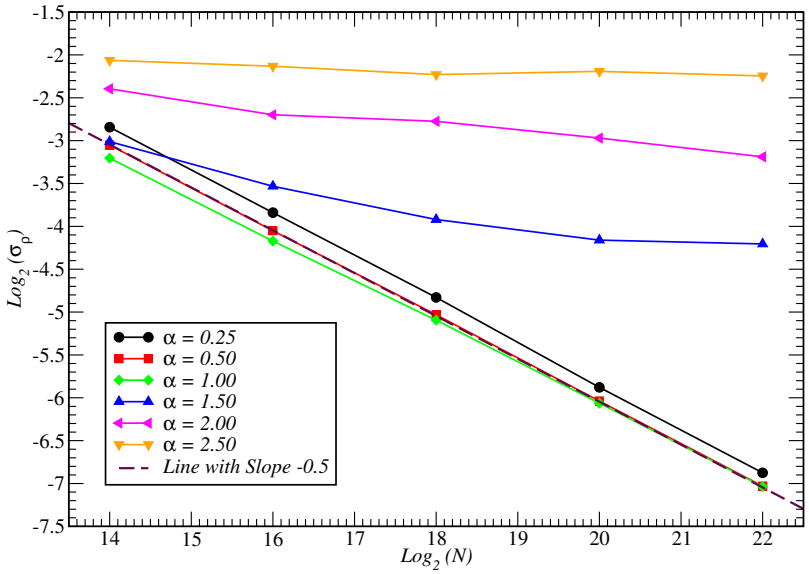

Figure 4.8: Scaling of the standard deviation of $\rho(k, E)$ for $k = \frac{\pi}{2}$ and $E = 0$, as a function of the system's size. The dashed line stands for the usual $N^{-1/2}$ scaling.

(σ_ρ) can be seen. To sum up these results, we present in Fig. 4.8, a plot showing the scaling of σ_ρ at the central energy, with the increase in the chain size.

4.4 Analytical Results and Discussion

If the initial plane-wave excitation state at $t = 0$ is $|\psi(0)\rangle = |k\rangle$, the amplitude that the state at time t is still the same is $\langle k| e^{-i\mathcal{H}t/\hbar} |k\rangle$. Using a complete set of energy eigenstates $\{|\psi_\beta\rangle : \beta = 0, \ldots, N-1\}$, we can see that this amplitude is the Fourier transform of the spectral function defined in Eq. 2.36:

$$\begin{aligned}
\langle k| e^{-i\mathcal{H}t/\hbar} |k\rangle &= \sum_\beta e^{-iE_\beta t/\hbar} |\langle \psi_\beta | k\rangle|^2 \\
&= \int_{-\infty}^{+\infty} dE e^{-iEt/\hbar} \sum_\beta |\langle \psi_\beta | k\rangle|^2 \, \delta(E - E_\beta) \\
&= \int_{-\infty}^{+\infty} dE e^{-iEt/\hbar} \rho(k, E). \qquad (4.23)
\end{aligned}$$

Expanding both sides in powers of t and averaging over disorder, we get the following expression for the n^{th}-moment of the disorder-averaged spectral function $\overline{\rho(k, E)}$:

$$\overline{\langle k| \mathcal{H}^n |k\rangle} = \int_{-\infty}^{+\infty} dE E^n \overline{\rho(k, E)}. \qquad (4.24)$$

The Hamiltonian is the one defined in Eq. 2.1 and can be written as $\mathcal{H} = \mathcal{H}_0 + \mathcal{V}$ where

$$\mathcal{H}_0 = \sum_k E_k \left|k\right\rangle \left\langle k\right| \tag{4.25a}$$

$$\mathcal{V} = \sum_m \varepsilon_m \left|\varphi_m\right\rangle \left\langle \varphi_m\right|, \tag{4.25b}$$

with the band Hamiltonian $\mathcal{H}_0$ being diagonal in the Bloch basis, and the disordered potential, $\mathcal{V}$, in the local Wannier basis. In the calculation of $\langle k| \mathcal{H}^n |k\rangle$, we will assume that $\mathcal{H}_0 |k\rangle = E_k |k\rangle = 0$. This is strictly true for the states in the center of the band (i.e $k = \pm\pi/2$), for which we calculated numerically the spectral function. However, this assumption implies no loss of generality, since for an arbitrary value k, we can add an irrelevant constant to $\mathcal{H}$,

$$\mathcal{H}_0 \to \mathcal{H}_0 := \sum_{k'} \left(E_{k'} - E_k\right) \left|k'\right\rangle \left\langle k'\right|, \tag{4.26}$$

such that $\mathcal{H}_0 |k\rangle = 0$, remains true. The calculation will show that changing k only shifts the spectral function in energy.

4.4.1 Gaussian case

As a justification for our numerical results, we managed to calculate the average spectral function for the infinite chain, with a Gaussian model of correlated disorder. Generally, our analytical results will be valid in the limits when $2\pi/N \ll q_c \ll \pi$ and $q_c \ll \sigma_\varepsilon/\hbar v_k$.

4.4.1.1 Lowest Order Terms

To illustrate the gist of the argument, we begin by looking at the lowest order moments, using the Eq. 4.24. It is obvious that for $n = 1$ the result is zero, because $\mathcal{H}_0 |k\rangle = 0$ and $\overline{\mathcal{V}} = 0$. For $n = 2$,

$$\begin{aligned}
\overline{\langle k| \mathcal{H}^2 |k\rangle} &= \overline{\langle k| (\mathcal{H}_0 + \mathcal{V})(\mathcal{H}_0 + \mathcal{V}) |k\rangle} \\
&= \overline{\langle k| \mathcal{H}_0^2 + \mathcal{H}_0\mathcal{V} + \mathcal{V}\mathcal{H}_0 + \mathcal{V}^2) |k\rangle} \qquad (4.27) \\
&= \overline{\langle k| \mathcal{V}^2 |k\rangle}, \qquad (4.28)
\end{aligned}$$

Resolving the identity in the Bloch basis,

$$\overline{\langle k| \mathcal{H}^2 |k\rangle} = \sum_q \overline{\langle k| \mathcal{V} |k+q\rangle \langle k+q| \mathcal{V} |k\rangle}. \tag{4.29}$$

Recalling Eq. 2.11,

$$\overline{\langle k| \mathcal{H}^2 |k\rangle} = \sum_q V^2(q) = \sigma_\varepsilon^2, \tag{4.30}$$

By the same arguments, in the third moment only one term survives:

$$\begin{aligned}\overline{\langle k|\,\mathcal{H}^3\,|k\rangle} &= \overline{\langle k|\,\mathcal{V}\mathcal{H}_0\mathcal{V}\,|k\rangle} \\ &= \overline{\langle k|\,\mathcal{V}\,|k+q\rangle\,\langle k+q|\,\mathcal{H}_0\,|k+q\rangle\,\langle k+q|\,\mathcal{V}\,|k\rangle} \qquad (4.31)\\ &= \sum_q V^2(q)E_{k+q}, \qquad (4.32)\end{aligned}$$

where $\mathcal{H}_0\,|k+q\rangle = E_{k+q}\,|k+q\rangle$. In the thermodynamic limit, the sum over q turns into an integral and if $q_c \ll \pi$, we can extend the integration range to $q \in\,]-\infty, \infty[$ and expand $E_{k+q} \approx \hbar v_k q$. In this case, the integrand is odd in q and the right-hand side of Eq. 4.32 vanishes upon integration.

Finally, we tackle the 4^{th}-moment (the last, before presenting the general argument), whose the only non-zero terms are

$$\begin{aligned}\overline{\langle k|\,\mathcal{H}^4\,|k\rangle} &= \overline{\langle k|\,(\mathcal{H}_0+\mathcal{V})^4\,|k\rangle} \qquad (4.33)\\ &= \overline{\langle k|\,\mathcal{V}\mathcal{H}_0^2\mathcal{V}\,|k\rangle} + \overline{\langle k|\,\mathcal{V}^4\,|k\rangle}. \qquad (4.34)\end{aligned}$$

Using the same technique as above, the first term is

$$\sum_q V^2(q)E_{k+q}^2 = \sum_q V^2(q)\left(\hbar v_k q\right)^2, \qquad (4.35)$$

which is a complete Gaussian integral (in the limit $q_c \ll \pi$), whose value is

$$\langle k|\,\mathcal{V}\mathcal{H}_0^2\mathcal{V}\,|k\rangle = \sigma_\varepsilon^2\left(\hbar v_k q\right)^2. \qquad (4.36)$$

On the other hand, the term containing the 4^{th} power of $\mathcal{V}$ is

$$\begin{aligned}\overline{\langle k|\,\mathcal{V}^4\,|k\rangle} = &\sum_{q_1,q_2,q_3} V(q_1)V(q_2)V(q_3)V(-q_1-q_2-q_3)\\ &\times\overline{e^{i\phi_{q_1}}e^{i\phi_{q_2}}e^{i\phi_{q_3}}e^{i\phi_{-q_1-q_2-q_3}}},\end{aligned}$$

The averages of these random phase factors are discussed in the Appendix. A. In particular, we show that, in the thermodynamic limit ($N\to\infty$), the expression above reduces to

$$\overline{\langle k|\,\mathcal{V}^4\,|k\rangle} = 3\left(\sum_q V^2\left(q\right)\right)^2 = 3\sigma_\varepsilon^4. \qquad (4.37)$$

Finally, by looking at the Eqs. 4.36 and 4.37, we see that, as long as $\sigma_\varepsilon^2 \gg \left(\hbar v_k q_c\right)^2$, we can ignore terms that have insertions of $\mathcal{H}_0$. Then, we simply write $\overline{\langle k|\,\mathcal{H}^4\,|k\rangle}$ as:

$$\overline{\langle k|\,\mathcal{H}^4\,|k\rangle} \approx \overline{\langle k|\,\mathcal{V}^4\,|k\rangle} = 3\sigma_\varepsilon^4. \qquad (4.38)$$

4.4.1.2 General Expression for the Moments of $\rho(k, E)$

Inspired on the results above, we argue that the general form of the terms in Eq. 4.24 is:

$$\overline{\langle k|\,\mathcal{H}^{2p}\,|k\rangle} \approx \overline{\langle k|\,\mathcal{V}^{2p}\,|k\rangle}, \tag{4.39}$$

$$\overline{\langle k|\,\mathcal{H}^{2p+1}\,|k\rangle} \approx 0. \tag{4.40}$$

Furthermore, in the Appendix. A we show that the averages $\overline{\langle k|\,\mathcal{V}^{2p}\,|k\rangle}$ have the following general form

$$\overline{\langle k|\,\mathcal{V}^{2p}\,|k\rangle} = (2p-1)!!\left(\sigma_\varepsilon^2\right)^p\left[1+\mathcal{O}\left(\frac{1}{N}\right)\right]. \tag{4.41}$$

Using the Eqs. 4.39-4.41, in the thermodynamic limit ($N \to \infty$), we can rebuild the entire Taylor series for the averaged diagonal propagator, and re-sum it as follows:

$$\begin{aligned}
\overline{\langle k|\,e^{-i\mathcal{H}t/\hbar}\,|k\rangle} &= \sum_{p=0}^{\infty}\frac{1}{(2p)!}\left(\frac{-it}{\hbar}\right)^{2p}\overline{\langle k|\,\mathcal{V}^{2p}\,|k\rangle} \\
&= \sum_{p=0}^{\infty}\frac{(-1)^p(2p-1)!!}{(2p)!}\left(\frac{\sigma_\varepsilon^2 t^2}{\hbar^2}\right)^p \\
&= \sum_{p=0}^{\infty}\frac{1}{2^p p!}\left(-\frac{\sigma_\varepsilon^2 t^2}{\hbar^2}\right)^p = e^{-\sigma_\varepsilon^2 t^2/2\hbar^2}
\end{aligned}$$

The spectral function is the time-domain Fourier transform of this last expression, yielding

$$\overline{\rho(k=\pm\frac{\pi}{2},E)} = \frac{1}{\sqrt{2\pi\sigma_\varepsilon^2}}e^{-\frac{E^2}{2\sigma_\varepsilon^2}}, \tag{4.42}$$

which agrees with the results found in our numerical calculations, using the KPM.

For the sake of completeness, we also state the result for a general value of k, which can be obtained from Eq. 4.42 simply by shifting the energy variable by the corresponding band energy E_k of that state, i.e.

$$\overline{\rho(k,E)} = \frac{1}{\sqrt{2\pi\sigma_\varepsilon^2}}e^{-\frac{(E-E_k)^2}{2\sigma_\varepsilon^2}}. \tag{4.43}$$

In conclusion, we found that, if $q_c \ll \pi$ and $(v_k q_c)^2 \ll \sigma_\varepsilon^2$, then the disorder-averaged spectral function, in the thermodynamic limit, will have a Gaussian shape. This is true, even if the disorder strength (measured by σ_ε) is small, as long as this is matched by a decrease of q_c and corresponding increase of the correlation length of the potential. For instance, the mean free path, estimated by $\ell = \hbar v_k/\sigma_\varepsilon$ can still be much larger that the lattice parameter, so long as $\ell < \xi$, where ξ is the disorder correlation length.

4.4.1.3 Emergence of the Classical Limit for the Spectral Function

We were able to establish precise conditions in which the classical limit of the spectral function, found by Trappe *et. al.* [63], appears. The statement of this limit is equivalent to Eq. 4.39, and reads ($E_k = 0$)

$$\overline{\langle k|\, e^{-i\mathcal{H}t/\hbar}\, |k\rangle} = \overline{\langle k|\, e^{-i\mathcal{V}t/\hbar}\, |k\rangle}. \tag{4.44}$$

so that

$$\overline{\rho(k,E)} = \int dt e^{iEt/\hbar} \overline{\langle k|\, e^{-i\mathcal{V}t/\hbar}\, |k\rangle}. \tag{4.45}$$

Using the Wannier basis (eigenbasis of $\mathcal{V}$) and its transformation law to the Bloch basis $\langle \varphi_n|k\rangle = \exp(ikn)/\sqrt{N}$, we can rewrite the above equation (with $E_k = 0$) as

$$\begin{aligned}\overline{\langle k|\, e^{-i\mathcal{V}t/\hbar}\, |k\rangle} &= \sum_{n,m} \overline{\langle k|\varphi_n\rangle \langle \varphi_n|\, e^{-i\mathcal{V}t/\hbar}\, |\varphi_m\rangle \langle \varphi_m|k\rangle} \\ &= \frac{1}{N}\sum_m \overline{e^{-i\varepsilon_m t/\hbar}} = \int dE P(E) e^{-iEt/\hbar},\end{aligned} \tag{4.46}$$

where $P(E)$ is the probability distribution of a site energy. Comparing the above with Eq. 4.23, we have

$$\overline{\rho(k,E)} = P(E). \tag{4.47}$$

Thus, the averaged spectral function is just the probability distribution of a single site energy. As it is clear for the definition of the disordered potential (Eq. 2.5), the distribution $P(E)$ must be a Gaussian according of the Central Limit Theorem.

4.4.2 Power-Law Correlated Disorder

4.4.2.1 Validity of the Classical Limit

In the case of Power-law correlated disorder, the argument leading to the Eq. 4.39 still holds, as long as $\alpha > 1$, but requires a slightly different formulation. To see how this comes about, let us consider Eq. 4.35 as an example. In this case, we have

$$\begin{aligned}\sum_q V^2(q) E_{k+q}^2 &= \frac{2\pi}{N} A^2(\alpha) \sum_{q\neq 0} \frac{1}{|q|^\alpha} \left[E_{k+q}\right]^2 \\ &= \frac{\sigma_\varepsilon^2}{2\zeta(\alpha)} \sum_{p=1}^{N/2} \frac{1}{p^\alpha} E_{k+2\pi p/N}^2.\end{aligned} \tag{4.48}$$

As before, if we expand E_{k+q} in powers of p, we get terms of the form

$$\left[\frac{1}{n!}\frac{d^n E_k}{dk^n}\right] \frac{\sigma_\varepsilon^2}{2\zeta(\alpha)} \left(\frac{2\pi}{N}\right)^n \sum_{p=1}^{N/2} \frac{1}{p^{\alpha-n}} \tag{4.49}$$

If $\alpha - n > 1$ the sum above is convergent and the result vanishes, in the large-N limit, as N^{-n}. On the other hand, if $\alpha - n < 1$ the sum diverges, but instead it can be written as an integral over the First Brillouin Zone, as follows

$$\left(\frac{2\pi}{N}\right)^n \sum_{p=1}^{N/2} \frac{1}{p^{\alpha-n}} = \left(\frac{2\pi}{N}\right)^{\alpha-1} \int_{\frac{2\pi}{N}}^{\pi} dq \frac{1}{q^{\alpha-n}}$$
$$= \frac{1}{n-\alpha+1}\left[\frac{2^{\alpha-1}\pi^n}{N^{\alpha-1}} - \left(\frac{2\pi}{N}\right)^n\right]. \tag{4.50}$$

Both terms in the equation above go to zero in the thermodynamic limit, since $\alpha > 1$ and $n \geq 1$. This argument is obviously true for every term in $\langle k| \mathcal{H}^n |k\rangle$, containing insertions of $\mathcal{H}_0$. Hence, in the $N \to \infty$ limit, the only finite contributions come from the all-$\mathcal{V}$ terms, and we re-obtain the classical result expressed in Eq. 4.47.

In this limit the spectral function can only depend on the parameters of the disordered potential, namely σ_ε and α. Since α is dimensionless, there is a single energy scale, σ_ε, in $\overline{\rho(k,E)}$. The scaling of Eq. 4.22, illustrated in Fig. 4.6, follows at once. It should be noted, however, that as α gets closer to 1, this scaling is not observed numerically. This is due to finite size effects that we have not accounted for. An example is the very slow convergence of $\sum_{p=1}^{N/2} p^{-\alpha}$ to $\zeta(\alpha)$. For $\alpha = 1.1$, for instance, the truncation error is still of order 10% for $N \sim 10^{10}$.

4.4.2.2 The Limiting Cases ($\alpha \to 1$ and $\alpha \to +\infty$) And The Double-Peaked Shape

Despite the validity of the classical limit for the averaged spectral function, we have shown in the Appendix. A that it is not clear how to obtain a closed form for the n^{th}-moment of $\overline{\rho(k,E)}$ even in this limit. Nevertheless, the limit $\alpha \to 1^+$ revealed itself as very special case, where the exact averaged spectral function is found to be a Gaussian,

$$\overline{\rho(k,E)} = \frac{1}{\sqrt{2\pi\sigma_\varepsilon^2}} e^{-\frac{(E-E_k)^2}{2\sigma_\varepsilon^2}}. \tag{4.51}$$

This result is consistent with the numerical results obtained in the last section (see fig. 4.5).

For $\alpha > 1$, however, the higher cumulants of the spectral function cease to be zero, and $\overline{\rho(k,E)}$ drifts away from a Gaussian shape. For illustration, we have calculated the 4^{th} – cumulant of the averaged spectral function, as a function of the exponent α . This has the following definition:

$$m_4 = \int_{-\infty}^{+\infty} dE E^4 \overline{\rho\,(k,E)} - 3\left[\int_{-\infty}^{+\infty} dE E^2 \overline{\rho\,(k,E)}\right]^2, \tag{4.52}$$

and can be directly computed using the expressions obtained in the Appendix. A, *i.e.*

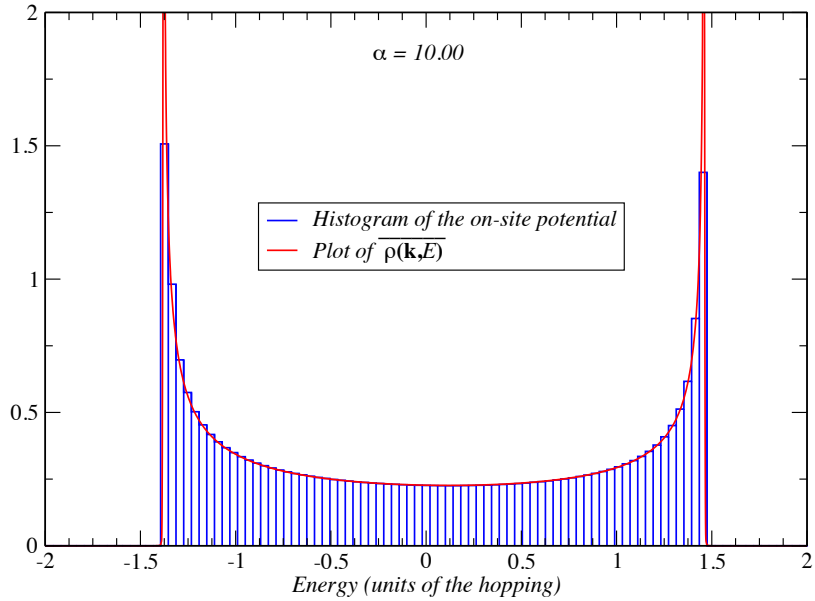

Figure 4.9: Comparison of the local energy distribution $P(E)$ and the disorder-averaged spectral function $\overline{\rho(k,E)}$, obtained for a system of size $N = 2^{17}$ with $M = 8192$ Chebyshev expansion coefficients and a single realization of disorder. The calculation was done for $k = \pi/2$.

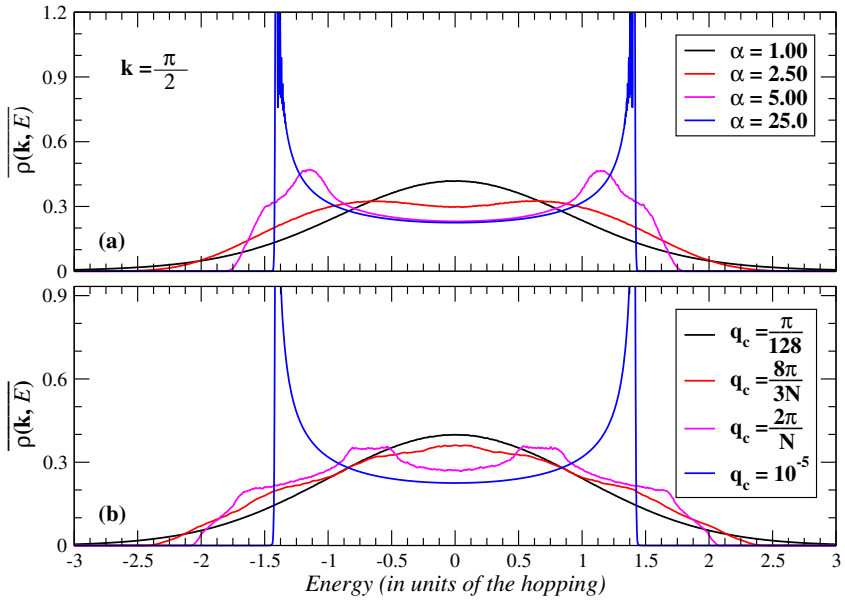

Figure 4.10: Spectral function $\rho(\mathbf{k}, E)$ for the disordered system of size $N = 2^{14}$ with 8192 Chebyshev moments for different values of α (top panel) and q_c (lower panel). The limits $\alpha \gg 1$ and $q_c \ll 2\pi/N$ are identical.

$$m_4(\alpha) = -3\sigma_\varepsilon^4 \frac{\zeta(2\alpha)}{2\zeta(\alpha)}. \tag{4.53}$$

Other than explaining the deviations from the Gaussian shape that we found in the numerical plots of $\overline{\rho(k,E)}$, these effects have another striking consequence. According to our earlier remarks, in the classical limit, the averaged spectral function is the same as the probability distribution of the site energies [63]. Since the value of the disordered potential in a single point is described as a sum of a large number of independent random variables (see Eq. 2.24), the non Gaussian shape shows that these do not obey the **Central Limit Theorem**. To see how this comes about, we start by looking at Eq. 4.10, where

$$\sigma_\varepsilon^2 \propto \sum_{p=1}^{N/2} \frac{1}{p^\alpha}. \tag{4.54}$$

When $\alpha > 1$, this sum is convergent in the $N \to \infty$ limit, which means that only a number of $\mathcal{O}(1)$ of terms actually contribute to the variance of the local disorder ε_n. Furthermore, as α increases, this sum is dominated by less and less terms, meaning that we are never in the conditions of the central limit theorem (which assumes a large number of summed random independent variables).

This becomes particularly clear in the extreme case $\alpha \to \infty$. In this limit, the local value of the disordered potential is dominated by a single term, $p = 1$, and the disorder is a static cosine potential with a wavelength N and a random phase,

$$\varepsilon_n \sim \sqrt{2}\sigma_\varepsilon^2 \cos(\frac{2\pi n}{N} + \phi_{2\pi/N}). \tag{4.55}$$

The corresponding probability density function can be calculated, yielding the expression:

$$P(E) = \frac{1}{\pi} \frac{1}{\sqrt{2\sigma_\varepsilon^2 - E^2}}. \tag{4.56}$$

As an illustration, we depict in Fig. 4.9 the KPM calculated the spectral function for $\alpha = 10$, and the normalized histogram of site energies for a single realization of disorder. As α increases above 1, the spectral function smoothly approaches the limiting form of Eq. 4.56, by first displaying a two peaked shape as illustrated in Fig. 4.10a.

The expression of Eq. 4.56 also corresponds to the one we obtain numerically for Gaussian disorder case when $q_c \ll 2\pi/N$ (see Fig. 4.10.b). In either case, of course, a single value q dominates the sum

$$\varepsilon_n = 2\sum_{q>0} V(q)\cos\left(qn + \phi_q\right) \tag{4.57}$$

and the two models of disorder cannot be distinguished.

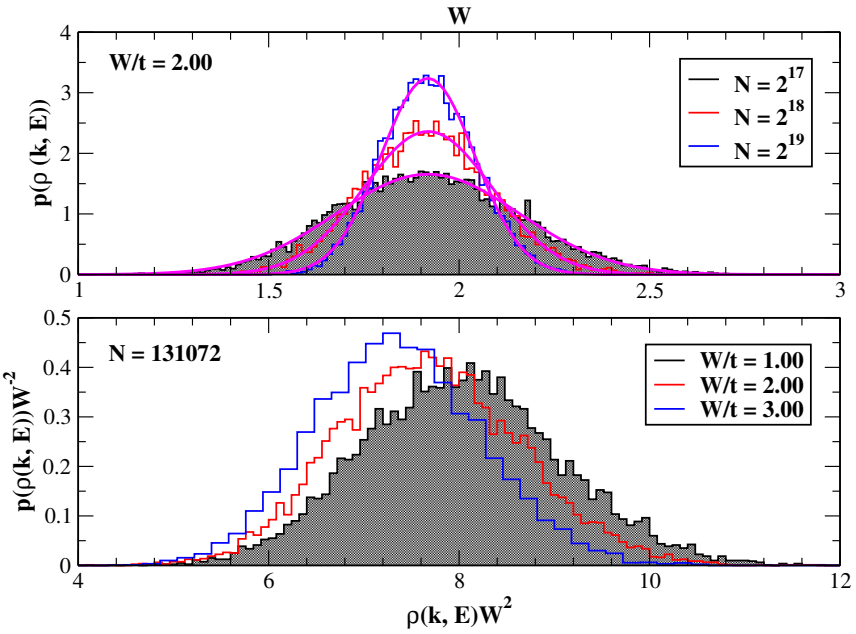

Figure 4.11: The spectral function distributions $p(\rho(\mathbf{k}, E))$ of 1D Anderson model with different system sizes for $W/t = 2$ (top panel). The spectral function distributions for the system of size $N = 2^{17}$, with various disorder strength (lower panel). The calculations are carried out for $M = 8192$ Chebyshev moments and by keeping PBC.

4.5 Probing MIT with Spectral Function

The understanding of Anderson localization has been significantly enriched by studying the statistical properties of conductance [64, 65, 16], inverse participation ratio (IPR) [66], and local density of states (LDOS) [44, 67]. For instance, the probability distributions of the conductance show a universal and a Gaussian nature in the metallic regime, while a system-size dependent and a log-normal distribution behavior is found in the insulating regime.

We are now going to address the scaling behavior of the distribution of spectral function for a non-interacting disordered system. It is useful to study a very well-established one-dimensional model as a guiding example. In this model, an infinitesimal amount of disorder can confine all the energy eigenstates of an electron to a finite region of space. This insulating character of the system has been probed by incorporating various physical quantities.

What would be the probability distribution of the spectral function in this limit? We have pointed out that this distribution depends on the microscopic details of the system as depicted in Fig. 4.11 (upper panel). In fact, the distribution tends to concentrate more in a narrow Gaussian peak around its mean value with increasing system size.

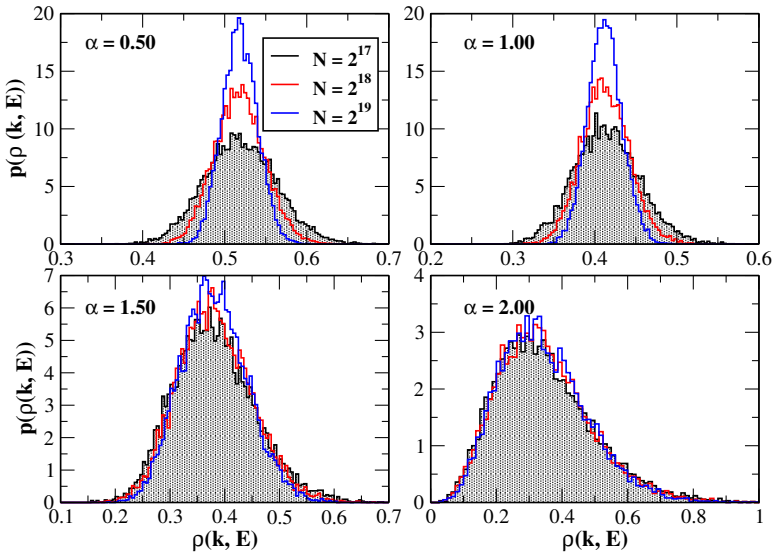

Figure 4.12: The distributions of spectral function for one-dimensional lattice with power-law correlated disorder of unit variance $\sigma_\epsilon^2 = 1$, for $\alpha = 0.50,\ 1.00,\ 1.50,$ and 2.00 at the band's center. The distribution of spectral functions is size independent for $\alpha \geq 2$.

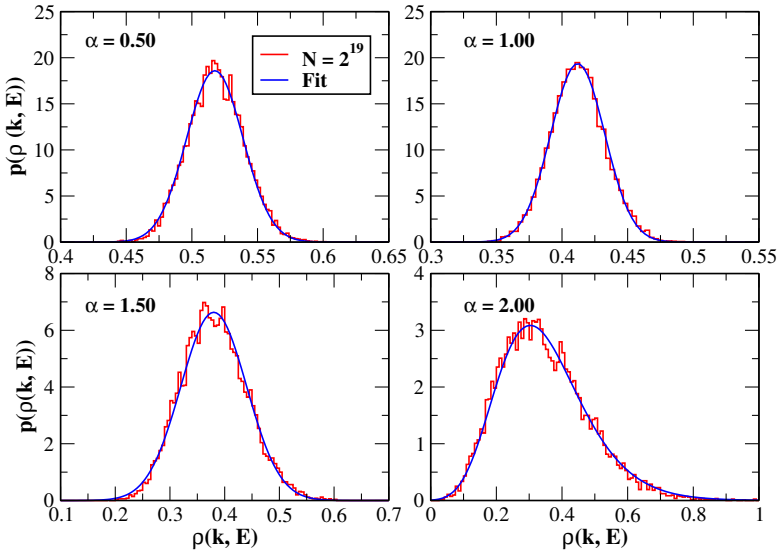

Figure 4.13: The distributions of spectral function for one-dimensional lattice with power-law correlated disorder of unit variance $\sigma_\epsilon^2 = 1$, for $\alpha = 0.50,\ 1.00,\ 1.50,$ and 2.00 at the band's center. The spectral functions are reasonably fitted by a Gaussian function for $\alpha < 2$. For $\alpha = 2$, the distribution is well fitted by a log-normal function.

This system-size dependence nature of the spectral function distribution agree with the previously obtained result [44] for the distribution of LDOS in the localized regime. However, it is figured out that unlike LDOS, which has a log-normal distribution form, the spectral function distribution has a Gaussian nature in this limit. Moreover, the spectral function distribution starts to shrink and moves toward zero with increasing disorder for a fixed system size as presented in Fig. 4.11 (lower panel).

We now characterize the physical behavior of power-law correlated disorder model (see subsection. 2.1.1.4) from the perspective of spectral function distributions. The spectral function distributions show system size-dependent nature for $\alpha < 2$ as illustrated in Fig. 4.12. This is the property of the system in insulating regime, and has been already shown for the 1D Anderson model (see Fig. 4.11). On other hand, the distributions turned out to be universal for $\alpha \geq 2$, which is a clear indication of the existence of extended states in the system [44]. In addition, the spectral function distributions are symmetric and Gaussian distributed around the mean value in the localized regime as shown in Fig. 4.13. In contrast, the distributions are found highly asymmetric and follows a log-normal distribution for the extended states.

By studying the spectral function distributions of power-law correlated disorder model (de Moura-Lyra model), we verified that the correlation-induced metal-insulator transition happens at correlation exponent $\alpha = 2$ [4, 17]. However, most recently [27] we investigated that this system undergoes localization-delocalization transition in the perturbative regime at $\alpha = 1$ in the thermodynamic limit, will be discuss in next chapter.

Chapter 5

Delocalization in the de Moura-Lyra Model

This chapter, based on [27], examines the physical properties of a one-dimensional tight-binding non-interacting lattice with diagonal power-law correlated disorder (de Moura-Lyra model). We will study the normalized two point correlator of the power-law correlated disorder for $\alpha \lesssim 1$ in both finite and infinite system limit and will discuss the normalized single-bond discontinuity parameter, which measures the variance of the nearest neighbor onsite energies difference.

In addition, we will calculate the localization length of the system by using a generalized Thouless formula derived by Izrailev and Krokhin [43]. The localization length in the perturbative regime diverges as $(1-\alpha)^{-1}$ in the thermodynamic limit.

We will review the Landauer formalism for the calculations of conductance, g[1]. At first we will compute the conductance distributions of a well-established one-dimensional Anderson model. We will calculate the localization length of the Anderson model by fitting the mean of $-\ln \mathrm{g}$, and will compare with the analytical perturbative results. In addition, we will verify that the variance of $-\ln \mathrm{g}$ is proportional to $1/\sqrt{N}$, where N is the system size.

Our main focus is to investigate the delocalization transition in the de Moura-Lyra model at zero temperature. In particular, we will report the first numerical evidences that a localization-delocalization transition happens at $\alpha = 1$, where the localization length (measured from the scaling of the conductance) is shown to diverge as $(1-\alpha)^{-1}$ in the thermodynamic limit. These numerical results are confirmed by analytical perturbative calculations of the localization length. The persistent finite-size scaling of the data is shown to be caused by a very slow convergence of the nearest-neighbor correlator to its infinite-size limit, and controlled by the choice of a proper scaling parameter. This last conclusion leads to the re-interpretation of the localization in these models to be caused by an effective Anderson uncorrelated model at small length-scales.

[1] $\mathrm{g} = \mathrm{G}\hbar/e^2$, where g is a dimensionless conductance

At the end of the chapter, we will implement and discuss the kernel polynomial method for the localization length of the de Moura-Lyra model. In fact, finding an analytical expression for the localization length of the model and comparing with the KPM estimates of the localization length is one of the intents of this chapter. The main advantage of using KPM is that it compute the localization length with a controlled accuracy and a low computational complexity.

5.1 Correlation Function of the Local Disorder

To study the thermodynamic limit ($N \to \infty$) properties of the system with power-law correlated disorder potential (see Eq. 2.24), for $\alpha \lesssim 1$, we replaced all the sums over q by integrals (see Eq. 4.2) and analytically calculate the normalized two point correlator, $\Gamma(\alpha, r)$ of the random potential, as given by

$$\Gamma(\alpha, r) = \frac{A^2(\alpha)}{\sigma_\varepsilon^2} \int_0^\pi \frac{\cos qr}{|q|^\alpha} dq, \qquad q > 0, \tag{5.1}$$

$$= \frac{A^2(\alpha)}{2\sigma_\varepsilon^2} \int_{-\pi}^\pi \frac{e^{-iqr}}{|q|^\alpha} dq, \qquad q \neq 0, \tag{5.2}$$

where α is the correlation exponent, and $q = 2\pi p/N$, $p \in \mathbb{Z} \setminus \{0\}$. For the case when $\alpha < 1$, the corresponding integral does not have a low-q singularity and the situation is be very similar to a system with uncorrelated disorder. The local variance (see Eq. 4.3) has the form

$$\sigma_\varepsilon^2 = 2A^2(\alpha) \int_0^\pi \frac{1}{|q|^\alpha} dq, \qquad q > 0, \tag{5.3}$$

$$= 2A^2(\alpha) \frac{\pi^{1-\alpha}}{1-\alpha}. \tag{5.4}$$

where $A(\alpha)$ is the normalization constant, and can be obtained as

$$A(\alpha) = \sigma_\varepsilon \sqrt{\frac{(1-\alpha)\pi^{\alpha-1}}{2}}. \tag{5.5}$$

The auto-correlation function can be rewritten as

$$\Gamma(\alpha, r) = \frac{(1-\alpha)\pi^{\alpha-1}}{2} \int_{-\pi}^\pi \frac{e^{-iqr}}{|q|^\alpha} dq, \qquad q \neq 0. \tag{5.6}$$

Eq. 5.6, can be simplified as

$$= (1-\alpha)\pi^{\alpha-1} \int_0^\pi \frac{1}{|q|^\alpha} \cos(qr) dq = (1-\alpha)(\pi r)^{\alpha-1} \int_0^{\pi r} \frac{1}{|z|^\alpha} \cos(z) dz, \tag{5.7}$$

$$=_1 F_2(\frac{1-\alpha}{2}; \frac{1}{2}, \frac{3-\alpha}{2}; -(\frac{\pi r}{2})^2). \tag{5.8}$$

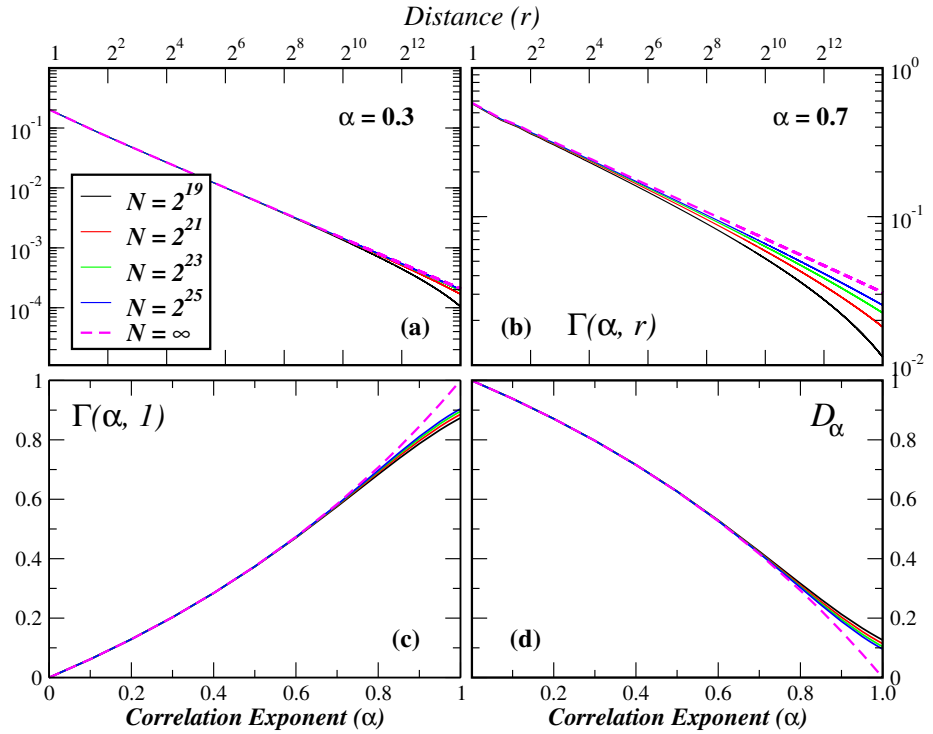

Figure 5.1: Correlation function of the power-law decay type correlated disorder potential as a function of lattice sites for (a) $\alpha = 0.3$ and (b) $\alpha = 0.7$. The (c) normalized correlator and (d) single-bond discontinuity as a function of α for various system size.

where ${}_pF_q$ is a hyper-geometric series, given by

$$ {}_pF_q\left(a_1, a_2, ...a_n; b_1, b_2, ...b_n; z\right) = \sum_{n=0}^{\infty} \frac{(a_1)_n (a_2)_n ... (a_p)_n}{(b_1)_n (b_2)_n ... (b_p)_n} \frac{z^n}{n!}. \tag{5.9} $$

It is clear from Eq. 5.8, that the pair correlation function is size independent. Moreover, the correlation function for various α in the limit of $\alpha < 1$, is always positive (no anti correlation exist).

In the asymptotic limit, $1 \ll r \ll N$, the auto correlation function has a rather simple asymptotic expansion in r,

$$ \Gamma(\alpha, r) = (1-\alpha)\pi^{\alpha-1} \int_0^{\pi} \frac{1}{|q|^{\alpha}} \cos(qr) dq, \tag{5.10} $$

$$ = (1-\alpha)(\pi r)^{\alpha-1} \Gamma(1-\alpha) \sin(\frac{\pi\alpha}{2}). \tag{5.11} $$

where $\Gamma(x)$ is a Gamma function of the variable x. The expression Eq. 5.11, shows that there is no anticorrelation in the limit $\alpha < 1$, and the correlations falling-off as $r^{\alpha-1}$ as illustrated in Fig. 5.1 (upper panel).

Other than the slow decay of the correlations at large distances, one also notices that there is a very sharp uncorrelation across a single bond (short-scale noise) as shown in

Fig. 5.1 (lower panel). This features disappear as $\alpha \to 1^-$, but for any smaller value of the exponent it is enough to generate a small scale random noise with an amplitude of the order of σ_ε. An appropriate measure for this noise is the (squared) normalized single-bond discontinuity parameter D_α, defined as

$$D_\alpha \equiv \frac{\overline{(\varepsilon_n - \varepsilon_{n+1})^2}}{2\sigma_\varepsilon^2} = 1 - \Gamma(\alpha, 1). \tag{5.12}$$

This parameter roughly measures the dispersion of onsite energies, relative to the previous value. In the limit, $\alpha \to 1^-$, this quantity may be shown to be proportional to $(1 - \alpha)$.

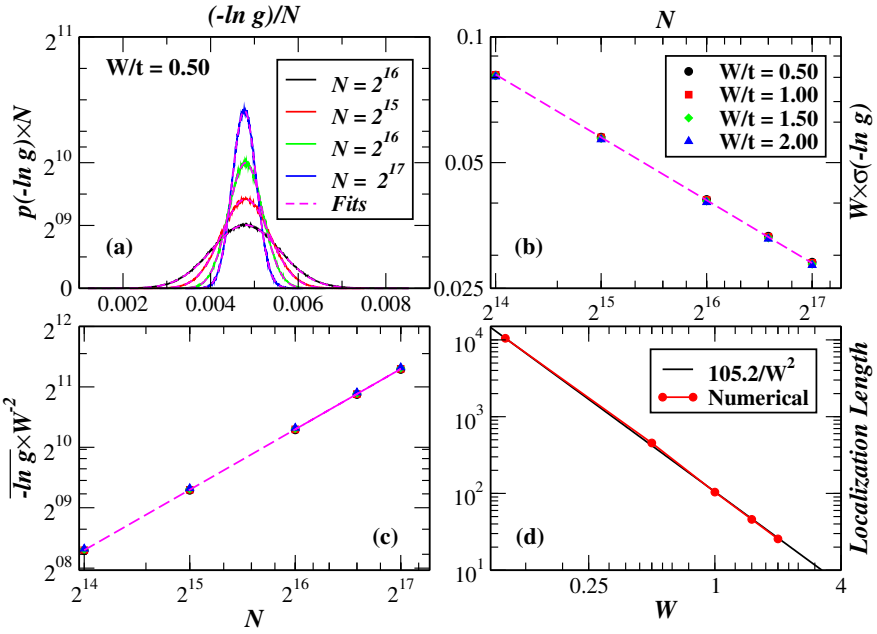

Figure 5.2: (a) The conductance distributions of the one-dimensional Anderson model for various system sizes with $W = 0.50$ at the band's center. The distributions of conductance are very well fitted by a Gaussian function. The rescaled (b) variance and (c) mean of $-\ln g$ vs system size N for various disorder. The variance of $-\ln g$ follow "law of large numbers", $\sigma(-\ln g) \propto 1/\sqrt{N}$. (d) A comparison of localization length obtained by fitting the data in (c) with the theoretical value [3].

Above, all the statistical properties of the disordered potential were calculated in the thermodynamic limit. On the contrary, the two-point correlator of the finite system of size N has the following form [27]

$$\Gamma^N(\alpha, r) = \frac{\sum_{i=1}^{N/2} i^{-\alpha} \cos(\frac{2\pi i r}{N})}{\sum_{i=1}^{N/2} i^{-\alpha}}. \tag{5.13}$$

with an analogous expression for the normalized single-bond discontinuity

$$D_\alpha^N = 1 - \Gamma^N(\alpha, 1). \tag{5.14}$$

In Fig. 5.1 (lower panels), we compare exact correlator and D_α of infinite and finite system of different sample sizes. The very slow convergence towards the thermodynamic limit value is quite evident, especially for values of α close to 1. This very slow convergence of the $\Gamma^N(\alpha, 1)$ or D_α to its limiting value is shown to cause a persistent finite-size scaling of the calculated localization length. This is also the reason for the persistence of the small-scale uncorrelated noise, even when α is very close to 1.

5.2 Localization Length

We study the perturbative calculation of the localization length for one-dimensional tight-binding system with diagonal disorder. This analytical calculation is based on Hamiltonian map approach [68], introduced by Izrailev *et. al.* [43, 3]. The general expression of localization length ξ in units of lattice spacing, is given by [43],

$$\xi^{-1}(k) = \frac{\sigma_\varepsilon^2}{8\sin^2 k}\varphi(k). \tag{5.15}$$

where σ_ε^2 is the variance of the local disorder potential in units of t, and the function $\varphi(k)$ is the Fourier transform of correlator $\Gamma(r)$, of the site potential ε_n. The function $\varphi(k)$ is given by

$$\varphi(k) = 1 + 2\sum_{r=1}^{\infty}\Gamma(r)\cos 2kr. \tag{5.16}$$

where $k = \arccos(E/2)$, is a (positive) wave-number associated to an unperturbed band energy E. For a non-interacting one-dimensional Anderson model, the localization length turns out

$$\xi = \frac{96}{W^2}(1 - \frac{E^2}{4}). \tag{5.17}$$

where the variance of the local disorder potential, $\sigma_\varepsilon^2 = W^2/12$, with $\Gamma(r) = 0$, $r \neq 0$, (the Anderson disorder has no correlation). Eq. 5.17, was found to work well over all energies, except $E = 0$ [2, 69]. This anomaly has also been studied in chapter. 2, where the KPM estimates of localization length revealed a clear deviation from $96/W^2$ at the band center (see Fig. 3.8), and are in good agreement with the numerical results [2, 69], where the correct expression for the localization length of the Anderson model is $105.2/W^2$ [3, 2, 69].

For the case of potentials correlated in space, for instance, a power-law correlated disorder potential, we employ the same generalized Thouless expression (see Eq. 5.15),

for localization length. In this case, the function $\varphi(k)$ in terms of normalized two point correlator $\Gamma(\alpha, r)$ of the correlated disorder potential can be expressed as

$$\varphi(k) = 1 + 2\sum_{r=1}^{\infty} \Gamma(\alpha, r) \cos 2kr, \tag{5.18}$$

$$= \sum_{r=-\infty}^{\infty} \Gamma(\alpha, r) e^{2ikr}, \tag{5.19}$$

Plugging Eq. 5.6 into Eq. 5.19, we get

$$\varphi(k) = \frac{1}{2}\frac{(1-\alpha)}{\pi^{1-\alpha}} \int_{-\pi}^{\pi} \sum_{r=-\infty}^{\infty} \frac{e^{ir(2k-q)}}{|q|^{\alpha}} dq, \tag{5.20}$$

$$= \pi^{\alpha}(1-\alpha) \int_{-\pi}^{\pi} \frac{\delta(2k-q)}{|q|^{\alpha}} dq, \tag{5.21}$$

$$= \pi^{\alpha}(1-\alpha) \frac{1}{|2k|^{\alpha}}. \tag{5.22}$$

Inserting in Eq. 5.15, we obtain

$$\xi^{-1}(k) = \frac{\sigma_{\varepsilon}^2}{8\sin^2 k} \frac{\pi^{\alpha}(1-\alpha)}{|2k|^{\alpha}} \tag{5.23}$$

It is easy to express the localization length in terms of energy E, as [27]

$$\xi(E) = \frac{8}{(1-\alpha)\sigma_{\varepsilon}^2}(1 - \frac{E^2}{4}) \left[\frac{2}{\pi} \arccos \frac{E}{2}\right]^{\alpha}. \tag{5.24}$$

From Eq. 5.24, it is evident that for any value of the band energy, the localization length is finite. However, as $\alpha \to 1^{-}$ this length diverges as $(1-\alpha)^{-1}$, signaling the existence of a global delocalization transition at this point, i.e without generating any mobility edge.

5.3 Conductance

Conductance is an essential ingredient for understanding the transport properties of mesoscopic systems [65, 16]. For a non-interacting Anderson model (of any dimension), the probability distribution of conductance deep in the insulating regime for a finite system follows log-normal distribution function. Moreover, the averaged conductance decays exponentially with increasing system size and vanishes in the thermodynamic limit [64, 65, 16]. On the other hand, the probability distribution of the conductance in the metallic regime is very well described by a Gaussian function for the 2D and 3D Anderson model [64, 16]. Nevertheless, the extended or localized nature of the system can also be characterized by the probability distribution of the logarithm of conductance [16]. It is found that [65], the distributions of the logarithm of conductance follow a Gaussian function for the localized states and a log-normal behavior for the extended states.

The existence of a finite localization length ξ_N leads to a quantum conductance which has a self-averaging log-normal statistics over the ensemble and a typical value that scales exponentially to zero with N/ξ_N. Hence, in order to measure it, we made use of the linearized Landauer formula [60, 61] for the conductance (of a two-terminal device)

$$\mathrm{g}(E_F) = \frac{e^2}{h}(4 - E_F^2)\left|\mathcal{G}^r_{0,N+1}(E_F)\right|^2 . \tag{5.25}$$

where N is the number of sites in the sample, E_F is the Fermi energy and $\mathcal{G}^r$ stands for the retarded real-space Green's function (see chapter 3 for detail). For a given sample of disorder, the $\mathcal{G}^r_{0,N+1}(E_F)$ is calculated by using the recursive Green function method (see in Appendix. C) with the exact surface Green's functions of the leads as boundary conditions.

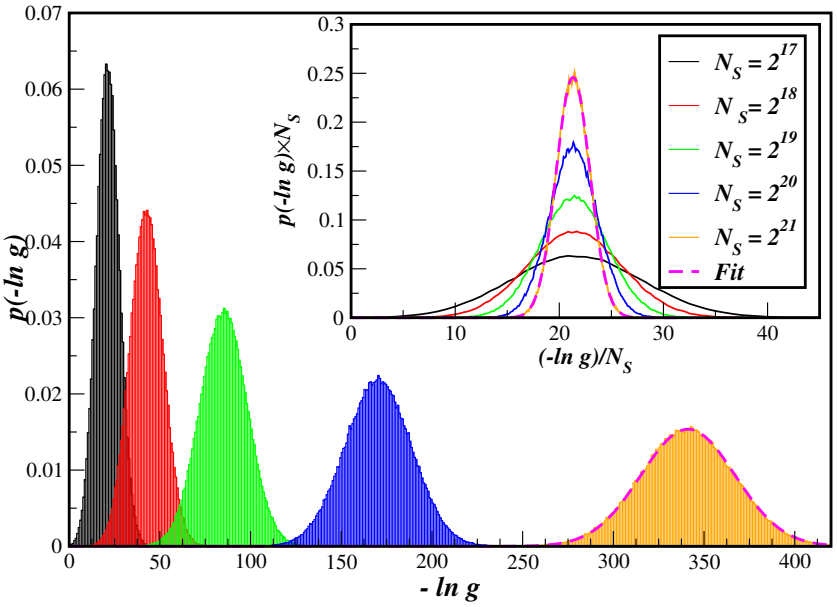

Figure 5.3: The logarithm of conductance distributions of the de Moura-Lyra class of model for various sub-chains N_S, drawn from a system of size $N = 2^{22}$ with 10^5 independent configurations of disorder at the band's center. The random potential is generated for $\alpha = 0.9$ with a variance $\sigma_\varepsilon = 0.10$. The logarithm of conductance distribution, for instance, for $N_S = 2^{21}$, is very well fitted by a Gaussian function. In the inset, we show the rescaled distributions of $(-\ln \mathrm{g})$, making clear that this quantity is self-averaging and with an average which scales linearly with N_S.

5.3.1 Anderson Model

In order to test the Landauer formalism, we calculate the conductance properties of one-dimensional Anderson model. In particular, we compute the distributions of conductance

at zero temperature. The distributions of $-\ln g$, turns out to be Gaussian in the presence of disorder as shown in Fig. 5.2(a). In addition, the distributions are size dependent, which is a clear signature of the existence of localized states of the system. Moreover, we have verified that the scaled variance of $-\ln g$ for a given disorder is proportional to $1/\sqrt{N}$, where N is the size of the system as illustrated in Fig. 5.2(b). This property show self-averaging, and simply means that in thermodynamic limit, a disordered sample will have a conductance equal to one, such that $\ln g = 0$.

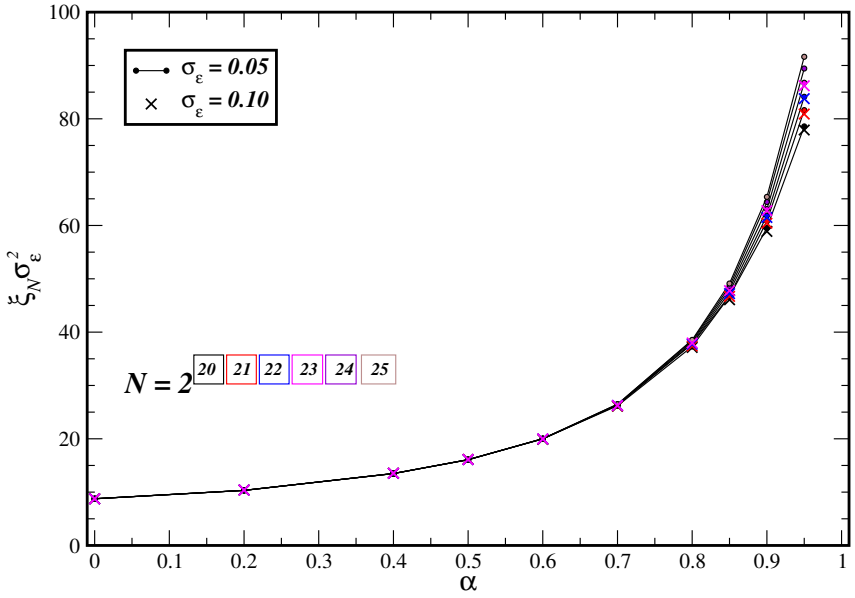

Figure 5.4: The rescaled localization length, $\sigma_\varepsilon^2 \xi_N$, as a function of α of the de Moura-Lyra class of model for different total system N. The localization lengths are obtained by fitting the mean of $-\ln g$.

Furthermore, we have studied the average of $-\ln g$ as a function of system size for various disorder strength as shown in Fig. 5.2(c). The scaled mean of $-\ln g$ for various disorder strength collapse perfectly. Since, all the energy eigenstates are localized in one-dimensional Anderson model, therefore the mean of $-\ln g$ decay exponentially with system size [16], as

$$\overline{-\ln g} := \frac{2N}{\zeta} = \frac{2N}{105.2} W^2, \tag{5.26}$$

$$\overline{-\ln g} W^{-2} = \frac{2}{105.2} N. \tag{5.27}$$

where $\xi = 105.2/W^2$, is the localization length for the Anderson model [3]. From Eq. 5.27, it is clear that the scaled mean of $-\ln g$ is independent of disorder strength and vary

linearly with L. By fitting the data in Fig. 5.2(c) for various disorder, we can obtain the localization length as depicted in Fig. 5.2(d). The numerically obtained localization length is in a very good agreement with theoretical value [3].

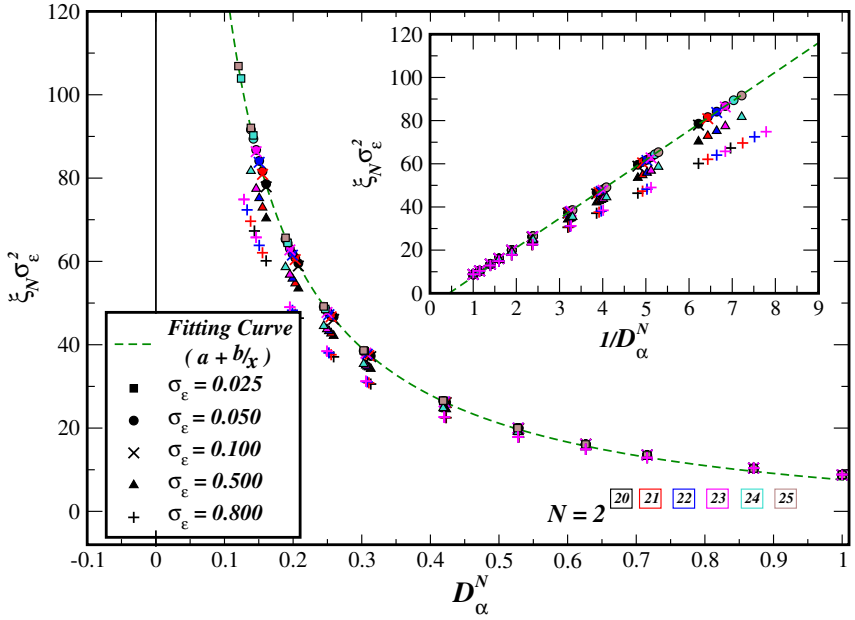

Figure 5.5: The rescaled localization length, $\sigma_\varepsilon^2 \xi_N$, as a function of short-scale normalized discontinuity D_α^N, for different variance of the local disorder σ_ε. The data are perfectly collapsed in the perturbative regime ($\sigma_\varepsilon \leq 0.1$) and very well fitted with a curve $y = a + b/x$ (green dashed curve). However, the data for $\sigma_\varepsilon = 0.50$, 0.80 already show a deviation from this fitted curve, due to the breakdown of perturbation theory. Inset: the same data are plotted as a function of $1/D_\alpha^N$.

5.3.2 Power-Law Correlated Disorder Model

In the presence of an infinitesimal disorder, all the eigenstates of electron in one-dimensional non-interacting lattice systems with large enough size are restricted in a small part of the space. However, the de Moura-Lyra class of models show a disorder-induced MIT due to the smoothing of the potential landscape for $\alpha > \alpha_c$, where α_c is a critical disorder. Thus, for α below α_c the states are localized and for α above α_c they are extended. Here, we considered the disordered samples to be different sized pieces (sub-chains of size N_S) cut from independently generated potentials with N sites. Then, N was increased in order to approach the thermodynamic limit.

In Fig. 5.3, we illustrate the results with an example, from where the referred features of localization are very evident. This same procedure was then repeated for different values of α, σ_ε and N, and the localization length was obtained from the inverse slope of a linear

fit to the mean of $-\ln g$ as function of N_S.

5.3.2.1 Finite-Size Scaling of Localization Length

A. Results and Interpretation

From Fig. 5.4, the localization length is seen to increase with α, as expected. Nevertheless, it is not evident that it is diverging in the way predicted by the perturbative expression Eq. 5.24, due to the persistent finite-size scaling present in the data for α close to 1. This scaling of the localization length is driven by the slow convergence of the disorder statistics to its thermodynamic limit. In particular, as referred in beginning, even for values of α very close to the transition point there is a sizable random noise at small distances, whose amplitude goes very slowly to zero as N is increased. Our central argument is that the main contribution to the eigenstates's localization comes from this small scale uncorrelated random potential, which has an effective strength measured by $\sqrt{D_\alpha^N}$. The later claim can be proven by plotting the data in Fig. 5.4 as a function of the parameter, D_α^N, instead of α. This is done in Fig. 5.5, and a perfect collapse of all the points is obtained for small enough values of σ_ε.

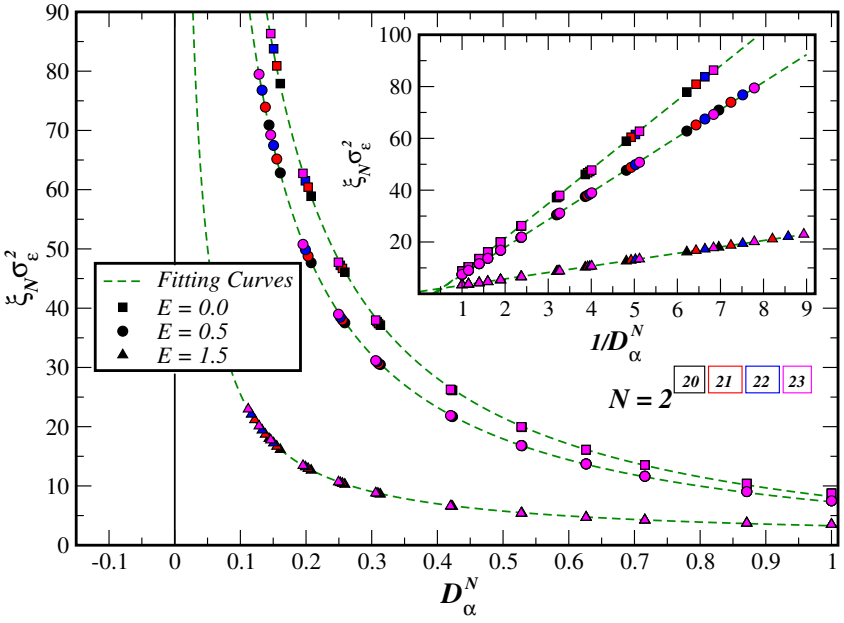

Figure 5.6: The rescaled localization length, $\sigma_\varepsilon^2 \xi_N$, as a function of normalized single-bond discontinuity D_α^N of the de Moura-Lyra class of model for various size of the system N. The data are computed for a fixed variance $\sigma_\varepsilon = 0.1$ with energies $E = 0.0$, 0.50, and 1.50. The data at the corresponding energies are perfectly collapsed and fitted with $y = a + b/x$ (green dashed curve).

The great advantage of this new representation is that we accomplish a complete control over the finite-size scaling phenomena: with increasing in N, all the points slide over the dashed curve, slowly approaching a fixed value.It is important to mention that, the rescaled localization length obey the scaling behavior as follow:

$$\sigma_\varepsilon^2 \xi_N \equiv f(N, \alpha) = f(D_\alpha^N). \tag{5.28}$$

This result was used to extrapolate the values of ξ_∞ to the thermodynamic limit, with the following procedure:

- Calculate the thermodynamic limit values of $D_\alpha^\infty = \lim_{N\to\infty} D_\alpha^N$ from Eq. 5.8 and Eq. 5.14 for each value of α.
- Use the finite-size scaling curves (dashed curves in Fig. 5.6) to read the values the thermodynamic limit of $\xi(\alpha)$.
- Plot the corresponding values as a function of α and compare them with the analytical expression of Eq. 5.24.

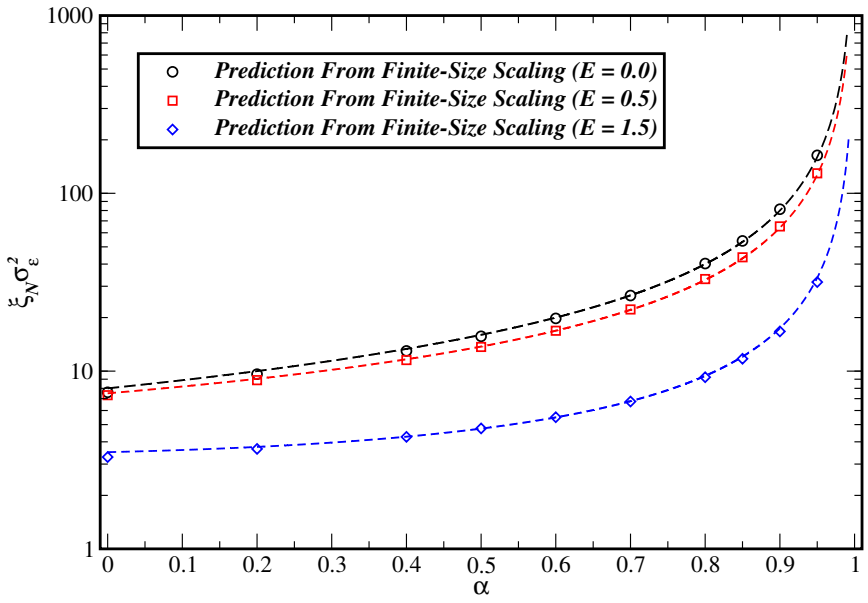

Figure 5.7: Comparison between the thermodynamic limit values of the rescaled localization length (predicted by the dashed curves in Fig. 5.6), with their corresponding analytical results, see Eq. 5.24 (dashed curves).

The final results are shown in Fig. 5.7, where it is clear that we have a perfect agreement with the analytical results given by Eq. 5.24. For completeness, we also checked this

E_F	α_c	ν
0.00	1.00 ± 0.0064	1.03 ± 0.068
0.50	0.99 ± 0.0073	0.95 ± 0.075

Table 5.1: The estimated critical correlation exponent and ν for $E_F = 0.00,\ 0.50$.

behavior for different energies, which yielded a similar collapse of the data (see Fig. 5.6) and agreement with Eq. 5.24, thus confirming the belief that this transition occurs over all the spectrum at once. A direct fit to the data points in Fig. 5.7, to a function of the form

$$\xi_N = C(\alpha_c - \alpha)^{-\nu}. \tag{5.29}$$

yields the following results given in the Table. 5.1, which are in numerical agreement with the analytical expression.

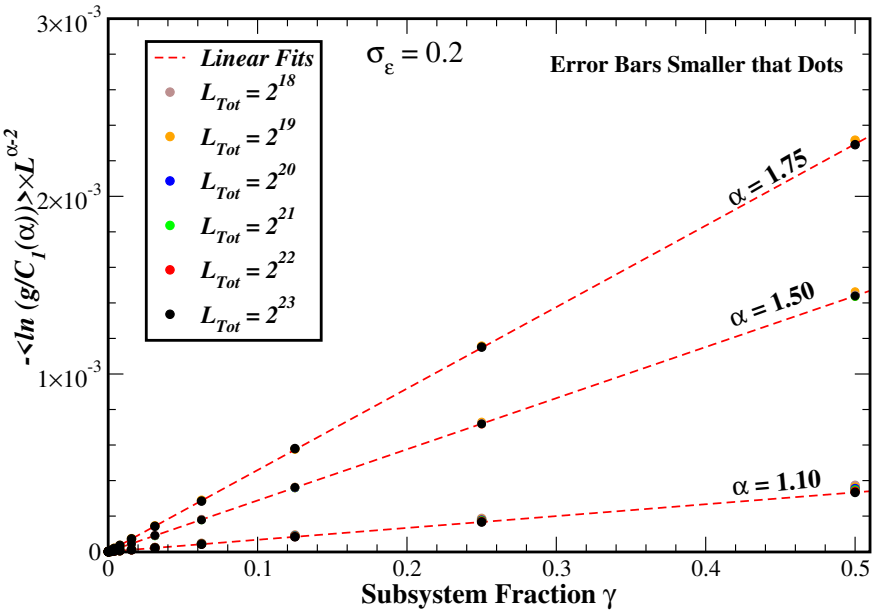

Figure 5.8: Plots of the $-\langle \ln(g/C_1(\alpha))\rangle\, L^{\alpha-2}$ as a function of the fraction chain used, $\gamma = N_S/N$, for three values of α above the critical point. The N dependence of the function $f(\gamma,\, N\,\alpha)$ in Eq. 5.31 was used to collapse the data for different different system sizes into a single straight line (dashed red lines). The value of the local variance used was $\sigma_\varepsilon = 0.20$.

B. Delocalization or Insulator-Metal Transition?

Before closing this section, it is imperative to make some further comments on the physical interpretation of this divergence of ξ. More precisely: Does this divergence signal a

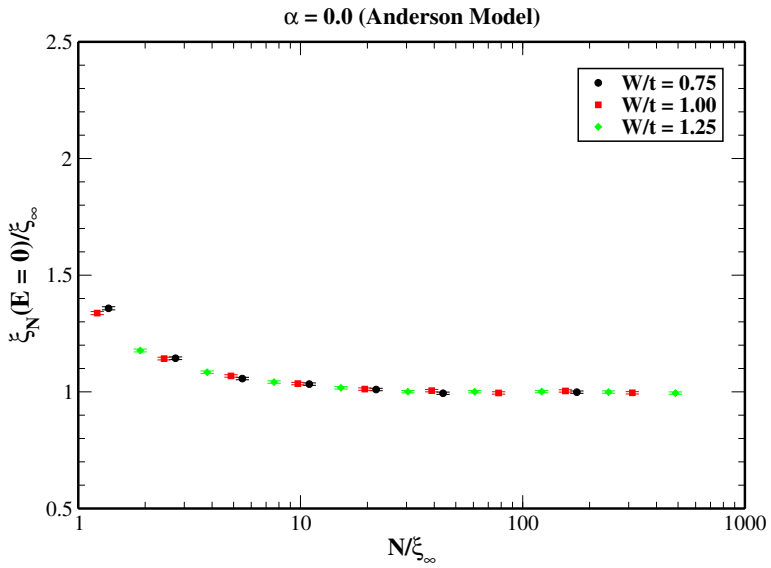

Figure 5.9: The numerical convergence of the KPM estimates of localization length $\xi_N(E = 0)/\xi_\infty$, as a function of N/ξ_∞, (N = system size) of the de Moura-Lyra model with OBC at zero temperature. The data are computed for $\alpha = 0$, $M = 1024$ with 1% estimated error. The parameter ξ_∞ is the analytically calculated localization length for the Anderson model in the perturbative regime [2, 3].

transition from an insulating to a metallic phase?

A first concern shall be raised about the applicability of our procedure of cutting subchains from a larger sample and study their conductance, when $\alpha \geq 1$. In this limit, the correlator of the local disorder C_α^∞ is non-stationary in the thermodynamic limit, as correlator is a function of r/N (see Refs. [1, 4]) and not simply of r, as in Eq. 5.8. One consequence of this is the following: If we take a fixed sized subchains from increasingly larger chains, the values of ε_n in the subchains will become more and more correlated and, in the limit $N \to \infty$, they will be a uniform potential inside the subchains. Hence, any finite subchain will be ordered in this limit and therefore metallic. Additionally, this argument invalidates immediately the existence of a finite localization length for any $\alpha \geq 1$. However, one could have used subchains whose size is a fixed fraction of N, i.e. $\gamma = N_s/N = \text{const}$. In such a case, the reasoning of last paragraph is no longer valid, even though the two procedures are precisely equivalent for $\alpha < 1$.

Are the subchains metallic in this case? To answer this, we must remark that in an insulator-to-metal transition, one has a diverging ξ, but also a linear scaling of ξ with the system size in the metallic phase. As is known from previous work [30], the scaling of the localization length with system size is in these systems is anomalous for any $\alpha > 1$, i.e. $\xi \propto N^{\alpha-1}$. An implication of this result is that the scaling of $-\ln \mathrm{g}$ is a function $f(\gamma, N, \alpha)$, of the following form:

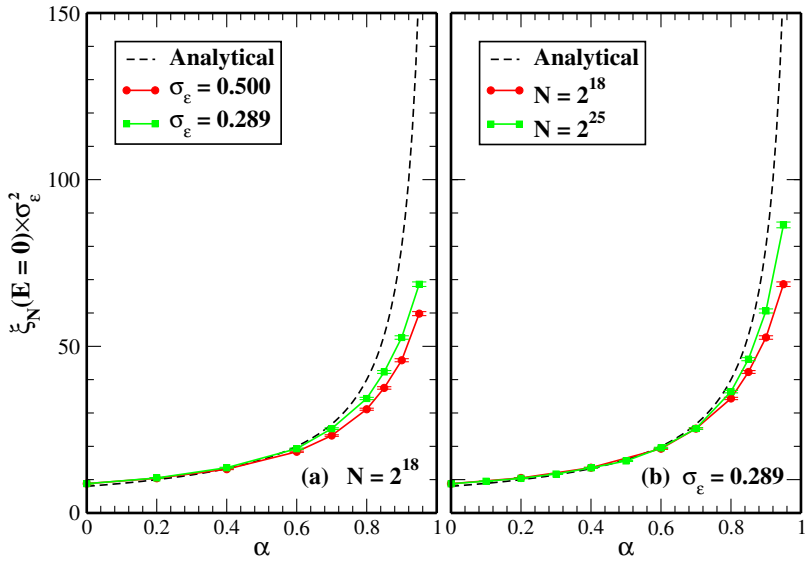

Figure 5.10: The KPM estimates of normalized localization length $\sigma_\varepsilon^2 \xi_N(E=0)$, as a function of α for the de Moura-Lyra model with OBC at zero temperature. Computations are carried out for a fixed (a) system of size $N = 2^{18}$ with various σ_ε, and (b) $\sigma_\varepsilon = 0.289$ with various system size, for $M = 2048$ Chebyshev moments and 1% estimated error. The numerical results for a fixed system size converge to Izrailev result in the perturbative regime as illustrated in (a). With increasing system size, the $\sigma_\varepsilon^2 \xi_N(E=0)$ starts to merge with Izrailev result for a fixed $\sigma_\varepsilon = 0.289$, reflecting strong finite size effect.

$$f(\gamma, N, \alpha) = -\ln C_1(\alpha) + \frac{N_S}{\xi\,(\alpha, N)}; \tag{5.30}$$

$$= -\ln C_1(\alpha) + C_2(\alpha)\gamma N^{2-\alpha} \tag{5.31}$$

From this it is clear that for $\alpha > 2$, the $-\ln \mathrm{g}$ converges to a finite constant $C_1(\alpha)$, in the limit $N \to \infty$ with γ fixed. This supports the results of G. M. Petersen [4] and explains the observed critical point at $\alpha = 2$ [17]. At any rate, the scaling of Eq. 5.31 may also be checked by calculations analogous to the ones we made for $\alpha < 1$. Our numerical results are shown in Fig. 5.8, where we show the data of $-\ln \mathrm{g}$ for six values of N can be collapsed into a linear curve after subtracting $C_1(\alpha)$ (obtained by fitting) and rescaling by $N^{2-\alpha}$. This corroborates the validity of Eq. 5.31 for $\alpha \geq 1$.

Summarizing, the behavior of this model for $\alpha \to 1^+$ is highly non-trivial and, in particular, deciding whether or not the phase is metallic and dependent on the way the thermodynamic limit is taken. Therefore, by keeping sub-chains constant and increasing $N \to \infty$ will form a uniform potential inside the subchain, and will induce delocalized phase without a well defined finite length scale ξ.

To finish, we summarize our main conclusions in two points:

- We were able to numerically observe the existence of a delocalization transition in these models, at $\alpha = 1$, and show that it agrees with analytical results in the weak-disordered regime. This settles the matter in favor of an expected global delocalization of the eigenstates for $\alpha \geq 1$.

- The way we were able to control the finite-size scaling of the localization length provides us with very clear evidence about the true nature of the said transition. As a matter of fact, the observed behavior of $\xi(D_\alpha^N)$ in the perturbative regime is exactly the same as one would expect from an uncorrelated Anderson disorder, with an effective strength given by $\sqrt{D_\alpha^N}$. This fact gives a strong indication that the variation of the localization length with the exponent α is mainly due to a varying effective strength of the short-scale noise, and not due to the change in the tail's exponent of the real-space disorder correlator. Nonetheless, the two effects cannot be decoupled in the de Moura–Lyra model as there is there is a single parameter α controlling both the vanishing of the local noise component and the power-law tail's exponent

5.4 The KPM Approximations of Localization Length

In the following section we show the kernel polynomial simulations of the localization length (see section. 3.3.3 for detail) for the de Moura-Lyra model. In order to test the method, we compute the localization length of the system in the limit of Anderson model ($\alpha \to 0$). In the process, we use exactly similar variance of the local power-law random potentials as used for the Anderson model. Therefore, the power-law correlated potentials have the following form

$$\varepsilon_i := \sigma_\varepsilon \varepsilon_i = \frac{W}{\sqrt{12}} \varepsilon_i. \tag{5.32}$$

where W defines the strength of disorder. The numerical convergence of the KPM approximation for the localization length of the de Moura-Lyra model at the band center $E = 0$, is illustrated in Fig. 5.9. One can clearly see that the KPM gives good account of the data for zero correlation exponent $\alpha = 0$ with $M = 1024$ Chebyshev moments and 1% estimated error in the data.

The localization-delocalization behavior of the de Moura-Lyra model is illustrated in Fig. 5.10. The rescaled localization length show large deviation from the Izrailev result for $\sigma_\varepsilon = 0.5$, (non-perturbative regime). However, it starts to converge with decreasing σ_ε for a fixed system size $N = 2^{25}$ as shown in Fig. 5.10.a. Nevertheless, there is a strong system size effect, as shown in 5.1(lower panel), and also clear in Fig. 5.10.b, where numerical results for a fixed $\sigma_\varepsilon = 0.289$ start converging with increasing system size.

Chapter 6

Entanglement Entropy and Contour

In the first part of this chapter, we review the ground state entanglement structure of a one-dimensional non-interacting tight-binding disordered chain. In particular, we study the behavior of entanglement for the quantum critical system influenced by a uniformly distributed on-site disorder at zero temperature. We shall concentrate on analysis of the famous entanglement area law and its violation for the quantum critical system.

In Sec. 6.2, we will discuss the kernel polynomial approximations of ground state entanglement entropy of a non-interacting one-dimensional Anderson model with PBC at zero temperature. We will show that the estimated correlation matrix for the model is non-idempotent, and as a consequence, the KPM does not converge fully for the entanglement entropy. In this case, the system has a non-vanishing spectral weight at Fermi level and the eigenvalues of the correlation matrix are no longer 0 or 1. In order to solve this issue, we propose McWeeny purification algorithm [70], which recursively drives the correlation matrix to idempotent. In fact, we will show that a highly accurate results of entanglement entropy can be obtained for only 2 Chebyshev moments after purification procedure. A major drawback in this method is that, the numerical complexity of the purification procedure ($\mathcal{O}(L^3)$) dominate the overall computational cost of the KPM.

In section. 6.3, we briefly review the concept of entanglement contour (EC) in the context of non-interacting one-dimensional electronic system [40, 71]. The EC turns out to be a useful theoretical tool in providing information about the spatial structure of entanglement. In particular, it quantifies the single site contributions for the entanglement entropy of a subsystem immersed in an extended lattice quantum system.

In section. 6.4, we employ the concept of EC to examine the disordered system. We report on the scaling behavior of entanglement from the EC perspective at zero temperature. We show that the exponential scaling of EC follows universal area law of entanglement entropy. Similarly, the power-law scaling of EC results the logarithmic scaling law. In addition, we demonstrate the contour function as a theoretical tool for the characterization of quantum phase transition in de Moura-Lyra model. More precisely, we numerically explore the scale invariant of the scaled EC in the vicinity of phase transition for the model.

6.1 Entanglement in Free Electronic System

The entanglement investigation of disordered fermionic systems has found a continuously increasing importance in condensed matter physics [26, 72]. In this section, we will focus on the ground state entanglement theory of the non-interacting one-dimensional Anderson model as discussed in chapter 2.

In order to study entanglement properties of a quantum system, it is necessary to define the measure of entanglement. The von Neumann entropy of the reduced density matrix has a favored theoretical measure for the degree of entanglement in a quantum system. Most importantly, it quantifies the ground state entanglement between the system and the complementary region of the system. In order to develop some intuition on quantum entanglement, we consider a composite system that can be partitioned into two sub-regions $\mathcal{A}$ and $\mathcal{B}$, which correspond to disjoint subsets of sites in real space. The Hilbert space of the composite quantum system is described by the tensor product of the individual Hilbert space $H_{\mathcal{AB}} = H_{\mathcal{A}} \otimes H_{\mathcal{B}}$. Following Eq. 2.102, one finds the von Neumann entropy of the subsystem $\mathcal{A}$ of size l, i.e., $S_{\mathcal{A}} = S(l, L)$, where L is the total size of the system. It is noticed that for a composite system in pure state, the von Neumann entropy of the reduced density matrix of other subsystem is the same, $S_{\mathcal{A}} = S_{\mathcal{B}}$. In the following section we will discuss the entanglement analysis of the 1D Anderson model by imposing PBC and OBC in detail.

6.1.1 Area Law of Entanglement Entropy

The quantum correlation (two-point correlation function) of the ground states of physical Hamiltonian [73] in the presence of a mass gap decreases exponentially with the separation of points, or algebraically if the gap vanishes at critical points. That is, only local interactions (local degrees of freedom interact with their neighbors) will take part in the ground state correlation of the gaped system. Hence, the system is non-critical and the energy gap gives rise to a finite correlation length. Therefore, in gaped one-dimensional quantum systems with local interactions there always emerges an area law [35], which states that entanglement entropy is proportional to the surface area of the subsystem, i.e., independent of size of the system. However, the state of the gapless system is critical, and there is a logarithmic divergence of entanglement entropy explained by conformal field theory [6].

Wolf [36] demonstrated the violation of the entanglement entropy area law in gapless fermionic systems of arbitrary spatial dimensions. That is, for a finite nonzero Fermi surface, the entanglement grows proportional to the surface of the subsystem times a logarithmic correction. For a d-dimensional cube with edge length L, it can be expressed as

$$S_{\mathcal{A}} \sim L^{d-1} \log L. \tag{6.1}$$

The understanding of entanglement properties of disordered fermionic systems is not as

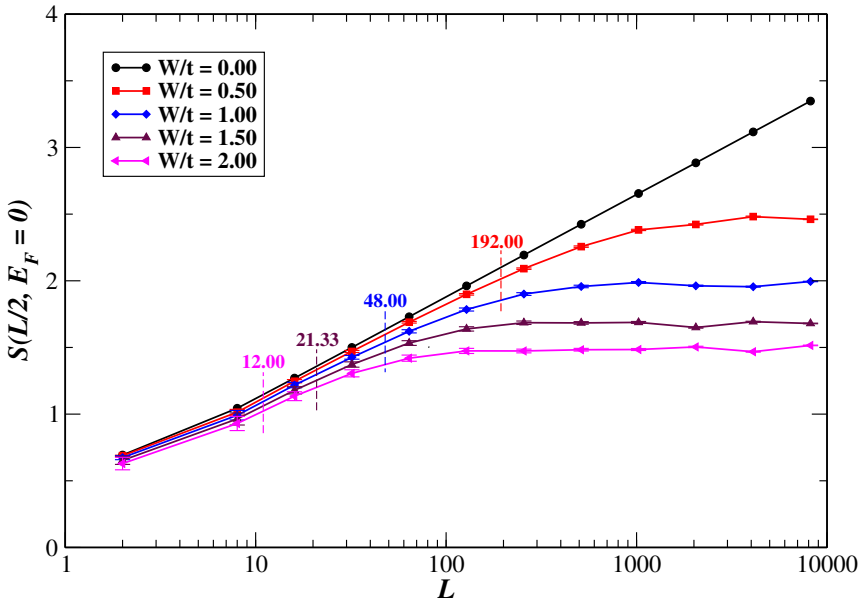

Figure 6.1: The entanglement entropy (calculated by exact diagonalization method) of the half subsystem $\mathcal{A}$, of the one-dimensional Anderson model with PBC for various disorder strength at half filling. We use 2^{18-n} realizations of disorder for the system of size $L = 2^n$ with $n \in \mathbb{N}$ [5]. The vertical dashed lines with data are the exact mean free path of the corresponding disorder.

advanced. It is well known that an infinitesimal disorder of the standard Wigner-Dyson disorder class localizes all electronic states in one and two dimensions. One can expect localization to restore area law, even if there is no electronic excitation gap. If the states are localized, the entanglement between the two parts should arise from states at the boundary of the two parts. For a $d-$dimensional space, the area law of entanglement entropy of a sub-region $\mathcal{A}$ can be written as

$$S_{\mathcal{A}} \sim \beta L^{d-1} + \mathcal{O}(L^{d-2}). \tag{6.2}$$

where β is a non-universal constant.

As illustrated in Fig. 6.1, the area law of entanglement entropy will be obeyed as long as the linear size of the subsystem is sufficiently larger than the mean free path or localization length. In general, the mean free path and the localization length of 1D Anderson model scale similarly with disorder. In addition, the area law of entanglement entropy of free fermion ground states may also be verified for two, and three-dimensional disordered quantum critical system [5].

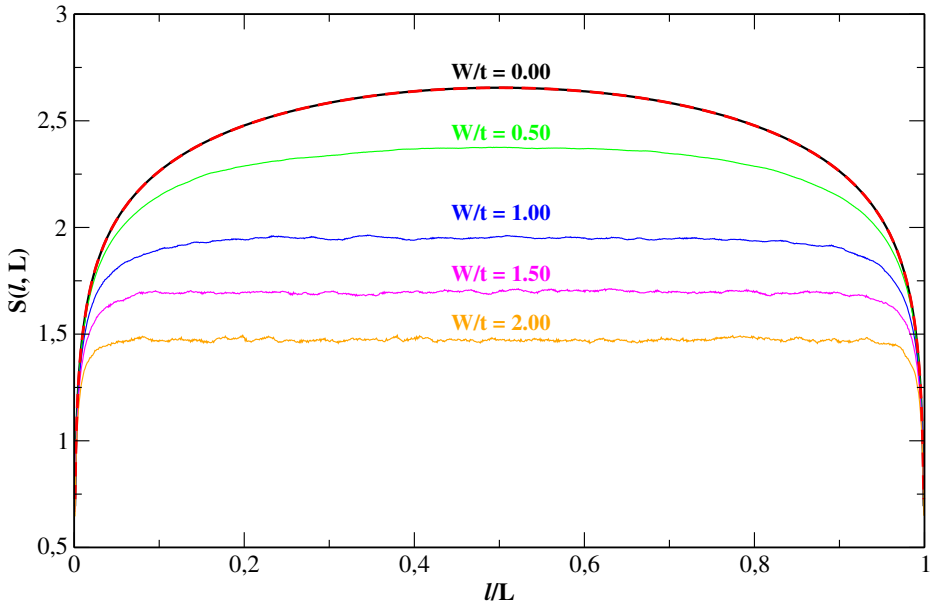

Figure 6.2: Entanglement entropy vs l/L of a one-dimensional Anderson model for various disorder strength at half filling ($E_F = 0$), and keeping PBC. The data are computed (see Eq. 2.102) for a subsystem l of the composite system of size $L = 1024$ with 512 disorder configurations by using exact diagonalization method. The entanglement entropy is well fitted (red dashed curve) by Eq.6.3 for a perfectly clean system [6].

The states of the system can also be characterized by the behavior of the entanglement entropy in the disordered system. More specifically, the states satisfying the area law will be localized. In contrast, the entanglement of the extended states will have a logarithmic correction.

In order to explore the behavior of quantum entanglement, we calculate the entanglement of a finite chain as a function of l/L with PBC, Fig. 6.2, and OBC, Fig. 6.3, where l is the size of a subsystem. The entanglement of the subsystems are computed for half filled non-interacting fermions at zero temperature with 512 realizations of disorder.

Most theoretical work [6, 7], show that the entanglement entropy of the subsystem in a perfectly clean system follow logarithmic scaling law with system size. Here we verify the logarithmic scaling law of entanglement entropy by fitting (red dashed curve) the entanglement entropy of the subsystem of a clean composite system. The entanglement entropy of a subsystem of length l embedded in 1D critical chain of length L scales as [6, 7],

$$S(l, L) = \frac{1}{3} \log \left[\frac{L}{\pi} \sin(\frac{\pi l}{L}) \right] + 0.726, \tag{6.3}$$

In the thermodynamic limit ($L \to \infty$), the entanglement entropy of the subsystem of length

l can be expressed as

$$S(l, L \to \infty) = \frac{1}{3} \log l + 0.726. \tag{6.4}$$

On the other hand, the entanglement entropy of the 1D finite critical chain with OBC is shown in Fig. 6.3. In this case, the entanglement entropy of sub-region of length l in the clean limit scales as [6, 7],

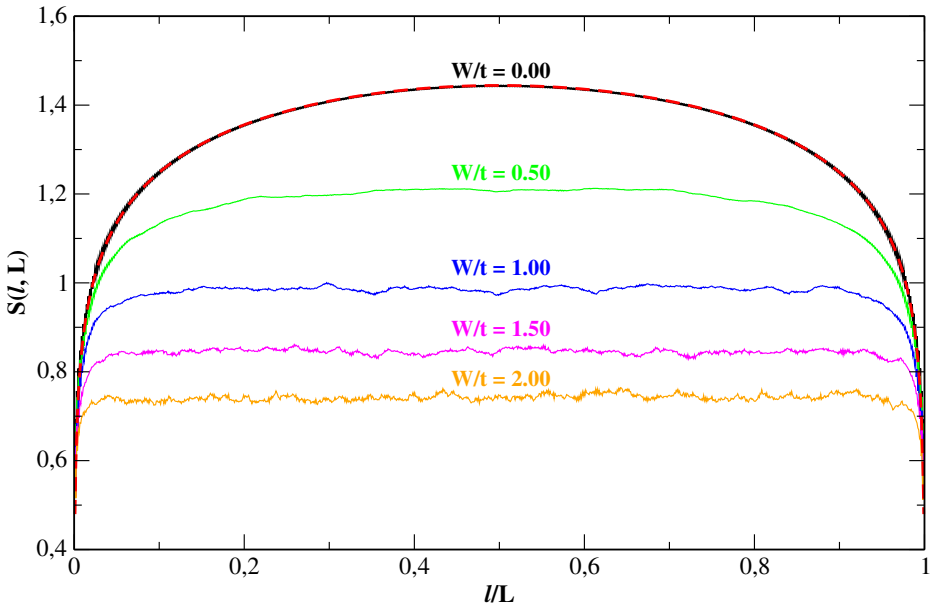

Figure 6.3: Entanglement entropy l/L of a one-dimensional Anderson model for various disorder strength at half filling ($E_F = 0$), and keeping OBC. The data are computed (see Eq. 2.102) for a subsystem l of the composite system of size $L = 1024$ with 512 disorder configurations by using exact diagonalization method. The entanglement entropy is well fitted (dashed curve) by Eq.6.5 for perfectly clean system [7].

$$S(l, L) = \frac{1}{6} \log \left[\frac{2L}{\pi} \sin(\frac{\pi l}{L}) \right] + \frac{0.726}{2}. \tag{6.5}$$

It is important to mention that the logarithmic behavior of the entanglement entropy of the subsystem of length l embedded in a finite 1D critical chain is the indication of the presence of extended states. The entanglement entropy of the 1D critical lattice chain are the known conformal predictions [6].

Introducing disorder leads to a decrease in the entanglement entropy. It is clear from Fig. 6.2 and 6.3, that the entanglement degradation for a fixed total system size depends on the amount of disorder.

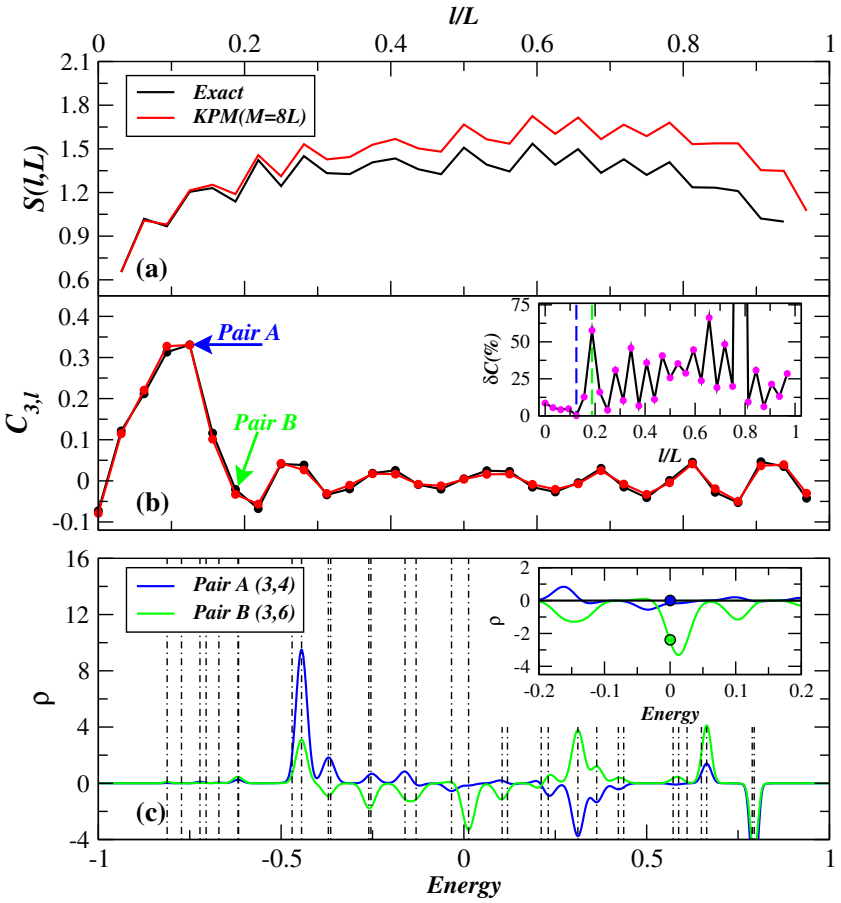

Figure 6.4: The KPM and exact (diagonalization method) computations of (a) entanglement entropy and (b) correlation functions and their percentage relative error (inset), of finite 1D disordered lattice of size $L = 32$ as a function of systems size ratio l/L, where l is the subsystem size. In (c), we show the spectral density of the two pairs of the correlation function as a function of energy spectrum. In the inset (c), we enlarge the central region to show the peak of the spectral density at the band center. Here, we use exactly same random potential (single realization of disorder) for both KPM and exact calculation of entanglement entropy with disordered strength $W/t = 2$, and $8L$ Chebyshev moments at zero temperature.

6.2 The KPM Estimates of Entanglement Entropy

In this section, we briefly explain the spectral expansion technique for the ground states entanglement entropy of 1D Anderson model with periodic boundary conditions at half filling. We ensure, by adequate rescaling that all the energy scales and the Hamiltonian matrix $\hat{\mathcal{H}}$ (see Eq. 2.1) are in the standard domain of orthogonality of the Chebyshev polynomials[1]; then the two-point correlation function, $\mathcal{C}_{ij}$ (see Eq. 2.86), can be approximated as

[1]The Hamiltonian matrix $\hat{\mathcal{H}}$ and all energy scales can be fit into the standard domain of orthogonality of the Chebyshev polynomials, by dividing $(2D + W/2)$, where D is the dimension of the quantum system and W is the strength of Anderson on-site disorder.

$$\mathcal{C}_{ij} = \int_{-1}^{1} \rho^{ij}_{KPM}(E) f(E) dE, \tag{6.6}$$

where $f(E)$ is the Fermi-Dirac distribution function, and $\rho^{ij}_{KPM}(E)$ is the KPM expansion of the spectral matrix correlation (see Eq. 3.64). After inserting Eq. 3.64, into Eq. 6.6, results the following form of the $\mathcal{C}_{ij}$ [19],

$$\mathcal{C}_{ij} = \sum_{m=0}^{M-1} \frac{2 g_m \mu^{ij}_m}{1+\delta_{m,0}} \int_{-1}^{1} \frac{f(E) T_m(E)}{\pi\sqrt{1-E^2}} dE, \tag{6.7}$$

where μ^{ij}_m are the coefficients of expansion for the truncated polynomial series and are given by Eq. 3.65. The integral in Eq. 6.7 can easily be solved by Gaussian quadrature method (GQM) [74]. In this method, the integrand is approximated by summing its functional values at a sequence of abscissas within the range of integration. The explicit expression of the approximated correlation function can be written as [19],

$$\mathcal{C}_{ij} \quad = \quad \tfrac{1}{\mathcal{M}} \textstyle\sum_{q=0}^{\mathcal{M}-1} \mu_q f(E_q), \tag{6.8}$$

where μ_q is the cosine transformation of the kernel improved Chebyshev moments and $\{E_q\}$ are the finite set of $\mathcal{M}$ points over the interval of integration. Usually the number of data points $\mathcal{M}$ is greater than the number of moments M. The analytic expression for Gauss-Chebyshev abscissas are [74],

$$E_q = \cos(\frac{\pi(q+0.5)}{\mathcal{M}}), \text{ with } q = 0, 1, 2, 3.....\mathcal{M}-1, \tag{6.9}$$

and μ_q can be expressed as

$$\mu_q = \sum_{m=0}^{M-1} \frac{2 g_m \mu^{ij}_m}{1+\delta_{m,0}} \cos(\frac{m\pi(q+1/2)}{\mathcal{M}}). \tag{6.10}$$

We compute the KPM estimates of the ground state entanglement entropy (by diagonalizing Eq. 6.8 and using Eq. 2.102) of the one-dimensional non-interacting disordered fermions with periodic boundary conditions at zero temperature. For comparison, we also calculate the entanglement entropy of the system by exact diagonalization method. The main difference between these two methods are in the calculations of correlation matrix.

The computations are carried out for the system of size $L = 32$, with $W = 2$ disorder strength at half filling ($E_F = 0$). In the absence of disorder, a higher KPM resolutions can be obtained for $8L$ Chebyshev moments. However, we have pointed that, the KPM with $8L$ Chebyshev moments for a single realization of disorder does not give a good estimate of the entanglement entropy for a disordered case as shown in Fig. 6.4.a. It is important to mention that, we have used exactly same disordered potentials for both methods.

To shed further light on the entanglement entropy, we compare the correlation function,

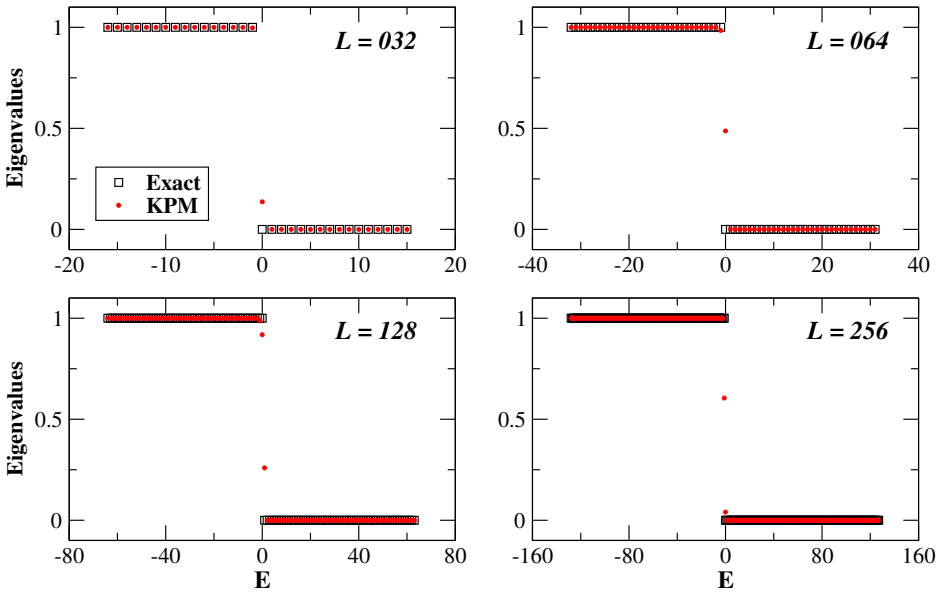

Figure 6.5: Eigen spectra of the correlation matrix computed by KPM (red dots) and exact diagonalization (empty squares) at half filling with $8L$ Chebyshev moments.

$\mathcal{C}_{3,l}$ of the model using exactly similar random potential. We also calculate their percentage relative error $\delta\mathcal{C}_{3,l}(\%)$ (see inset in Fig. 6.4.b). In particular, we focus on two pairs, *Pair A* (small $\delta\mathcal{C}(\%)$) and *Pair B* (large $\delta\mathcal{C}(\%)$). In order to know the origin of small or large percentage relative error, we compute the spectral density functions at *Pair A* and *B* as a function of energy spectrum. As illustrated in Fig. 6.4.c, the spectral density of *Pair B* has nonzero value at Fermi energy (see the magnified and more clear version in the inset). The spectral density of *Pair B* partially contributed to the correlation function and leads to a non-idempotent correlation matrix. However, the zero temperature correlation matrix of a composite system in pure state is idempotent, i.e.,

$$\mathcal{C}^2 = \mathcal{C} \tag{6.11}$$

Its eigenvalues are restricted to 0 for empty states and 1 for occupied states of the electronic system. However, the KPM estimated correlation function has some eigenvalues in between 0 and 1 as illustrated in Fig. 6.5. It is noticed that, for any amount of Chebyshev moments the KPM will not converge fully for the case of non-vanishing spectral density at exactly $E = 0$. To solve that problem and to get an idempotent matrix, we need to apply a purification algorithm.

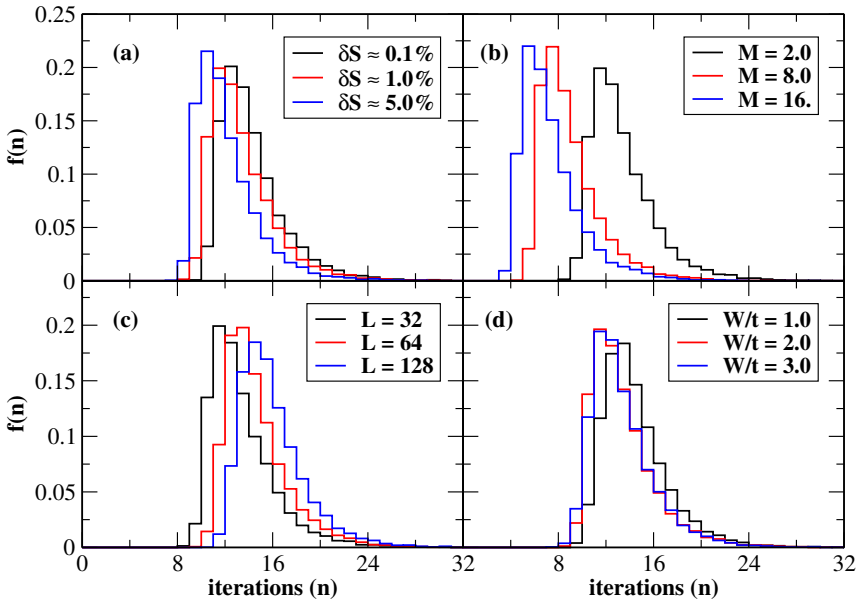

Figure 6.6: Purification of $\mathcal{C}$ (Eq. 6.13): Frequency of iterations f(n), for (**a**) $L = 32$, $M = 2.0$, and $W/t = 2.0$, (**b**) $L = 32$, $W/t = 2.0$, and $\delta S \approx 1.0\%$, (c) $M = 2.0$, $W/t = 2.0$,and $\delta S \approx 1.0\%$, and (**d**) $L = 32$, $M = 2.0$, and $\delta S \approx 1.0\%$.

6.2.1 The Purification Scheme

The correlation matrix $\mathcal{C}$ of the ground state non-interacting lattice chain at absolute zero temperature should be idempotent (see Eq. 6.11). In contrast, the KPM results give a non-idempotent correlation matrix, irrespective of the number of moments and the kernel. In order to obtain the correct correlation matrix for the system, we use the idea of purification technique proposed by McWeeny [70]. The general form of the McWeeny's purification algorithm for a nearly idempotent density matrix ρ is define as

$$\varrho = 3\rho^2 - 2\rho^3. \tag{6.12}$$

where ϱ is a purified density matrix. In general, the purification procedure recursively drives eigenvalues of the nearly idempotent matrix to 1 or 0 for eigenvalues (of the original matrix) greater or less than 1/2, respectively. Moreover, the purified version of the density matrix can be obtained after sufficient number of purification steps.

We demonstrate the McWeeny's purification algorithm for the KPM approximated correlation matrix in Fig. 6.6. For a better resolution, one requires large number purification iterations for a fixed system size and disorder with small expansion coefficients. It worthwhile to mention that we can get an accurate estimate of the entanglement entropy for only

2 Chebyshev moments as can be seen in (a). It is because, for 2 moments, the correlation matrix, Eq. 6.7, have the form

$$\begin{aligned}
\mathcal{C}_{ij} &= \frac{\mu_0^{ij}}{\pi}\int_{-1}^{1}\frac{f(E)}{\sqrt{1-E^2}}dE + \frac{2}{\pi}g_1\mu_1^{ij}\int_{-1}^{1}\frac{Ef(E)}{\sqrt{1-E^2}}dE, \\
&= \frac{\mu_0^{ij}}{\pi}\int_{-1}^{\mu}\frac{1}{\sqrt{1-E^2}}dE + \frac{2}{\pi}g_1\mu_1^{ij}\int_{-1}^{\mu}\frac{E}{\sqrt{1-E^2}}dE, \\
&= \frac{\mu_0^{ij}}{\pi}\left(\frac{\pi}{2}\right) + \frac{2}{\pi}g_1\mu_1^{ij}\left(-1\right), \\
&= \frac{\mu_0^{ij}}{2} - \frac{2}{\pi}g_1\mu_1^{ij}. \qquad (6.13)
\end{aligned}$$

where μ in the upper limit of the integral is the chemical potential for the system, and at half filling, $\mu = 0$. The zeroth order moment μ_0^{ij} in Eq. 6.13, is an identity matrix of system Hamiltonian dimension, while μ_1^{ij} gives the rescaled Hamiltonian. It is important to mention that the correlation matrix commutes with the system Hamiltonian. Thus, the eigenstates of the Hamiltonian and the correlation matrix are same. As a consequence, one can get an accurate estimation of the entanglement entropy only for 2 moments after purification's process.

It most of the applications except entanglement entropy for some cases, the accuracy and resolutions of the KPM estimates are controlled by expansion coefficients and appropriate kernel [19]. However, we show that accuracy of the estimated entanglement entropy can be strongly controlled by a purification's algorithm as illustrated in Fig. 6.6(b). One can see that large number of purification iterations are required for small amount of Chebyshev moments for fixed, $\delta S \approx 0.1\%$ entanglement entropy. Interestingly, one can gets a controlled accuracy of the estimated entropy for only two moments. In (c), we demonstrate the effect of size on the purification algorithm for a fixed disorder, moments and cut off. In the limit large system size, there is a higher probability of eigenvalues lying in between 0 and 1. As a consequence, larger system needs large number of iterations for purification's. In (d), we discuss the effect of disorder by keeping other parameter constant. The purification algorithm needs almost the same steps for a strong disorder. We have tested our problem for sufficiently small number of ($M \geq 2$) moments with Jackson kernel and came up with the conclusion that, for this specific problem, the accuracy and resolutions of the KPM can only be controlled by the purification algorithm.

In conclusion, we have computed the KPM estimates of the ground-state entanglement entropy the quantum critical 1D Anderson model at $T = 0$. In the process we have uncovered some limitations of the this method for this type of calculation, which are not apparent in other calculations such as density of states. More specifically, the KPM results deviated significantly form analytical results. We traced that to a fundamental limitation of KPM, its finite energy resolution; the spectral contribution of states very close to the Fermi energy, where at $T = 0$ the Fermi occupation factor is discontinuous, is

not properly calculated. That affects only slightly the correlation matrix, but drastically the entanglement entropy, which acquires a thermal component that scales as the volume of the subsystem, rather than the area of its boundary. We were eventually able to bypass this difficulty and calculate entanglement entropies accurately, using a purifying procedure. Unfortunately this procedure requires repeated multiplication of the correlation matrix produced by KPM, and since it is a dense matrix, this method, although it can be faster for small systems, does not scale more favorably than an exact diagonalization with sample size.

6.3 Entanglement Contour

The field of quantum entanglement have been successfully used to characterize the physical properties of condensed matter systems. In an attempt to characterize the spatial distributions of entanglement, Chen and Vidal [40] introduced the entanglement contour for free electronic system. The entanglement contour quantifies the contributions of the real-space degrees of freedom in site i to the entanglement between subsystem and its complement. Moreover, the entanglement contour can be used to determine the central charge of the underlying conformal field theory [40].

Let consider a spatially extended $d-$dimensional quantum system at zero temperature. We begin by partitioning the system into two regions $\mathcal{A}$ and $\mathcal{B}$. The entanglement entropy $S_{\mathcal{A}}$ of the subsystem $\mathcal{A}$ can be written as

$$S_{\mathcal{A}} = -\boldsymbol{Tr}\left(\rho^{\mathcal{A}} \log \rho^{\mathcal{A}}\right). \tag{6.14}$$

where $\rho^{\mathcal{A}}$ is the reduced density operator of the subsystem $\mathcal{A}$. The reduced density matrix $\rho^{\mathcal{A}}$ or $\rho^{\mathcal{B}}$ can be obtained by tracing over degrees of freedom of their complement subsystem. In general, the ground state entanglement for a system with local interactions and energy gap typically obeys boundary law (see sec. 6.1 for detail). Moreover, the area law is not always satisfied for the one-dimensional quantum critical system. For gapless fermionic systems of arbitrary spatial dimensions with finite nonzero Fermi surface, the entanglement grows proportional to the surface of the subsystem times a logarithmic correction

$$S_{\mathcal{A}} \sim L^{d-1} \log L. \tag{6.15}$$

In order to identify the lth site contribution of entanglement to the entanglement entropy between $\mathcal{A}$ and $\mathcal{B}$, Chen and Vidal [40] construct a positive function $C_s(l)$. The function $C_s(l) : \mathcal{A} \to \mathbb{R}$ assign a real number to each site in the sub-regions $\mathcal{A}$ such that

$$S_{\mathcal{A}} = \sum_{l \in \mathcal{A}} C_s(l), \tag{6.16}$$

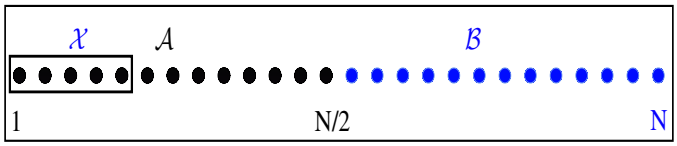

Figure 6.7: The position-space partitioning of a 1D lattice chain into two equal subsystems $\mathcal{A}$ and $\mathcal{B}$. The sub-region $\mathcal{X}$ is the subset of $\mathcal{A}$.

where $C_s(l)$ represents the entanglement contributions of the individual lth site for the structure of entanglement entropy. Eq. 6.16 illustrates that the contour functions can satisfy the sum rule. It must be noted that the van Neumann entropy of the reduced density matrix ρ^l at site l is not equivalent to the entanglement contour $C_s(l)$. Furthermore, the sum of entanglement of the individual sites in subsystem $\mathcal{A}$ does not give the total entanglement entropy of the subsystem,

$$S_{\mathcal{A}} \neq \sum_{l \in \mathcal{A}} S_l \tag{6.17}$$

where S_l is the von Neumann entropy of the reduced density matrix ρ^l at site l. The entanglement contour vanishes for a site l entangled with only neighbor sites in the subsystem $\mathcal{A}$, whereas the one-site von Neumann entropy takes a nonzero value $\sim \log 2$ due to the presence of local entanglement within region $\mathcal{A}$. The modal decomposition of entanglement can be determined by introducing mode dependent normalized weight function $\mathcal{F}_k^l$, such as

$$S_{\mathcal{A}} = \sum_{l \in \mathcal{A}} \sum_k \mathcal{F}_k^l S_{\mathcal{A}}(\lambda_k), \tag{6.18}$$

where $S_{\mathcal{A}}(\lambda_k)$ is the local entropy (see Eq. 2.104) of the subsystem with λ_k eigenvalues (see Eq. 2.101) of the correlation matrix. The weight function satisfies $\sum_{l \in \mathcal{A}} \mathcal{F}_k^l = 1$. On comparing Eq. 6.16 and Eq 6.18 leads to the contour

$$C_s(l) = \sum_k \mathcal{F}_k^l S_{\mathcal{A}}(\lambda_k). \tag{6.19}$$

Eq. 6.19, defines a weighted sum of $\mathcal{F}_k^l$ and $S_{\mathcal{A}}(\lambda_k)$, which is positive in the range $0 \leq \lambda_k \leq 1$.

6.3.1 Properties of Entanglement Contour

The entanglement contour should have the following properties [40]:

- **Positivity:** The entanglement contour should be a real and positive number, $C_s(l) \geq 0$.
- **Normalization:** The entanglement contour of individual sites in subsystem $\mathcal{A}$ sat-

isfies the sum rule, such as

$$\sum_{l\in\mathcal{A}} C_s\left(l\right) = S_{\mathcal{A}}. \tag{6.20}$$

For the case of sub-regions $\mathcal{X}$ with in subsystem $\mathcal{A}$, such that $\mathcal{X} \subseteq \mathcal{A}$, with a vector space

$$\mathbb{V}^{\mathcal{X}} = \bigotimes_{l\in\mathcal{X}} \mathbb{V}^{l}, \tag{6.21}$$

the entanglement contour of the sub-regions $\mathcal{X}$ is,

$$s_{\mathcal{A}}^{\mathcal{X}} = \sum_{l\in\mathcal{X}} C_s\left(l\right). \tag{6.22}$$

It follows that the entanglement contour for any two disjoint subsets $\mathcal{X}_a, \mathcal{X}_b \subseteq \mathcal{A}$, with $\mathcal{X}_a \cap \mathcal{X}_b = \emptyset$ is additive,

$$C_s\left(\mathcal{X}_a \cup \mathcal{X}_b\right) = C_s\left(\mathcal{X}_a\right) + C_s\left(\mathcal{X}_b\right)$$

It is also noticed that the entanglement contour of the sub-region $\mathcal{X}_a$ will be larger than the entanglement contour contained in the sub-region $\mathcal{X}_b$, if $\mathcal{X}_b$ is the subset of $\mathcal{X}_a$, i.e.,

$$C_s\left(\mathcal{X}_a\right) \geq C_s\left(\mathcal{X}_b\right) \quad \text{if} \quad \mathcal{X}_a \supseteq \mathcal{X}_b \tag{6.23}$$

- **Symmetry:** The entanglement contour is invariant if $T\rho^{\mathcal{A}}T^{\dagger} = \rho^{\mathcal{A}}$, where T is the symmetry of $\rho^{\mathcal{A}}$ that exchanges site l with m in the subsystem $\mathcal{A}$, i.e.,

$$C_s\left(l\right) = C_s\left(m\right) \tag{6.24}$$

This proves that the two sites i and j have the same entanglement contour of the subsystem $\mathcal{A}$.

- **Invariance:** The entanglement contour is invariant under local unitary transformations. If a unitary transformation $\mathcal{U}^{\mathcal{X}}$ acts on a sub-region $\mathcal{X}$ with $\mathcal{X} \subseteq \mathcal{A}$, such that

$$\left|\tilde{\Psi}\right\rangle = \mathcal{U}^{\mathcal{X}}\left|\Psi\right\rangle \tag{6.25}$$

where $|\Psi\rangle$ is the ground state of the full system, then the entanglement contour remains the same after the unitary transformation.

- **Upper and Lower Bound:** The entanglement contour of the sub-regions $\mathcal{X}$ with $\mathcal{X} \subseteq \mathcal{A}$ contained in factor space $\Omega_{\mathcal{A}}$ is always be smaller than the entanglement entropy of the subsystem $\mathcal{A}$, as

$$C_s(\mathcal{X}) \leq S_{\Omega_{\mathcal{A}}} \tag{6.26}$$

where the decomposition of subsystem $\mathcal{A}$ is $\mathbb{V}^{\mathcal{A}} = \mathbb{V}^{\Omega_{\mathcal{A}}} \otimes \mathbb{V}^{\bar{\Omega}_{\mathcal{A}}}$, with $\mathbb{V}^{\Omega_{\mathcal{A}}}$ and $\mathbb{V}^{\bar{\Omega}_{\mathcal{A}}}$ are the factor spaces of $\mathbb{V}^{\mathcal{A}}$. This means that the entanglement contour in any sub-region $\mathcal{X}$ is upper bounded by $S_{\Omega_{\mathcal{A}}}$. Indeed, the upper bound can be alternatively announced as a lower bound, which identify that the entanglement contour of sub-region $\mathcal{X}$ is at least equal to the entanglement entropy.

It is noticed that for an equal bipartite subsystems, the entanglement contour has a reflective symmetry with respect to half of the system. On comparing Eq. 6.19 and Eq. 2.103, the weight function is,

$$\mathcal{F}_k^l = |\langle \phi_l | \psi_k \rangle|^2 . \tag{6.27}$$

where ϕ_l gives the lth lattice site contribution to the entanglement entropy in sub-region $\mathcal{A}$ and ψ_k is the kth eigenstate of the correlation matrix.

Furthermore, Frerot .et. al. [71], introduced the concept of particle-number fluctuations contour, which is is related to the correlations of the particle number fluctuations between each site of the subsystem $\mathcal{A}$ and its complement $\mathcal{B}$. For a gapless free fermions with a finite density of states at Fermi energy E_F, the fluctuations $\delta^2 N_{\mathcal{A}}$ of the subsystem $\mathcal{A}$ at zero temperature is

$$\delta^2 N_{\mathcal{A}} = \left\langle \left(\hat{N}_{\mathcal{A}} - \left\langle \hat{N}_{\mathcal{A}} \right\rangle \right)^2 \right\rangle . \tag{6.28}$$

where $\hat{N}_{\mathcal{A}}$ counts the number of particles in subsystem $\mathcal{A}$. The variance of the particle number of the subsystem $\mathcal{A}$ is,

$$\delta^2 N_{\mathcal{A}} = \sum_{l \in \mathcal{A}} C_n(l) \tag{6.29}$$

with

$$C_n(l) = \langle \delta n_l \delta N_{\mathcal{A}} \rangle \tag{6.30}$$

where $C_n(l)$ is the contour of the particle-number fluctuations at site l and has a similar spatial symmetries as those of subsystem $\mathcal{A}$. Thus, the fluctuation contour is the correlation function between the density fluctuations at site l and the subsystem $\mathcal{A}$. It can also be describe as [71]

$$C_n\left(l\right) = \sum_k |\langle \phi_l | \psi_k \rangle|^2 \lambda_k (1 - \lambda_k). \tag{6.31}$$

It is worthwhile to mention that the fluctuation and the entanglement contour has exactly similar behavior (as they have exactly same wight function and the behavior of $\lambda_k(1-\lambda_k)$ is very similar to mode entanglement), in particular for free fermions. In fact, it is pointed out [71] that the contour functions are related by the following equation,

$$C_s\left(l\right) \approx \frac{\pi^2}{3} C_n\left(l\right) + \mathcal{O}\left(1\right), \qquad l \in \mathcal{A}. \tag{6.32}$$

In the following we will show that this relation hold even in the disordered free fermions system.

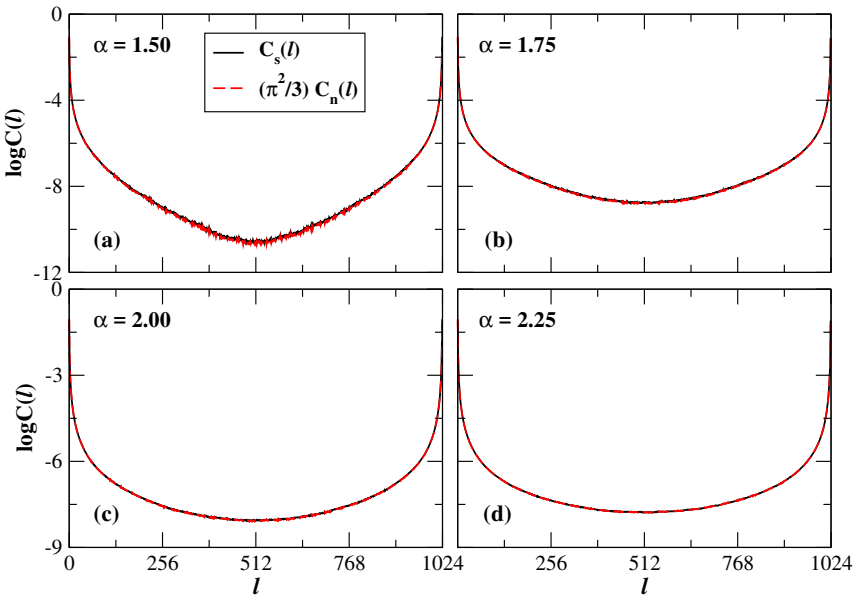

Figure 6.8: Comparison of entanglement and fluctuation contour of a sub-region $\mathcal{A}$ for the quantum critical 1D model in the presence of power-law correlated onsite random potentials with PBC for $L = 1024$. The parameter α is the correlation exponent, which controls the strength of disorder.

6.4 Entanglement Contour of the Disordered free Fermions

Here we focus on an examination of entanglement contour for a non-interacting 1D quantum critical chain with two different models of disorder, the Anderson model and the power-law correlated disorder model. In the Anderson model, the disorder is considered to be an independent random variables uniformly distributed in the interval $[-\frac{W}{2}, \frac{W}{2}]$ as discussed in chapter 2. In the power-law correlated disorder, the randomness is manifested as a long-range correlated disorder with power-law spectral density. The most detailed studies of the system Hamiltonian are discussed in chapter 2, (see Eq. 2.1).

The contour function quantifies the part of the total entanglement entropy associated with the distant state of the system. In order to develop some intuition on metal-insulator transition in the disordered system, we turn to the quantum entanglement contour. We begin by partitioning the system into two regions, $\mathcal{A}$ and $\mathcal{B}$. The sub-region $\mathcal{A}$ or $\mathcal{B}$ corresponds to a subset of lattice sites in real-space.

In practice, it turns out that for all cases of interest, the fluctuations contour have exactly similar physical behavior as the entanglement contour. Indeed, we have pointed out that the contour functions are related by Eq. 6.32, even in the disordered system as shown in Fig. 6.8.

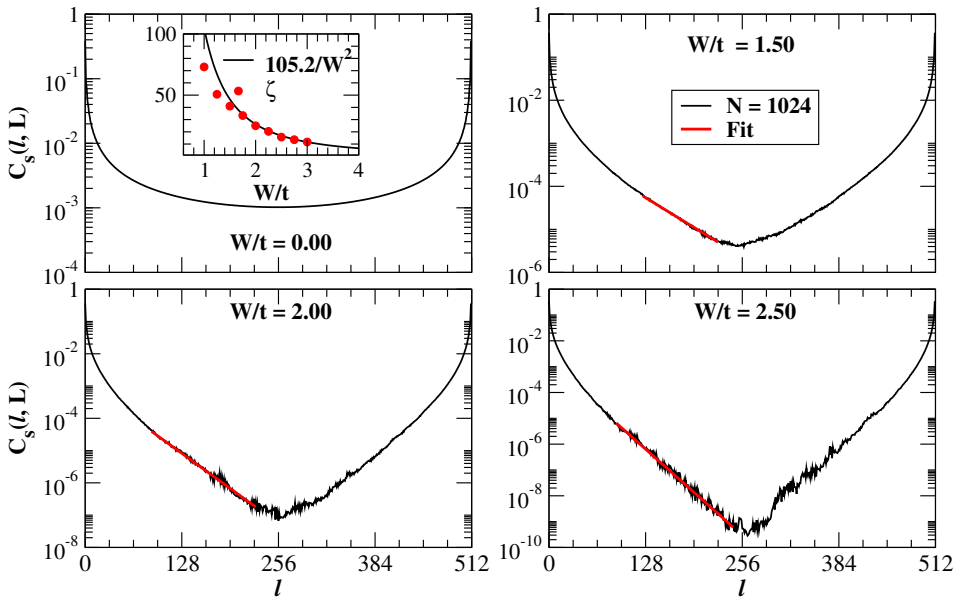

Figure 6.9: Entanglement contour of sub-region $\mathcal{A}$ for the quantum critical 1D Anderson model with PBC. The red dots in the inset are the the correlation length calculated by fitting the EC; the black line is the Born approximation.

6.4.1 Contour Function for the Anderson Model

We now list our preliminary results about the contour function for the quantum critical system under the influence of random onsite potentials. It is important to note that the disordered-averaged entanglement contour profiles of the two intervals ($\mathcal{A}$ and $\mathcal{B}$), like in perfectly clean systems, are completely symmetric in the presence of disorder.

Fig. 6.9, illustrates the contour function as a function of sub-system lattice sites l for various disorder strength at zero temperature. The entanglement contour is computed for a sub-region $\mathcal{A}$ of size $L = N/2$ with 2^{15} realizations of disorder and imposing PBC. One can clearly observe that the entanglement contour exhibits roughly algebraic decaying behavior with distance in the clean system limit ($W/t = 0$). We can also extrapolate the scaling behavior of the entanglement entropy in terms of entanglement contour. We noticed that the power-law decay of entanglement contour implies logarithmic scaling law of entanglement entropy [6].

As we are dealing a system with PBC, therefore the boundary of sub-region $\mathcal{A}$ consists of cuts at lattice site $l = 0$ and $l = L$. Hence, the entanglement contour for the ground state of Hamiltonian decays with the distance to the closest boundary.

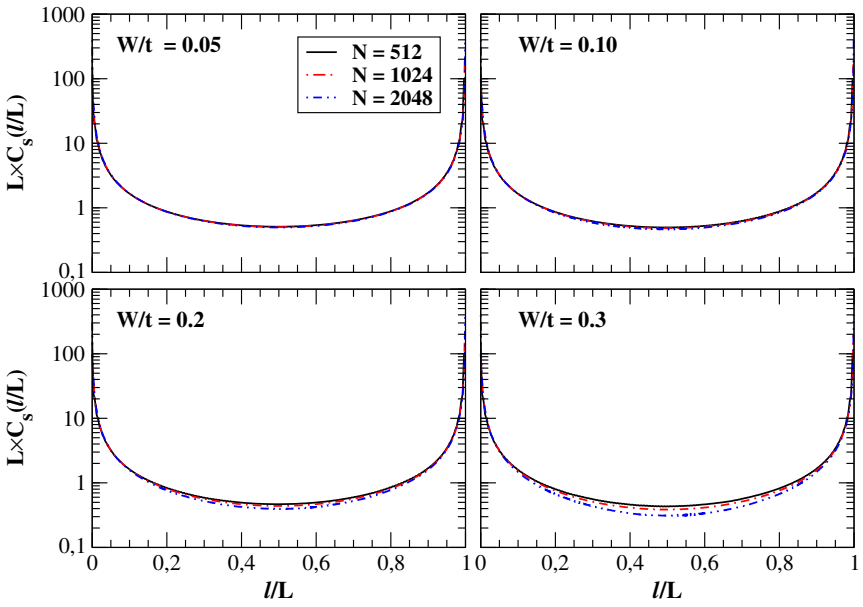

Figure 6.10: Scaled entanglement contour of the sub-region $\mathcal{A}$ for the quantum critical 1D Anderson model with PBC for various system size.

For the finite disordered case, the contour function accelerates to decay faster from the boundary, depending on the amount of disorder as illustrated in Fig. 6.9. In other words, for a sufficiently strong disorder, the entanglement contour decays exponentially close to the boundary of the subsystem for $l \gg \zeta$,

$$C_s(l, L) := C_s(l) \propto e^{-l/\zeta}, \qquad l \gg \zeta. \tag{6.33}$$

where ζ is the correlation length. The exponentially decay of the entanglement contour leads us to the area law of entanglement entropy for the system. In this case, the off-diagonal elements of the correlation matrix are expected to decay exponentially with the distance to the diagonal of correlation matrix. Thus, all the ground state correlations decay exponentially with distance.

In order to clarify the numerical analysis for the system in the context contour function, we calculate the correlation length ζ by fitting the entanglement contour near the boundary. The comparison of correlation length ζ (red dots) with the localization length ξ (black line) is illustrated in the inset of Fig. 6.9. According to Born approximation [12], the localization length in weak disorder limit scales as

$$\xi = \frac{105.2t^2}{W^2}. \tag{6.34}$$

It can be seen that the correlation function has a very good agreement with Born approximation. Hence,

$$\zeta \approx \xi. \tag{6.35}$$

It is interesting to observe that the correlation length has qualitatively similar behavior as the localization length of the quantum critical Anderson model.

To examine the essential aspects of contour function, for instance the MIT, we focus our attention on scaling properties of the entanglement contour for the Anderson model. For a finite-size systems, the scaled entanglement contour is size independent in the limit of vanishing disorder ($W/t \sim 0$), as depicted in Fig. 6.10. Indeed, no significant finite-size effects should be observed for $L \ll \zeta$. This is a clear signature of extended states. On the other hand, for $W/t \geq 0.1$, the scaled entanglement contour depends on system size, signaling the existence of localized states.

6.4.2 de Moura-Lyra Model

In this section, we numerically investigate the contour function for the de Moura-Lyra model at zero temperature. The computations are carried out for different system sizes with large number of realizations of disorder at half filling.

It is important to study two extreme cases of correlation exponent. In the case of infinite α, the system Hamiltonian corresponds to a tight-binding model with a sinusoidal potential of wavelength N. As a consequence, the eigenstates of the system are extended, due to the effective absence of disorder. In contrast, the eigenstates of the system are strongly localized in the case of zero α. In this limit, one recovers the Anderson model with uncorrelated disorder.

We have pointed out that the disorder-averaged entanglement contour show roughly power-law decay behavior in the limit of infinite α. In the opposite limit $\alpha = 0$, the entanglement contour turned out to decay exponentially with distance closest to boundary for $l \gg \zeta$. In this limit, the eigenstates for finite system are exponentially decaying in space at infinity. The most detailed studies of localization in this system predicts MIT at critical correlation exponent α_c. From entanglement perspective [26], all the eigenstates of the system are localized for $\alpha \leq \alpha_c$. In contrast, the system shows metallic behavior for $\alpha > \alpha_c$.

The disorder induced localization-delocalization transition may also be investigated in the framework of contour function. For this purpose, we perform the scaling collapses of the entanglement contour for various size and correlation exponent as illustrated in Fig. 6.11 for PBC and Fig. 6.12 for OBC. We have noticed that, the contour function at the vicinity of critical exponent satisfy the following universal scaling function,

$$C_s(1, L) \simeq L C_s(l/L, L). \tag{6.36}$$

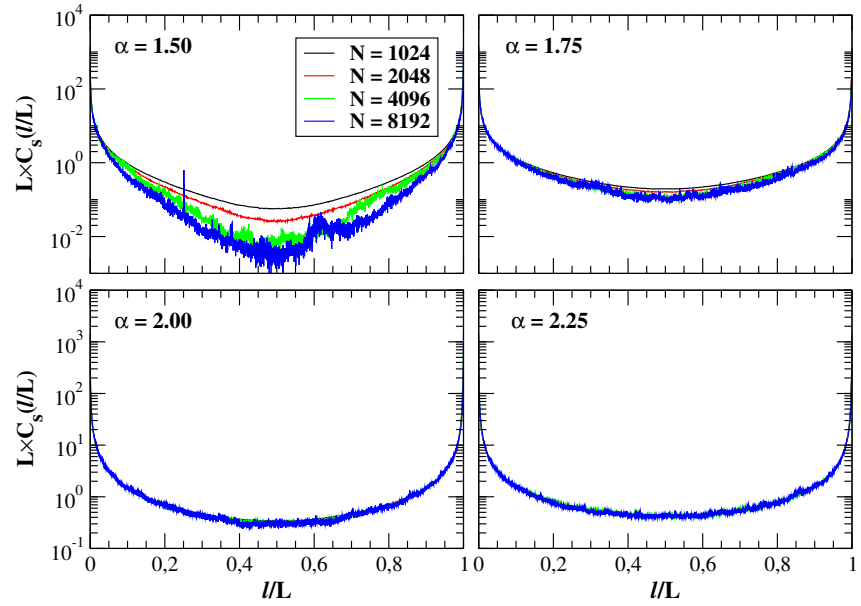

Figure 6.11: The contour function associated with electronic system of sub-region $\mathcal{A}$ of size L for various disorder strength parameter α with PBC.

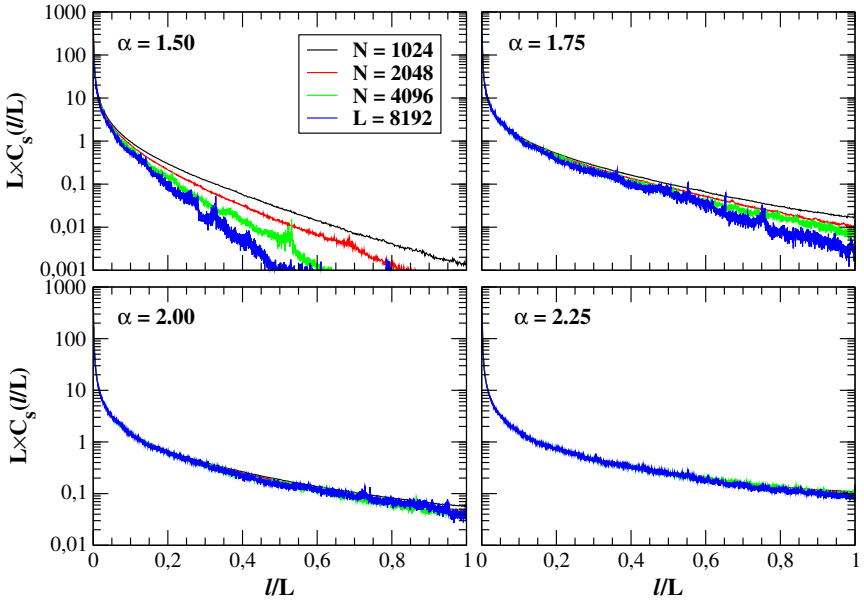

Figure 6.12: The entanglement contour associated with electronic system of sub-region $\mathcal{A}$ of size L for various disorder strength parameter α with OBC.

The scaled entanglement contour turns out to be size dependent for $\alpha < 2$ as shown in Fig. 6.11 and Fig. 6.12. This feature of entanglement contour indicate the localized nature of the system. On other hand, for $\alpha \geq 2$, the scaled entanglement contour is size independent. Most precisely, the data collapses of the scaled entanglement contour signaling the existence of delocalized states. Furthermore, the entanglement contour of the subsystems will decay algebraically for extended and exponentially for localized states near the subsystems boundary.

The behavior of de Moura-Lyra model for $\alpha \to 1^+$ is highly nontrivial and, in particular, deciding whether or not the phase is metallic is dependent on the way the thermodynamic limit is taken. For $\alpha > 1$, the thermodynamic limit correlator is non-stationary ($\mathcal{C}_\alpha^\infty \propto r/N$), and if we take a fixed sized subchain from increasingly larger chains, the values of ε_n in the subchain will become more and more correlated and, in the limit $N \to \infty$ is therefore metallic with no mobility edge [27]. It is important to mention that the entanglement contour are computed for systems with fixed fraction of N, i.e. $\gamma = N_s/N = 1$ [27] (full system sizes are considered for the calculations, $N_s = N$), and hence the data supports the results of G. M. Petersen [4] and explains the observed critical point at $\alpha = 2$ [17].

Chapter 7

Conclusions and Outlook

In this dissertation, we have addressed the statistical properties of a one-dimensional tight-binding system with different models of random site energies at zero temperature. We have investigated various models of disorder, as well as, important tools for the characterization of physical properties of the system.

We have reported numerical simulations in Chapter 3, based on the kernel polynomial method (KPM) of the disordered electronic systems. We have numerically computed various physical quantities such as spectral function, density of states and localization length of the systems with an $\mathcal{O}(NMR)$ numerical complexity, where N, M and R are the system size, moments and random vectors respectively. At first, we have studied the disorder-averaged single-particle spectral function of the Anderson model. It has been shown that disorder-induced spectral width verifies the Born approximation in the perturbative regime. We have also computed the localization length of the Anderson model, and verified by comparing with the analytical perturbative result.

In Chapter 4, we found an Anderson-like behavior of spectral function for the power-law correlated disorder model (power-law decay of the spectral density, $S(k) \sim k^{-\alpha}$) in the limit of space-correlations $\mathcal{C}_{0,n} = \delta_{0,n}$, of disordered potential ($\alpha \to 0$). By varying the correlation exponent, we observed a change from a Lorentzian shape to a Gaussian line shape for $\alpha \to 1^+$, that reflects the classical limit. In this limit, the spectral function turns out to be the probability distribution of the random potential. In addition, the spectral function is self-averaging for $\alpha \leq 1$, as the standard deviations decay $1/\sqrt{L}$, with size L of the system, at the band center, but ceases to be so for $\alpha > 1$. In the extreme limit, $\alpha \to \infty$, the correlated disorder system corresponds to a tight-binding model with a cosine potential of wavelength L, and the spectral function displays similar behavior as the density of states in real space. Furthermore, we have also investigated spectral function for the Gaussian correlated disorder case (Gaussian decay of the spectral density). It is shown that the correlation length of disorder in the regime $\sigma_\varepsilon \gg \hbar v_k q_c$, is much larger than the lattice spacing ($q_c a \ll 1$) but much smaller than the system's size, and the spectral function has a Gaussian shape with mean E_k and variance σ_ε^2, the variance of the random

site energy.

An important conclusion of this thesis is the problem of delocalization transition in the de Moura-Lyra model. Indeed, in Chapter 5, we have calculated the localization length of the model by applying a generalized Thouless formula in the perturbative regime, and observed a divergence behavior of the localization length at $\alpha = 1$, in the thermodynamic limit. These results were confirmed by a direct evaluation of the localization length from the linear scaling of the typical Landauer conductance, which was shown to suffer from a persistent finite-size scaling near the transition point. We have pointed out that the persistent finite-size scaling of the data is caused by a very slow convergence of the nearest-neighbor correlator to its infinite-size limit, and controlled by the choice of a proper scaling parameter. We have conclusively established that nature of localization-delocalization at $\alpha = 1$ quite different in nature of the transition observed at $\alpha = 2$.

Finally, in the Chapter 6, we have studied the ground-state entanglement in the Anderson model. It was shown that the entanglement entropy scales logarithmically with system size for a perfectly clean quantum critical systems. In this limit, the localization length exceeds system size and all the eigenstates are delocalized. However, the entanglement entropy of the Anderson model with size larger than the localization length turned out to be constant. As a consequence, the entanglement entropy obey the famous area law, $S \propto L^{d-1}$, where d is the dimension of the system. In addition, we have presented the kernel polynomial approximations of the ground-state entanglement entropy of the 1D Anderson model at $T = 0$. The KPM results are shown to be deviated significantly form analytical results (exact diagonalization method). We have pointed out that the KPM estimate of the correlation matrix is non-idempotent for the Anderson model. The origin of non-idempotent correlation matrix is the partial contributions of the spectral density at Fermi energy in the calculations of correlation matrix. We have pointed out that the accuracy and numerical convergence of this particular problem can be only controlled by purifying procedure (McWeeny's algorithm). A major drawback in this method is that the computational cost of purification procedure $\mathcal{O}(N^3)$ dominate the overall computational cost of the KPM. We have also presented evidence regarding the area law of entanglement entropy by employing entanglement contour. Furthermore, entanglement contour is used as a diagnostic tool for the metal insulator transition —where the rescaled entanglement contour becomes universal in the vicinity of critical exponent $\alpha = 2$— for the de Moura-Lyra model.

An interesting follow-up to the present work would be finding new ways of simulating stationary disorder landscapes having power-law tails with tunable exponents but a possibly negligible and independently determined short-scale noise. Analyzing systems with such potentials would give us information about the importance of algebraic correlation tails in the physics of one-dimensional localization.

Appendix A

Random Phase Averages

In section 4.4, we needed to calculate terms of the form

$$\overline{\exp\left(i\phi_{q_1}\right)\exp\left(i\phi_{q_2}\right)\ldots\exp\left(i\phi_{-q_1-q_2-\ldots q_{n-1}}\right)} \tag{A.1}$$

where ϕ_q are independent random phases with an uniform distribution in the circle and obeying the constraint $\phi_q = -\phi_q$. These expressions appear inside sums over momenta, of the form

$$\sum_{q_1\neq 0}\cdots\sum_{q_{n-1}\neq 0} V(q_1)\ldots V(q_{n-1})V(-q_1\cdots-q_{n-1}) \times\overline{\exp\left(i\phi_{q_1}\right)\ldots\exp\left(i\phi_{-q_1-q_2-\ldots q_{n-1}}\right)}, \tag{A.2}$$

where $V(q) = V(-q)$. Clearly, since these phases are uniformly distributed independent variables (except in the case $q_2 = \pm q_1$), we have

$$\overline{\exp\left(i\phi_{q_1}\right)} = 0, \tag{A.3a}$$

$$\overline{\exp\left(i\phi_{q_1}\right)\exp\left(i\phi_{q_2}\right)} = \delta_{q_1+q_2,0}. \tag{A.3b}$$

Therefore, we can only obtain a non zero result if all the phase factors are paired. This means that $F(q_1,\ldots,q_n) = \overline{\exp\left(i\phi_{q_1}\right)\exp\left(i\phi_{q_2}\right)\ldots\exp\left(i\phi_{q_n}\right)}$ is zero unless $\sum_i q_i = 0$.

A.1 General Procedure

To actually calculate the phase averages, we may start with the following illustrative case:

$$F\left(q_1,q_2,q_3,q_4\right) := \overline{\exp\left(i\phi_{q_1}\right)\exp\left(i\phi_{q_2}\right)\exp\left(i\phi_{q_3}\right)\exp\left(i\phi_{q_4}\right)} \tag{A.4}$$

To prevent lengthy notation, we define

$$\begin{aligned}\delta_{q_i+q_j,0} &\to \delta_{ij}\\ 1-\delta_{q_i+q_j,0} &\to \overline{\delta_{ij}} = 1-\delta_{ij}\end{aligned}$$

such that $\delta_{ij} + \overline{\delta_{ij}} = 1$. Note also, that since $V(q) = V(-q)$, the contraction of two momenta is equivalent to a Kronecker delta in the momentum sums.

Hence, we can write

$$\begin{aligned}F(q_1,\ldots,q_4) &= \delta_{12}F(q_3,q_4) + \overline{\delta_{12}}F(q_1,\ldots,q_4)\\ &= \delta_{12}\delta_{34} + \overline{\delta_{12}}F(q_1,\ldots,q_4),\end{aligned}$$

and repeat the process until we exhaust all possibilities. In this case, we just need to do it once,

$$\begin{aligned}\overline{\delta_{12}}F(q_1,\ldots,q_4) &= \overline{\delta_{12}}\left[\delta_{13}\delta_{24} + \overline{\delta_{13}}F(q_1,\ldots,q_4)\right]\\ &= \overline{\delta_{12}}\left[\delta_{13}\delta_{24} + \overline{\delta_{13}}\delta_{14}\delta_{23}\right]\end{aligned}$$

so

$$F(q_1,\ldots,q_4) = \delta_{12}\delta_{34} + \overline{\delta_{12}}\delta_{13}\delta_{24} + \overline{\delta_{12}\delta_{13}}\delta_{14}\delta_{23}.$$

Finally, if we express everything in terms of Kronecker deltas (using $\overline{\delta_{ij}} := 1-\delta_{ij}$), we get

$$\begin{aligned}F(q_1,\ldots,q_4) =& \delta_{12}\delta_{34} + \delta_{13}\delta_{24} + \delta_{14}\delta_{23}\\ &-\delta_{12}\delta_{13}\delta_{24} - \delta_{12}\delta_{14}\delta_{23} - \delta_{13}\delta_{14}\delta_{23}\\ &+\delta_{12}\delta_{13}\delta_{14}\delta_{23}.\end{aligned} \tag{A.5}$$

The left-hand side of the above equation can be divided in three groups of terms:

1. The first three terms correspond to all the pairwise contractions of momenta, which gives a contribution of the form:

$$3\left(\sum_q V^2(q)\right)^2 = 3\left(\overline{\epsilon^2}\right)^2 = 3\sigma_\varepsilon^4;$$

2. The following three involve double contractions (coincidences of momenta) which imply $V(q_1) = V(q_2) = V(q_3) = V(q_4)$. This contribution is $-3\sum_q V^4(q)$;

3. The last term gives no contribution, since it implies that $q_1 = -q_2 = -q_3 = -q_4$ and $q_2 = -q_3$. This will always yield a factor of $V(0) = 0$.

Consequently, the four momentum sums of Eq. A.2 have the value

$$3\left(\sum_q V^2(q)\right)^2 - 3\sum_q V^4(q) \tag{A.6}$$

This procedure is trivially generalized to any number of phase factors, although the structure becomes rather complicated for higher order terms. Fortunately, we will see that in certain limits, we may ignore the contributions coming from the coincidences of momenta, and only the pairwise contractions will contribute.

A.2 Phase Averages in the Gaussian Disorder Case

In the case of the Gaussian correlated disorder, the normalization of the Fourier transform implies that $V^2(q) \sim \mathcal{O}(1/N)$. The momentum sums give a factor of $\mathcal{O}(N)$, which means that the two terms in Eq. A.6 will be of order

$$3\left(\sum_q V^2(q)\right)^2 \sim \mathcal{O}(1),$$
$$3\left(\sum_q V^4(q)\right) \sim \mathcal{O}(N) \times \mathcal{O}(\frac{1}{N^2}) \sim \mathcal{O}(\frac{1}{N}).$$

This means that the second term is negligible in the thermodynamic limit. This argument can actually be carried through to any order, since any term of the form $\sum_q V^n(q)$ goes to zero in the limit $N \to \inf$, which renders all the contributions coming from the coincidence of indices irrelevant in this limit.

Therefore, if we want to calculate a general $F(q_1, \ldots, q_n)$, we may only consider the sum of all pairwise contractions of momenta. The total number of different contractions is $(n-1)!!$, and each one contributes with a term $\left(\sum_q V^2(q)\right)^{n/2}$ to the sum over momenta. Hence, we have

$$\sum_{q_1 \ldots q_{n-1}} V(q_1) \ldots V(-q_1 \ldots - q_{n-1}) \overline{e^{i\phi_{q_1}} \ldots e^{i\phi_{-q_1 \cdots - q_{n-1}}}} =$$
$$= (n-1)!! \left(\sum_q V^2(q)\right)^{\frac{n}{2}} \left[1 + \mathcal{O}\left(\frac{1}{N}\right)\right] \tag{A.7}$$

Phase Averages in the Power-Law Disorder Case

For the case of Power-Law Correlated Disorder, the Eq. A.6 is still valid, but one cannot generally ignore the V^4 term. Let us consider only the cases where $\alpha > 1$, meaning that

$$V(q) = A(\alpha)\left(\frac{2\pi}{N}\right)^{\frac{1}{2}} \frac{1}{|q|^{\frac{\alpha}{2}}} \tag{A.8}$$

with the normalization

$$A(\alpha) = \frac{\sigma_\varepsilon}{\sqrt{2\zeta(\alpha)}} \left(\frac{2\pi}{N}\right)^{(\alpha-1)/2}. \tag{A.9}$$

Like before, we have $\sum_{q\neq 0} V^2(q) = \sigma_\varepsilon^2$, but the calculation of $\sum_q V^4(q)$ is now, slightly different, i.e.

$$\begin{aligned}\sum_{q\neq 0} V^4(q) =& A^4(\alpha) \left(\frac{2\pi}{N}\right)^2 \sum_{q\neq 0} \frac{1}{|q|^{2\alpha}} \\ =& 2A^4(\alpha) \left(\frac{2\pi}{N}\right)^{2(1-\alpha)} \sum_{p=1}^{N/2} \frac{1}{p^{2\alpha}}\end{aligned}$$

In the large N limit, the last sum converges if $\alpha > 1/2$ and it gives $\zeta(2\alpha)$. Using Eq. A.9, we finally obtain $\sum_{q\neq 0} V^4(q) = \frac{\zeta(2\alpha)}{2\zeta(\alpha)}\sigma_\varepsilon^4$, which does not scale with the system size N. This interesting result suggests that the argument made for the Gaussian case does not work here, and any calculation of the moments of $\rho(k, E)$ must account for the coincidences of momenta. In fact, this is easily seen to be true for any term of the form $\sum_q V^{2n}(q)$, yielding the general form

$$\sum_q V^{2n}(q) = \frac{\zeta(n\alpha)}{2^n \zeta(\alpha)^n} \sigma_\varepsilon^{2n} \tag{A.10}$$

Nevertheless, a special case happens when $\alpha \to 1$. In this limit, the denominator of Eq. A.10 diverges as $(\alpha-1)^{-n}$, while the numerator remains finite near $\alpha = 1$. This means that, for $\alpha \to 1$ the corrections due to the coincidence of momenta become negligible, and we have

$$\begin{aligned}\sum_{q_1 \cdots q_{n-1}} V(q_1) \ldots V(-q_1 \ldots - q_{n-1}) \overline{e^{i\phi_{q_1}} \ldots e^{i\phi_{-q_1 \cdots - q_{n-1}}}} =& \\ = (n-1)!! \left(\sum_q V^2(q)\right)^{2n} [1 + \mathcal{O}(\alpha - 1)]& \end{aligned} \tag{A.11}$$

Appendix B

Generation of Correlated Random Potential

Fast Fourier Transform (FFT) is one of the most powerful mathematical algorithms and can reduce the numerical complexity by an order of magnitude. The numerical complexity of this algorithm is only $\mathcal{O}(L \log L)$, where L is the size of the system.

The correlated disorder potential can be efficiently computed by employing FFT. The key idea is to generate the correlated random potential in momentum space and then convert it into real space.

In general, the discrete inverse Fourier transform of a function $\phi(k)$ is

$$V(r) = \sum_{k=0}^{L-1} \phi(k) \exp(i\frac{2\pi k}{L} r), \tag{B.1}$$

For the case of even function of $\phi(k)$, we can expand the above equation as

$$V(r) = \sum_{k=-\frac{L}{2}+1}^{\frac{L}{2}} \phi(k) \exp(i\frac{2\pi}{L} kr), \tag{B.2}$$

$$= \sum_{k=-\frac{L}{2}+1}^{1} \phi(k) \exp(i\frac{2\pi}{L} kr) + \sum_{k=0}^{\frac{L}{2}} \phi(k) \exp(i\frac{2\pi}{L} kr), \tag{B.3}$$

$$= \sum_{k=1}^{\frac{L}{2}-1} \phi(k) e^{i\frac{2\pi}{L} kr} + \phi(0) + \sum_{k=1}^{\frac{L}{2}-1} \phi(k) e^{i\frac{2\pi}{L} kr} + \phi(\frac{L}{2}) e^{i\frac{2\pi}{L}\frac{L}{2} r}, \tag{B.4}$$

$$= \phi(0) + \phi(\frac{L}{2}) e^{i\pi r} + 2 \sum_{k=1}^{\frac{L}{2}-1} \phi(k) e^{i\frac{2\pi}{L} kr}, \tag{B.5}$$

$$= \phi(0) + \phi(\frac{L}{2}) e^{i\pi r} + 2 \sum_{k=1}^{\frac{L}{2}-1} \phi(k) (\cos(\frac{2\pi k}{L} r) + i \sin(\frac{2\pi k}{L} r)). \tag{B.6}$$

The correlated random potential for one-dimensional lattice can be written as

$$\varepsilon_r = \sum_{k=1}^{L/2} V(k) \cos\left(\frac{2\pi k}{L} r + \varphi_k\right), \tag{B.7}$$

In order to obtain the coefficient of FFT algorithm, we first expand the correlated disorder as

$$\varepsilon_r = \sum_{k=1}^{\frac{L}{2}} V(k)(\cos\left(\frac{2\pi k}{L} r\right)\cos(\varphi_k) - \sin\left(\frac{2\pi k}{L} r\right)\sin(\varphi_k)), \tag{B.8}$$

$$= V(\frac{L}{2})\cos(\pi r)\cos(\varphi_k) + \sum_{k=1}^{\frac{L}{2}-1} V(k)(\cos(\frac{2\pi k}{L} r)\cos(\varphi_k) - \sin(\frac{2\pi k}{L} r)\sin(\varphi_k)), \tag{B.9}$$

$$= V(\frac{L}{2})\cos(\varphi_k)\, e^{i\pi r} + \sum_{k=1}^{\frac{L}{2}-1} V(k)(\cos(\frac{2\pi k}{L} r)\cos(\varphi_k) - \sin(\frac{2\pi k}{L} r)\sin(\varphi_k)), \tag{B.10}$$

where $e^{i\pi r} = \cos(\pi r) + i\sin(\pi r)$, ($\sin(\pi r) = 0$, for $r = \mathbb{R}$). Comparing Eq. (B.6) and (B.10), we have

$$\phi(0) = 0;\ \phi(\frac{L}{2}) = V(\frac{L}{2})\cos(\varphi_k)\,;\ \phi(k) = \frac{V(k)}{2}\cos(\varphi_k) + i\frac{V(k)}{2}\sin(\varphi_k) \tag{B.11}$$

Thus, having these coefficient in hand, we can first generate the correlated disorder potentials in momentum space, and then applying FFT, in order to convert it into required real space.

Appendix C

Recursion Green Function Method

In this section, we will explore how to calculate the Green's functions —$\mathcal{G}^{r/a}_{N+1,0}(E_F)$— between two positions inside the sample coupled (on both sides) to semi-infinite leads. As demonstrated in chapter 3, the non-equilibrium current which transverses the sample when the chemical potentials in both leads are different, can be entirely expressed in terms of a small number of matrix elements of $\mathcal{G}(E = E_F)$[1].

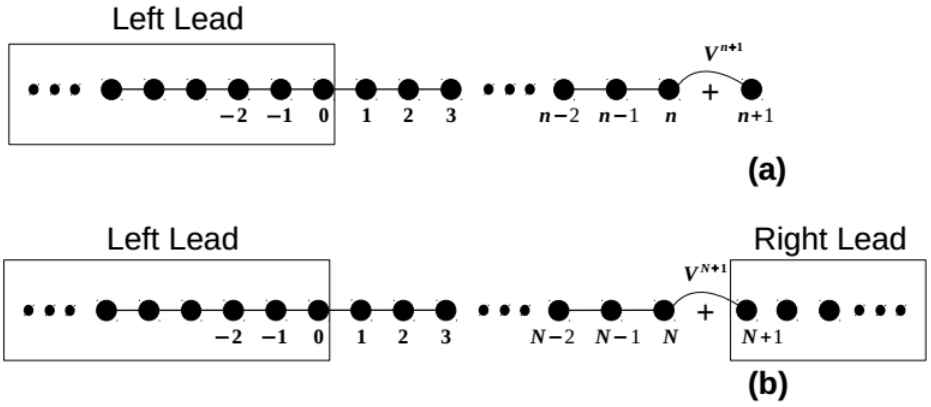

Figure C.1: Scheme showing the process of: (a) Adding the $(n+1)$th atom to the sample, as it is "grown" from the surface of the left lead; (b) Closing the recursion by coupling the sample to the right lead.

We start by pointing out that the method described here takes explicit advantage of both the 1D character of the system and the fact that the full Hamiltonian is band-diagonal in position-space. This is all we need in the context of one-dimensional systems, however there are many known generalizations of these recursive methods, which are applicable to other geometries and/or dimensions. The main idea behind the RGFM is the fact that one may divide the sample into its constituent sites and reconstruct it, site by site, on top of the left lead's surface. Accordingly, we may define the propagator associated to the system containing the left lead coupled to the n first sites of the sample as $\mathcal{G}^n_{i,j}(E)$. By definition,

[1]We omit from now on, the labels r/a, since it is obvious that all equations will apply equally well to the retarded and advanced propagators.

we take the 0-layer propagator to be $\mathcal{G}^0_{i,j}(E) = G^N_{i,j}(E)$. The process of adding the $(n+1)$th site of the sample is represented in Fig. C.1, where $V^{n+1} = -t\delta_{i,n}\delta_{j,n+1} - t\delta_{i,n+1}\delta_{j,n}$ is the interaction term which couples it to the rest of the sites at its left.

The Left-to-Right Recursion

The $(n+1)$-layer propagator —$\mathcal{G}^{n+1}_{i,j}(E)$— can be related to the propagator of the uncoupled system, by means to the Dyson Equation. The propagator of the uncoupled system is just the direct product of the $\mathcal{G}^n_{i,j}(E)$ with the one of the isolated $(n+1)$th site, i.e.

$$G^0_{i,j}(E) := \left[\mathcal{G}^n(E) \bigotimes g^{n+1}(E)\right]_{i,j}, \tag{C.1}$$

For an isolated atom, which is a single-level quantum system, it is obvious that we have

$$g^{n+1}_{i,j}(E) = \frac{\delta_{i,n+1}\delta_{j,n+1}}{E - \varepsilon_{n+1} \pm i0^+} = \delta_{i,n+1}\delta_{j,n+1}g_{n+1}(E), \tag{C.2}$$

where ε_{n+1} stands for the value of the local potential at site $n+1$, and $g_{n+1}(E) = G^0_{n+1,n+1}(E) = 1/(E - \varepsilon_{n+1} \pm i0^+)$. Given, the above facts, we can write the Dyson equation as follows:

$$\begin{aligned} \mathcal{G}^{(n+1)}_{i,j}(E) &= G^0_{i,j}(E) + \sum_{k,l} G^0_{i,k}(E)V^{(n+1)}_{k,l}\mathcal{G}^{n+1}_{l,j}(E), \\ &= G^0_{i,j}(E) - t\left(G^0_{i,n}(E)\mathcal{G}^{n+1}_{n+1,j}(E) + G^0_{i,n+1}(E)\mathcal{G}^{n+1}_{n,j}(E)\right), \end{aligned} \tag{C.3}$$

We are interested in the calculations of

$$\mathcal{G}^{n+1}_{n+1,n+1}(E) = g_{n+1}(E) - tg_{n+1}(E)\mathcal{G}^{n+1}_{n,n+1}(E), \tag{C.4}$$

$$\mathcal{G}^{n+1}_{n,n+1}(E) = -t\mathcal{G}^n_{n,n}(E)\mathcal{G}^{n+1}_{n+1,n+1}(E), \tag{C.5}$$

$$\mathcal{G}^{n+1}_{0,n+1}(E) = -t\mathcal{G}^n_{0,n}(E)\mathcal{G}^{n+1}_{n+1,n+1}(E), \tag{C.6}$$

Using these equations, we can obtain a recursion relation for $\mathcal{G}^n_{n,n}(E)$, as follows,

$$\mathcal{G}^{n+1}_{0,n+1}(E) = -\frac{t\mathcal{G}^n_{0,n}(E)}{E - \varepsilon_{n+1} - t^2\mathcal{G}^n_{n,n}(E)}, \tag{C.7}$$

$$\mathcal{G}^{n+1}_{n+1,n+1}(E) = \frac{1}{E - \varepsilon_{n+1} - t^2\mathcal{G}^n_{n,n}(E)}, \tag{C.8}$$

Clearly they show that if we start with the initial condition imposed by the left lead $\mathcal{G}^0_{0,0}(E, eV/2) = g_L(E, eV/2)$, where,

$$g_L(E, eV/2) = \frac{E + eV/2}{2t^2} \mp \frac{i}{2t^2}\sqrt{4t^2 - (E + eV/2)^2}. \tag{C.9}$$

in the presence of a constant potential V, we can determine $\mathcal{G}^n_{n,n}(E)$ and $\mathcal{G}^n_{0,n}(E)$ recursively, by adding each atom of the sample successively until the nth layer. However, this process cannot continue forever, since we which to couple to a semi-infinite lead on the right, once $n = N$, Thus, to close the iterative procedure, one must provide another Dyson equation, which describes the coupling of the "left lead + sample" subsystem, with the semi-infinite right lead (see Fig. C.1). The coupling between the two subsystems is written as, $V^{N+1}_{i,j} = -t\delta_{i,N}\delta_{j,N+1} - t\delta_{i,N+1}\delta_{j,N}$, and the corresponding Dyson equation is

$$\mathcal{G}_{i,j}(E) = G^0_{i,j}(E) - t\left(G^0_{i,N}(E)\mathcal{G}_{N+1,j}(E) + G^0_{i,N+1}(E)\mathcal{G}_{N,j}(E)\right), \tag{C.10}$$

After some algebra, we get the following final expression,

$$\mathcal{G}_{N+1,N+1}(E) = \frac{g_R(E)}{1 - t^2 g_R(E)\mathcal{G}^N_{N,N}(E)}, \tag{C.11}$$

$$\mathcal{G}_{0,N+1}(E) = -\frac{g_R(E)\mathcal{G}^N_{0,N}(E)}{1 - t^2 g_R(E)\mathcal{G}^N_{N,N}(E)}, \tag{C.12}$$

where $g_R(E, -eV/2) = \mathcal{G}^{N+1}_{N+1,N+1}(E, -eV/2)$ is the propagator of the right lead[2]

$$g_R(E, -eV/2) = \frac{E - eV/2}{2t^2} \mp \frac{i}{2t^2}\sqrt{4t^2 - (E - eV/2)^2}. \tag{C.13}$$

Similarly, the same could have been done starting from the opposite lead (right-to-left recursion) and can obtain the following recursion equations:

$$\mathcal{G}_{0,0}(E) = \frac{g_L(E)}{1 - t^2 g_L(E)\mathcal{G}^1_{1,1}(E)}, \tag{C.14}$$

$$\mathcal{G}_{N+1,0}(E) = -\frac{g_L(E)\mathcal{G}^1_{N+1,1}(E)}{1 - t^2 g_L(E)\mathcal{G}^1_{1,1}(E)}, \tag{C.15}$$

where $\mathcal{G}^1_{1,1}(E)$ and $\mathcal{G}^1_{N+1,1}(E)$ can be computed recursively by the using the following equations

$$\mathcal{G}^{n-1}_{N+1,n-1}(E) = -\frac{t\mathcal{G}^n_{N+1,n}(E)}{E - \varepsilon_{n+1} - t^2\mathcal{G}^n_{n,n}(E)}, \tag{C.16}$$

$$\mathcal{G}^{n-1}_{n-1,n-1}(E) = \frac{1}{E - \varepsilon_{n+1} - t^2\mathcal{G}^n_{n,n}(E)}, \tag{C.17}$$

Eqs. C.11 and C.14 are the central results for calculating transport properties in a tight-binding model.

[2] $\mp$: $-$ is for retarded, while $+$ is for advanced Green's function

Appendix D

Mean Free Path of the Anderson Model

The mean free path of the Anderson model in the perturbative regime (weak disorder limit) can be calculated analytically by the disorder averaged of the transition rate [75]. The transition rate for d-dimensional Anderson model with random potential V, can be found by applying the Fermi golden rule:

$$= \pi \sum_{k'} \left| \langle k \left| V \right| k' \rangle \right|^2 \delta(E_k - E_{k'}), \tag{D.1}$$

$$= \pi \sum_{k'} \left| \sum_j \varepsilon_j \langle k|j\rangle\langle j|k'\rangle \right|^2 \delta(E_k - E_{k'}), \tag{D.2}$$

$$= \pi \sum_{k'} (\sum_j \frac{\varepsilon_j^2}{L^{2d}} + \sum_{j \neq j'} \frac{\varepsilon_j \varepsilon_{j'}}{L^{2d}} \mathrm{e}^{i(k-k')(j-j')}) \delta(E_k - E_{k'}), \tag{D.3}$$

Tacking average over disorder, results

$$\frac{1}{\tau} = \pi \sum_{k'} \frac{W^2}{12 L^{2d}} \delta(E_k - E_{k'}), \tag{D.4}$$

in the thermodynamic limit,

$$\frac{1}{\tau} = \pi \frac{W^2}{12} \int \frac{\mathrm{d}k'}{(2\pi)^d} \delta(E_k - E_{k'}), \tag{D.5}$$

$$= \pi \frac{W^2}{12} \int dE' \rho(E') \delta(E_k - E'), \tag{D.6}$$

$$= \pi \frac{W^2}{12} \rho(E_k). \tag{D.7}$$

where $\rho(E_k)$ is the density of states for a d-dimensional clean system. For one-dimensional system, it is given by

$$\rho(E_k) = \frac{1}{\pi} \frac{1}{\sqrt{4t^2 - E_k^2}}, \tag{D.8}$$

The mean free path can be obtained by $l = v\tau$, where v is the typical velocity of the particle in between scattering events and can be obtained as

$$v \equiv \partial E_k / \partial k = \sqrt{4t^2 - E_k^2} \tag{D.9}$$

The mean free path is given by

$$l = \frac{12(4t^2 - E_k^2)}{W^2}, \tag{D.10}$$

Eq. D.10, clearly show that, the mean free path and the localization length in 1D Anderson model are the same.

Bibliography

[1] N. A. Khan, J. M. Viana Parente Lopes, J. P. Santos Pires, and J. M. B. Lopes dos Santos. Spectral functions of one-dimensional systems with correlated disorder. *J. Phys.: Condens. Matter*, 31(17):175501, feb 2019.

[2] G. Czycholl, B. Kramer, and A. MacKinnon. Conductivity and localization of electron states in one dimensional disordered systems: Further numerical results. *Zeitschrift für Physik B Condensed Matter*, 43(1):5–11, Mar 1981.

[3] F. M. Izrailev, A. A. Krokhin, and N. M. Makarov. Anomalous localization in low-dimensional systems with correlated disorder. *Physics Reports*, 512(3):125 – 254, 2012.

[4] G. M. Petersen and N. Sandler. Anticorrelations from power-law spectral disorder and conditions for an anderson transition. *Phys. Rev. B*, 87:195443, May 2013.

[5] M. Pouranvari, Y. Zhang, and K. Yang. Entanglement area law in disordered free fermion anderson model in one, two, and three dimensions. *Advances in Condensed Matter Physics*, 2015:4, 2015.

[6] P. Calabrese and J. Cardy. Entanglement entropy and quantum field theory. *Journal of Statistical Mechanics: Theory and Experiment*, 2004(06):P06002, 2004.

[7] F. Iglio. and Yu-Cheng Lin. Finite-size scaling of the entanglement entropy of the quantum ising chain with homogeneous, periodically modulated and random couplings. *Journal of Statistical Mechanics: Theory and Experiment*, 2008(06):P06004, 2008.

[8] M. Imada, A. Fujimori, and Y. Tokura. Metal-insulator transitions. *Rev. Mod. Phys.*, 70:1039–1263, Oct 1998.

[9] N. F. Mott. *Metal Insulator Transitions*, pages 287–296. Springer Netherlands, Dordrecht, 1984.

[10] P. W. Anderson. Absence of diffusion in certain random lattices. *Phys. Rev.*, 109:1492–1505, Mar 1958.

[11] D. J. Thouless. Localization distance and mean free path in one-dimensional disordered systems. *Journal of Physics C: Solid State Physics*, 6(3):L49, 1973.

[12] D. J. Thouless. *Ill-Condensed Matter, Les Houches Session XXXI.* (North-Holland, New York, 1979), 1979.

[13] B. Kramer and A. MacKinnon. Localization: theory and experiment. *Reports on Progress in Physics*, 56(12):1469, 1993.

[14] A. MacKinnon. The conductivity of the one-dimensional disordered anderson model: a new numerical method. *Journal of Physics C: Solid State Physics*, 13(35):L1031, 1980.

[15] A. MacKinnon and B. Kramer. One-parameter scaling of localization length and conductance in disordered systems. *Phys. Rev. Lett.*, 47:1546–1549, Nov 1981.

[16] P. Markoš. Numerical analysis of the anderson localization. *Acta Physica Slovaca Reviews and Tutorials*, 56, 10 2006.

[17] F. A. B. F. de Moura and M. L. Lyra. Delocalization in the 1D Anderson model with long-range correlated disorder. *Physical Review Letters*, 81(17):3735–3738, OCT 26 1998.

[18] H. Fehske, R. Schneider, and A. Weiße (Eds.). *Computational Many-Particle Physics.* Lecture Notes in Physics 739. Springer-Verlag Berlin Heidelberg, 1 edition, 2008.

[19] A. Weiße, G. Wellein, A. Alvermann, and H. Fehske. The kernel polynomial method. *Rev. Mod. Phys.*, 78:275–306, Mar 2006.

[20] R. N. Silver, H. Roeder, A. F. Voter, and J. D. Kress. Kernel polynomial approximations for densities of states and spectral functions. *J. Comput. Phys.*, 124(1):115 – 130, 1996.

[21] R. N. Silver, A. F. Voter, J. D. Kress, and H. Roeder. *Polynomial approximations for materials simulations.* Feb 1995.

[22] J.C. Mason and D.C. Handscomb. *Chebyshev Polynomials.* CRC Press, 2002.

[23] H. Bruus and K. Flensberg. *Many-body quantum theory in condensed matter physics an introduction.* Oxford Graduate texts. Oxford University Press, 2004.

[24] C. A. Muller and D. Delande. *Disorder and interference: localization phenomena: Ultracold Gases and Quantum Information,.* (Les Houches Summer School Session XCI) ed C Miniatura et al (Oxford: Oxford University Press), 2010.

[25] V. V. Volchkov, M. Pasek, V. Denechaud, M. Mukhtar, A. Aspect, D. Delande, and V. Josse. Measurement of spectral functions of ultracold atoms in disordered potentials. *Phys. Rev. Lett.*, 120:060404, Feb 2018.

[26] E. C. Andrade, M. Steudtner, and M. Vojta. Anderson localization and momentum-space entanglement. *Journal of Statistical Mechanics: Theory and Experiment*, 2014(7):P07022, 2014.

[27] J. P. Santos Pires, N. A. Khan, J. M. Viana Parente Lopes, and J. M. B. Lopes dos Santos. Global delocalization transition in the de moura–lyra model. *Phys. Rev. B*, 99:205148, May 2019.

[28] C.-K. Peng, S. V. Buldyrev, A. L. Goldberger, S. Havlin, F. Sciortino, M. Simons, and H. E. Stanley. Long-range correlations in nucleotide sequences. *Nature*, 356(6365):168–170, March 1992.

[29] J. W. Kantelhardt, S. Russ, A. Bunde, S. Havlin, and I. Webman. Comment on "delocalization in the 1d anderson model with long-range correlated disorder". *Phys. Rev. Lett.*, 84:198–198, Jan 2000.

[30] S. Russ, J. W. Kantelhardt, A. Bunde, and S. Havlin. Localization in self-affine energy landscapes. *Phys. Rev. B*, 64:134209, Sep 2001.

[31] J. Cardy P. Calabrese and B. Doyon. Entanglement entropy in extended quantum systems. *Journal of Physics A: Mathematical and Theoretical*, 42(50):500301, 2009.

[32] N. Laflorencie. Quantum entanglement in condensed matter systems. *Physics Reports*, 646:1 – 59, 2016.

[33] J. C. F. Matthews and M. G. Thompson. Quantum optics: An entangled walk of photons. *Nature*, 484(7392):47–48, April 2012.

[34] M. A. Nielsen; I. L. Chuang. *Quantum computation and quantum information.* Cambridge University Press, 10th anniversary ed edition, 2010.

[35] M. B. Hastings. An area law for one-dimensional quantum systems. *Journal of Statistical Mechanics: Theory and Experiment*, 2007(08):P08024, 2007.

[36] M. M. Wolf. Violation of the entropic area law for fermions. *Phys. Rev. Lett.*, 96:010404, Jan 2006.

[37] M. Pouranvari and K. Yang. Maximally entangled mode, metal-insulator transition, and violation of entanglement area law in noninteracting fermion ground states. *Phys. Rev. B*, 89:115104, Mar 2014.

[38] N. Roy and A. Sharma. Entanglement contour perspective for "strong area-law violation" in a disordered long-range hopping model. *Phys. Rev. B*, 97:125116, Mar 2018.

[39] L. Pastur and V. Slavin. Area law scaling for the entropy of disordered quasifree fermions. *Phys. Rev. Lett.*, 113:150404, Oct 2014.

[40] Y. Chen and G. Vidal. Entanglement contour. *Journal of Statistical Mechanics: Theory and Experiment*, 2014(10):P10011, 2014.

[41] N. A. Khan, J. M. B. Lopes dos Santos, J. M. Viana Parente Lopes, and J. P. Santos Pires. Probing anderson transition with entanglement contour. 2019.

[42] K. Fernando. On computing an eigenvector of a tridiagonal matrix. part i: Basic results. *SIAM Journal on Matrix Analysis and Applications*, 18(4):1013–1034, 1997.

[43] F. M. Izrailev and A. A. Krokhin. Localization and the mobility edge in one-dimensional potentials with correlated disorder. *Phys. Rev. Lett.*, 82:4062–4065, May 1999.

[44] G. Schubert, J. Schleede, K. Byczuk, H. Fehske, and D. Vollhardt. Distribution of the local density of states as a criterion for anderson localization: Numerically exact results for various lattices in two and three dimensions. *Phys. Rev. B*, 81:155106, Apr 2010.

[45] E. Borland R. and P. J. Anthony. The nature of the electronic states in disordered one-dimensional systems. *Proceedings of the Royal Society of London. Series A. Mathematical and Physical Sciences*, 274(1359):529–545, August 1963.

[46] D. J. Thouless. A relation between the density of states and range of localization for one dimensional random systems. *Journal of Physics C: Solid State Physics*, 5(1):77, 1972.

[47] D. McMahon. *Quantum Computing Explained*. Wiley-Interscience :, IEEE Computer Society, 2008.

[48] D. Petrosyan P. Lambropoulos. *Fundamentals of quantum optics and quantum information*. Springer, 1 edition, 2007.

[49] D-L. Zhou B. Zeng, X. Chen and X-G. Wen. Quantum information meets quantum matter. *arXiv:1508.02595.*, 2016.

[50] I. Peschel. Calculation of reduced density matrices from correlation functions. *Journal of Physics A: Mathematical and General*, 36(14):L205, 2003.

[51] V. Eisler and I. Peschel. Free-fermion entanglement and spheroidal functions. *Journal of Statistical Mechanics: Theory and Experiment*, 2013(04):P04028, apr 2013.

[52] J. H. Wilkinson. *The algebraic eigenvalue problem*. Clarendon Press, Oxford, 1965.

[53] C. F. V. Loan G. H. Golub. *Matrix computations*. Johns Hopkins studies in the mathematical sciences. Johns Hopkins University Press, 3rd ed edition, 1996.

[54] A. Ferreira and E. R. Mucciolo. Critical delocalization of chiral zero energy modes in graphene. *Phys. Rev. Lett.*, 115:106601, Aug 2015.

[55] F. Lacopi, J. J. Boeckl, and C. Jagadish, editors. *2D Materials, Volume 95 (Semiconductors and Semimetals)*. Academic Press, 1 edition, 7 2016.

[56] A. Braun and P. Schmitteckert. Numerical evaluation of green's functions based on the chebyshev expansion. *Phys. Rev. B*, 90:165112, Oct 2014.

[57] S. Zhang, S. Yamagiwa, M. Okumura, and S. Yunoki. Performance acceleration of kernel polynomial method applying graphics processing units. *IPDPS/APDCM*, pages 564–571, !EEE CS (2011).

[58] N. Hatano and J. Feinberg. Chebyshev-polynomial expansion of the localization length of hermitian and non-hermitian random chains. *Phys. Rev. E*, 94:063305, Dec 2016.

[59] R. I. Gradshteyn I. *Table of integrals Series and Products*. Academic Press, 18th September 2014.

[60] R. Landauer. Electrical resistance of disordered one-dimensional lattices. *The Philosophical Magazine: A Journal of Theoretical Experimental and Applied Physics*, 21(172):863–867, 1970.

[61] M. Wimmer. *Quantum transport in nanostructures: From computational concepts to spintronics in graphene and magnetic tunnel junctions*, volume 5. December 2009.

[62] H. M. Srivastava, M. L. Glasser, and V. S. Adamchik. *Series Associated with the Zeta and Related Functions*. Oxford Graduate texts. Kluwer Academic Publishers, Dordrecht, Boston, and London, 2001.

[63] M. I. Trappe, D. Delande, and C. A. Mueller. Semiclassical spectral function for matter waves in random potentials. *Jour. Phys. A - Mathematical And Theoretical*, 48(24, SI), June 2015.

[64] P. Sheng and Zhao-Qing Zhang. Mesoscopic transport properties of 2d disordered metallic films: a proposal for the observation of anderson localization. *Journal of Physics: Condensed Matter*, 3(23):4257–4267, jun 1991.

[65] M. Ruhlander and C. M. Soukoulis. The probability distribution of the conductance at the mobility edge. *Physica B: Condensed Matter*, 296(1):32 – 35, 2001. Proceedings of the Symposium on Wave Propagation and Electronic Structure in Disordered Systems.

[66] F. Evers and A. D. Mirlin. Fluctuations of the inverse participation ratio at the anderson transition. *Phys. Rev. Lett.*, 84:3690–3693, Apr 2000.

[67] N. C. Murphy, R. Wortis, and W. A. Atkinson. Generalized inverse participation ratio as a possible measure of localization for interacting systems. *Phys. Rev. B*, 83:184206, May 2011.

[68] F. M. Izrailev, T. Kottos, and G. P. Tsironis. Hamiltonian map approach to resonant states in paired correlated binary alloys. *Phys. Rev. B*, 52:3274–3279, Aug 1995.

[69] M. Kappus and F. Wegner. Anomaly in the band centre of the one-dimensional anderson model. *Zeitschrift für Physik B Condensed Matter*, 45(1):15–21, Mar 1981.

[70] R. McWeeny. Some recent advances in density matrix theory. *Rev. Mod. Phys.*, 32:335–369, Apr 1960.

[71] I. Frérot and T. Roscilde. Area law and its violation: A microscopic inspection into the structure of entanglement and fluctuations. *Phys. Rev. B*, 92:115129, Sep 2015.

[72] F. G. S. L. Brandao. and M. Horodecki. An area law for entanglement from exponential decay of correlations. *Nat Phys*, 9(11):721–726, November 2013.

[73] J. I. Latorre and A. Riera. A short review on entanglement in quantum spin systems. *Journal of Physics A: Mathematical and Theoretical*, 42(50):504002, 2009.

[74] W.H. Press, S. A. Teukolsky, W. T. Vetterling, and B. P. Flannery. *Numerical Recipes in C book set: Numerical Recipes in C: The Art of Scientific Computing, Second Edition*. Cambridge University Press, 2 edition, 1992.

[75] T. Thiery A. Scardicchio. Perturbation theory approaches to anderson and many-body localization: some lecture notes. 2017.